A STUDY OF SAND-BED FILTERS: Filtration of Suspended Solids with Narrow Size Ranges

by

SHYH-HONG HWANG

B. S., NATIONAL TAIWAN UNIVERSITY, 1980

A MASTER'S THESIS

submitted in partial fulfillment of the

requirements for the degree

MASTER OF SCIENCE

Department of Chemical Engineering

KANSAS STATE UNIVERSITY
Manhattan, Kansas

1984

Approved by:

L. J. Fan

Major Professor

TABLE OF CONTENTS

LIST OF TABLES

LIST OF FIGURES

FIGURE

FIGURE

ACKNOWLEDGMENT

I wish to express my sincere gratitude to my major advisor, Dr. L. T. Fan, whose advice and guidance made possible the completion of this work. I am also grateful to National Science Foundation for financial assistance (Grant No. CPE-8209086). Special thanks are also given to my family, Hsao-Ying, and my friends for their continual encouragement.

CHAPTER I INTRODUCTION

The overall objective of this study is to carry out a comprehensive investigation of the performance of the semifluidized-bed filter. This filter has been proposed as a remedy for the inefficient operation of deep bed filters (Wen and Fan, 1979; Hsu and Fan, 1981; 1982; Fan and Hsu, 1984). Because the filtration in a semifluidized bed involves the deep bed filtration, a reasonable model of semifluidized-bed filtration requires the incorporation of a deep bed filtration model. Therefore, a companion study on the deep bed filter has also been carried out.

Deep bed filters, also known as granular filters, are extensively used in purification of potable water and in treatment of waste water (see, e.g., Fuller, 1898; Dunbar and Calvert, 1908; Hall, 1957). Much effort has been spent to study various types of deep beds under a wide range of operating conditions. It appears that so far little has been done to analyze and model mechanistically the results in a unified manner.

The use of stochastic models to simulate the deep bed filtration has been proposed by Litwiniszyn (1963; 1966; 1967; 1968a; 1968b; 1969). These stochastic models can be viewed as the intermediate between the phenomenological models (Iwasaki, 1937; Ives, 1960; 1961; Camp, 1964), in which the form of model equations is assumed from prior knowledge of the phenomena, and the trajectory analysis models (O'Melia and Stum, 1967; Yao et al., 1971; Payatakes, 1973; Rajagopalan and Tien, 1976; 1979; Pendse et al., 1978), in which the trajectories of the particles are determined painstakingly from the force balance equations. The filtration process is complicated and chaotic in nature, and the stochastic models, derived through probability considerations, often generate parameters that appear to describe adequately the behavior of the filter.

Litwiniszyn (1963) has used a pure birth process where the number of blocked pores in a unit volume of the bed is considered as the model variable. Hsu (1981), and Hsu and Fan (1984) have employed the pure birth process to model the pressure drop through the entire bed; in their model the number of blocked pores is related to the pressure drop by assuming that the scouring of deposited particles is negligible.

One group of research workers(see, e.g., Mintz, 1951; Mintz et al., 1967) have considered that deposits accumulated in the filter medium have a structure with uneven strength. This structure is partially destroyed by the hydrodynamic forces of the flow of water through the medium, which increase with an increase in the pressure drop; a portion of the particles less strongly linked to other particles is detached from the grains. Based on this observation, Litwiniszyn (1966) has developed a birth-death model. In the present work, this birth-death model, taking into account both blockage of pores by suspended particles and scouring of deposited particles, is combined with Carman-Kozeny equation for the pressure drop through the packed bed to describe its temporal change during a filtration run.

The applicability of the birth-death model to the experimental data has amply been demonstrated. It has been found, however, that in some situations the pressure drop characteristics of the deep bed filtration deviate from the behavior predicted by this model. To elucidate this deviation, a different stochastic model, namely, the second-order, pure birth process, has also been proposed.

The operation of deep bed filters is often inefficient; it is typically characterized by the shallow penetration of suspended solids and rapid clogging in the bed. Fortunately, these disadvantages can be overcome by the use of semifluidized-bed filters. An experimental study on the performance of the semifluidized-bed filter has been carried out to observe the

phenomena involved in the semifluidized-bed filtration and to determine advantages achievable. To this end, this work is divided into the following chapters.

In Chapter II, a review of the semifluidized bed literature is presented. A description is given of the methods of operating a semifluidized bed. Numerous articles pertaining to the fundamental aspects of semifluidization are reviewed; mass balance equations and empirical correlations relating the structure of the bed to operating parameters are presented. Also described in this chapter are some applications of the semifluidized bed.

The Master equation and one-step processes are described in Chapter III. The Master equation, governing the probability balance in a stochastic process, is relatively easy to manipulate; it can be related directly to the physical process to be modeled. The one-step processes are a special class of stochastic processes; it is characterized by the occurrence of birth and death events. The one-step operator technique is presented to obtain useful information, such as the mean and variance of the random variable, from the Master equation for a one-step process.

Chapters IV and V deal with the stochastic modeling of the deep bed filtration under the constant flow condition. Specifically, the pressure drop dynamics in the deep bed filter are simulated in Chapter IV by the linear, birth-death process. The model is relatively simple in that the entire bed is assumed to be spatially lumped. The available experimental data from numerous researchers are analyzed and simulated in the light of this model.

In some situations, the pressure drop dynamics in the filter bed deviate from the behavior predicted by the linear, birth-death process. To explain this deviation, a second-order, pure birth model has been proposed in Chapter V. The bed is divided into several spatially-lumped compartments; each depicted by one of the present models.

A large number of experimental runs were conducted with deep bed filters; analysis and simulation of the results based on the present models, namely, the linear, birth-death and second-order, pure birth processes, are presented in Chapter VI. The primary concern in this work is to investigate how the size distribution of suspended solids and suspension concentration affect the performance of the deep bed filtration.

In Chapter VII, an experimental study of the semifluidized-bed filter is presented. The results show that the filtration capacity of the semi-fluidized bed filter is considerably greater than that of an equivalent deep bed filter. In addition to pressure drop and effluent quality data, a series of photographs is included to describe and explain the mechanisms of the semifluidized-bed filter, giving rise to its superior performance over the deep bed filter.

In the final chapter, significant conclusions of this work are summarized and possible area of future research is suggested.

CHAPTER II PHENOMENA OF SEMIFLUIDIZATION

The idea of semifluidization was conceived by L. T. Fan (1958). Semifluidization refers to the phenomenon created when a mass of fluidized solid particles is partially restricted from above with a porous restraining plate, giving rise to the formation of a fixed bed and a fluidized bed in series within a single containing vessel.

A typical semifluidized bed, as shown in Figure II-1, consists of a vertically-extending column providing a bed section for the fluidized or fixed solid particles, a fluid distributor plate for introducing the fluid (gas or liquid) from the bottom of the bed, and a movable upper restraining plate which passes the fluid but prevents the passage of the solid particles. The degree of fluidization occurring in the bed can range from complete fluidization (conventional fluidized bed) to no fluidization (conventional fixed or packed bed) by lifting or lowering the upper restraining plate, while the fluid is being introduced at a flow rate greater than the minimum fluidization velocity for the bed. At a given fluid velocity greater than the minimum fluidization velocity and less than the maximum fluidization velocity, the upper restraining plate can be raised above a point where the entire bed is completely fluidized. When the restraining plate is lowered, the uppermost portion of the bed is first fixed, and as the lowering of the restraining plate continues, a progressively increasing portion of the bed becomes fixed. Simultaneously, the fluidized portion of the bed right above the distributor plate becomes progressively smaller until, finally, a condition is reached where the entire bed is fixed (Fan et al., 1959; Fan and Wen, 1960; 1968). Thus, for a given system, any degree of fluidization between the limits of a completely fluidized state and a completely fixed state may be attained by controlling the fluid flow rate and/or the restrain-

ing plate position. The mobility of the upper restraining plate, however, is not essential to the formation of a semifluidized bed.

In case where the density of the bed particles is less than that of the fluid, the structure of the semifluidized bed is reversed. The fluid is now introduced from the top of the bed. The force of the fluid on the particles counteracts the buoyancy of the particles in maintaining fluidization. The fixed section of the bed lies below the fluidized section and adjacently above the restraining plate as shown in Figure II-2.

STRUCTURE

A simple material balance yields a relationship expressing the height of the fixed or packed section in a semifluidized bed as a function of operating conditions (Fan et al., 1959; 1960; 1961). Under the assumptions that the particles are uniformly distributed in a fluidized bed, the movement of a particle in the suspension is completely independent of other particles, and the suppression of the expansion of the suspension and subsequent formation of the packed section does not change the average particle distance in the fluidized section; and the voidage of the packed section is constant and is that of the least dense static bed under resting conditions, the following equation for the height of the packed section can be obtained as (referring to Figure II-1)

$$h_{pa}\rho_s(1 - \varepsilon_{pa}) = [h_{pa} + (h_f - h)]\rho_s(1 - \varepsilon_f)$$

or

$$h_{pa} = (h_f - h)\frac{1 - \varepsilon_f}{\varepsilon_f - \varepsilon_{pa}} \qquad \text{(II-1)}$$

where h_{pa} is the height of the packed section, ρ_s, the density of the solid particles, ε_{pa}, the porosity of the packed section, h_f, the height of the fully

fluidized bed , h, the height of the semifluidized bed, and ε_f, the porosity of the fluidized section. It follows then, the weight fraction of the solid particles in the packed section, X, can be expressed as

$$X = \frac{\rho_s A(1 - \varepsilon_{pa})(h_f - h)(1 - \varepsilon_f)}{W(\varepsilon_f - \varepsilon_{pa})} \qquad \text{(II-2)}$$

where A is the cross-sectional area of the bed and W, the weight of the bed particles. The observed heights of the packed section have been plotted for comparison with the values calculated in accordance with Eq. II-1 by Fan and Wen (1961) as shown in Figure II-3.

FLOW EQUATION

Dimensional analysis of the continuity and momentum equations for particulate fluidization led to the expression (Beranek, 1958)

$$f[\frac{\varepsilon_f - \varepsilon_o}{1 - \varepsilon_o} , \frac{u - u_{mf}}{u_t - u_{mf}}] = 0 , \qquad \text{(II-3)}$$

where ε_o is the porosity of the static bed under the least dense condition, and u, u_{mf} and u_t are the superficial fluid velocity, the minimum fluidization velocity in terms of the superficial velocity and terminal velocity of the particles, respectively. Fan and Wen (1961) have applied similar analysis to semifluidization and obtained the relationship

$$f[\frac{h - h_o}{h - h_{pa}} , \frac{G - G_{mf}}{G_t - G_{mf}}] = 0 , \qquad \text{(II-4)}$$

where G_{mf} and G_t are the minimum fluidization velocity and the free fall terminal velocity, respectively, in mass flow rate per unit area of the empty bed. Experimental data from solid-liquid (Fan and Wen, 1961) and solid-gas (Wen et al., 1963) systems substantiate this relationship. A

two parameters fit by Kurian and Rao (1970) have yielded an explicit form of Eq. II-4 as

$$\left[\frac{G - G_{mf}}{G_t - G_{mf}}\right] = 0.61 \left[\frac{h - h_{oa}}{h - h_o}\right]^{-1.2} \qquad \text{(II-5)}$$

On the other hand, Rao and Sarma (1973) introduced the minimum semifluidization, G_{osf}, in place of the minimum fluidization velocity in Eq. II-4, and developed the following one parameter expression;

$$\frac{h - h_o}{h - h_{pa}} = \left[\frac{G - G_{osf}}{G_t - G_{osf}}\right]^{0.2} \qquad \text{(II-6)}$$

Equations II-4 through II-6 define the state of semifluidization. Other investigators (Babu Rao and Doraiswamy, 1967; Roy and Sarma, 1973; Roy and Sen Gupta, 1975; Roy, 1971) have correlated empirically the state of semifluidization in various forms of the function

$$f\left[\frac{G}{G_t}, \frac{h_{pa}}{h_o}, \frac{D_c}{d_p}, \frac{\rho_s}{\rho_f}, R, \frac{h_o}{D_c}\right] = 0 \qquad \text{(II-7)}$$

The correlations are listed in Table II-1.

The minimum semifluidization velocity, defined as the superficial fluid velocity at which the formation of the packed section initiates, can be obtained from Eq. II-5 or II-7 by allowing $h_{pa} \rightarrow 0^+$. Poddar and Dutt (1969) have employed the voidage function of Wen and Yu (1966) and the relationship between ε_f and the voidage function (Wilhelm and Kwauk 1948; Lewis et al., 1949; Richardson and Zaki, 1954) to obtain the condition of minimum semifluidization given below.

$$\frac{18Re_{osf} + 2.7Re_{osf}^{1.687}}{Ga\left[1 - \frac{h_o}{h}(1 - \varepsilon_{pa})\right]^{4.7}} = 0.966\phi_s^{0.88} \qquad \text{(II-8)}$$

where Re_{osf} is the Reynolds number at the onset of semifluidization, Ga,

the Galileo number, and ϕ_s, the sphericity of particles. Empirical correlations are also available in the form of (Roy and Sarma, 1972; Roy, 1971; Roy and Sen Gupta, 1975)

$$f[\frac{G_{osf}}{G_{mf}} \text{ or } \frac{G_{osf}}{G_{msf}}, \frac{D_c}{d_p}, \frac{\rho_s}{\rho_f}, R] = 0 \qquad \text{(II-9)}$$

where G_{msf} is the maximum fluidization velocity; these are listed in Table II-2. The minimum fluidization velocity, G_{mf}, in Roy and Sarma's correlations can be calculated from Leva's (1959) simplified equation in FPS units:

$$G_{mf} = 688\, d_p^{1.82}\, \frac{[\rho_f\,(\rho_s - \rho_f)]^{0.94}}{\mu^{0.88}} \qquad \text{(II-10)}$$

The maximum semifluidization velocity, defined as the superficial fluid velocity at which all solid particles are supported by the fluid in the packed portion of the bed, can be obtained by: (a) extrapolating, graphically or numerically, the ε_f vs. G curve to $\varepsilon_f = 1.0$ or the h_{pa}/h_o vs. G curve to $h_{pa}/h_o = 1.0$ (Fan and Wen, 1961); (b) approximating G_{msf} by the free fall terminal velocity of a single particle (Fan and Wen, 1961); (c) using the following semiempirical equation (Poddar and Dutt, 1969);

$$18\, Re_{msf} + 2.7\, Re_{msf}^{1.687} = Ga\ , \qquad \text{(II-11)}$$

where Re_{msf} is the Reynolds number at the maximum semifluidization velocity; (d) using any of the empirical correlations by Roy and Sarma (1974a), Roy and Sen Gupta (1975) or Roy (1971) listed in Table II-3.

PRESSURE DROP

The overall pressure drop of both fully fluidized and semifluidized beds with the parameter of the height of initial static bed at least dense condition, h_o, has been experimentally studied by Fan and Wen (1961) as shown in Figure II-4.

Because of the formation of the packed section when the fluidized suspension is suppressed, the total pressure drop should be the algebraic sum of the pressure drops across the fluidized section and the packed section, since these two sections are aligned in series in the direction of fluid flow. Therefore,

$$\Delta P_t = \left(\frac{\Delta P}{L}\right)_f (h - h_{pa}) + \left(\frac{\Delta P}{L}\right)_{pa} h_{pa} \qquad \text{(II-12)}$$

By substituting the effective weight of the particles into the first term in the right-hand side of Eq. II-12, the Ergun equation (Ergun, 1952) into the second term, and combining the resultant expression with Eq. II-1, Fan and Wen (1961) have obtained

$$\Delta P_t = \left[h_f - \frac{(1 - \varepsilon_{pa})(h_f - h)}{(\varepsilon_f - \varepsilon_{pa})}\right] (1 - \varepsilon_f)(\rho_s - \rho_f)$$
$$+ \left[\frac{150(1 - \varepsilon_{pa})^2}{\varepsilon_{pa}^3} \frac{\mu u}{(\phi_s d_p)^2} + 1.75 \frac{(1 - \varepsilon_{pa})}{\varepsilon_{pa}^3} \frac{Gu}{\phi_s d_p}\right]$$
$$\cdot \left[(h_f - h) \frac{(1 - \varepsilon_f)}{(\varepsilon_f - \varepsilon_{pa})}\right] \frac{1}{g_c} \qquad \text{(II-13)}$$

where ρ_f and μ are the density and the viscosity of the fluid, respectively, d_p, the equivalent particle diameter, ϕ_s, the sphericity of particles, u, the superficial velocity of the fluid, and G, the mass flow rate of the fluid per unit area of the empty bed. Equation II-13 was found to give a reasonably good agreement with the experimental results for solid-liquid solid-gas systems with particles of various sizes and shapes (Fan and Wen,

1961; Wen et al., 1963). However, due to difficulties in determining ε_f and ε_{pa} accurately, Eq. II-13 often led to values below those measured (Wen et al., 1963; Roy and Sen Gupta, 1973; Roy and Sarma, 1974b). Subsequently, the following correction factor was introduced (Roy and Sen Gupta, 1973; Roy and Sarma, 1974b);

$$C = \frac{(\Delta P_t)_{exp}}{(\Delta P_t)_{Eq.\ II\text{-}13}} \tag{II-14}$$

This correction factor was empirically correlated by Roy and Sen Gupta (1973) and Roy and Sarma (1974b) as a function of the system variables, i.e.,

$$C = f[\frac{D_c}{d_p}, \frac{\rho_s}{\rho_f}, \frac{h_o}{D_c}, R, \frac{h_{pa}}{h_o}] \tag{II-15}$$

in which D_c is the column diameter, h_o, the height of the static bed under the least dense condition, and R, the bed expansion ratio. These correlations are tabulated in Table II-4.

Similar to Eq. II-13, it has been postulated that in addition to the pressure drop for the fluid flowing through packed section, the fluid need support the solid particles in the entire bed (Yutani and Fan, 1984). This implies that

$$\Delta P_t = h_f(1 - \varepsilon_f)(\rho_s - \rho_f) + [\frac{150(1 - \varepsilon_{pa})^2}{\varepsilon_{pa}^3} \frac{\mu u}{(\phi_s d_p)^2} + 1.75 \frac{(1 - \varepsilon_{pa})}{\varepsilon_{pa}^3} \frac{Gu}{\phi_s d_p}] \cdot [(h_f - h) \frac{(1 - \varepsilon_f)}{(\varepsilon_f - \varepsilon_{pa})}] \frac{1}{g_c} \tag{II-16}$$

It appears that Eq. II-13 tends to underestimate the pressure drop while Eq. II-16 tends to overestimate it; the actual pressure drop is bounded by the values estimated by these two equations. Therefore, a

correction factor, c_f, which has the value between 0 and 1, may need be introduced to modify them as (Yutani and Fan, 1984)

$$\Delta P_t = (1 - c_f)\, h_f(1 - \varepsilon_f)(\rho_s - \rho_f) + c_f \left[h_f - \frac{(1 - \varepsilon_{pa})(h_f - h)}{(\varepsilon_f - \varepsilon_{pa})}\right] (1 - \varepsilon_f)(\rho_s - \rho_f) + \left[\frac{150(1 - \varepsilon_{pa})^2}{\varepsilon_{pa}^3} \frac{\mu u}{(\phi_s d_p)^2} + 1.75 \frac{(1 - \varepsilon_{pa})}{\varepsilon_{pa}^3} \frac{Gu}{\phi_s d_p}\right] \cdot \left[(h_f - h) \frac{(1 - \varepsilon_f)}{(\varepsilon_f - \varepsilon_{pa})}\right] \frac{1}{g_c} \qquad \text{(II-17)}$$

MASS TRANSFER

The mass-transfer property of the semifluidized bed was investigated by Fan et al. (1959; 1960), using the benzoic acid-water system. The performance of the semifluidized bed as a mass-transfer contactor has been found to be a linear combination of those of the packed and fluidized sections in the bed. The experimentally determined overall log-mean mass-transfer coefficient can be expressed by the correlation

$$k_{\ell m} = (1 - X)(k_f)_{\ell m} + X(k_{pa})_{\ell m} \qquad \text{(II-18)}$$

in which $(k_f)_{\ell m}$ and $(k_f)_{\ell m}$ are the log-mean mass-transfer coefficients determined for the fluidized bed and packed bed, respectively. Similar results were also obtained by Govindrajan et al. (1976).

ION EXCHANGE

Currently, semifluidized beds have been widely used in the field of ion exchange. Mobay Chemical Company, Asahi Chemical Company of Japan, Bayer AG (Germany) and its U.S. counter part, Lewatit Company, are advocating the use of semifluidized beds with ion exchange resins. This action

precipitated from the discovery that a fluidized bed, followed by a fixed bed, increased the efficiency of resin utilization by improving liquid-resin contact. The fixed bed acts as a polishing section, handles the ion leakage from the fluidized bed, and prevents elutriation of resin particles (Chementator, 1962; 1972; Lewatit, 1972). In addition to a higher resin utilization efficiency, semifluidization also minimizes the volume of regenerant and wash water needed, reduces pressure drop, and operates more consistently than the conventional fixed bed process.

ADSORPTION

Industrial applications of adsorption are conducted principally in columns of fixed, fluidized or moving sorbent beds. Fixed bed adsorbers are used in the majority of industrial applications due to the ease and reliability of operation of these units. Mass transfer rates are relatively higher in fixed beds, but pressure drop increases markedly as the particle size is decreased. Fluidized bed operation allows the use of relatively smaller particles and provides a lower pressure drop compared to packed beds.

A semifluidized bed adsorber employed to remove trace organics from aqueous solutions has been proposed by Mathews and Fan (1983a; 1983b). The adsorption column is operated as a semifluidized bed by fluidizing the bed initially and then compressing the fluid bed using a movable sieve plate. By positioning the sieve plate at various heights, different ratios of fluidized bed to packed bed heights can be obtained.

Mathews and Fan (1983a; 1983b) compared the performance of fluidized, semifluidized and packed beds for the adsorption of phenol from aqueous solutions onto activated carbon. It was reported that the same amount of adsorption can be obtained in semifluidized beds as in packed beds, but at a lower overall column pressure drop. Desorption was also found to be

achievable at essentially the same rate as in packed beds, again at a lower pressure drop. These studies indicate that solvent recovery operations involving adsorption-desorption operations can be more economically achieved in semifluidized beds. In their earlier work (Mathews and Fan, 1983a), adsorption studies were conducted using particles of a constant size at several fluidized to packed bed height ratios and flow rates, and those using a mixture of adsorbent particle sizes were also conducted by them in the later work (Mathews and Fan, 1983b).

The experimental breakthrough profiles for packed, semifluidized and fluidized beds and the pressure drops for packed and semifluidized beds presented by Mathews and Fan (1983a) are shown in Figures II-5 and II-6, respectively.

REACTOR

Some chemical or biochemical reactions can be carried out in the semifluidized bed with the definite advantage over the operation in the fluidized or fixed bed reactor.

Catalytic Chemical Reactor

The oxidation of benzene has been studied in the adiabatic semifluidized, fluidized and fixed bed reactors (Babu Rao and Doraiswamy, 1970). The catalyst used consisted of vanadium and molybdenum oxides on silica gel. Experiments were carried out at an inlet temperature of 380 °C and at several benzene-air ratios. A definite improvement has been observed when the oxidation was carried out in the semifluidized bed reactor by a comparison of the conversions obtained in three types of reactors.

Fixed Film Bioreactor

The use of the semifluidized bed as a bioreactor has been patented by Fan and Wen (1981; 1982). The idea was prompted by the development of fixed

film fluidized bed and fixed bed bioreactors (see, e.g., Besik, 1973; Jeris and Owens, 1975; Jewell et al., 1976; 1978; Scott and Hancher, 1976; Weber et al., 1970). In the fixed film fluidized bed bioreactor, the fluidizing particles, usually sand or activated carbon, are coated with viable microbial cells. This adhesion of microbes onto the enormous surface area provided by the fluidizing particles accounts for the high concentration of biomass. Jeris et al. (1977) reported the concentration of the mixed liquor volatile suspended solids (MLVSS) in the fluidized bed bioreactor to be between 8,000 and 40,000 mg/ℓ, an order of magnitude higher than that in a conventional suspended growth system. Thus, the residence time required for an equivalent task should be one to two orders of magnitude shorter in fixed film bioreactors than in conventional system (Besik, 1973; Jeris and Owens, 1975; Jewell et al., 1976; 1978). The use of semifluidized beds in place of fixed and fluidized beds in biological waste treatment should offer distinct advantages. Among these are the elimination of unstable bed expansion and elutriation of microbe coated particles in fluidized bed bioreactors, and the reduction of bed plugging by suspended solids experienced in fixed bed operations. Other possible advantages of using a semifluidized bed bioreactor in place of a fluidized bed bioreactor have been discussed by Fan and Hsu (1980).

The patent of the semifluidized bed bioreactor, proposed by Fan and Wen (1981), describes a method of carrying out a fluidized bed biological reaction for advanced treatment of wastewater in which the top of the bed is restrained with a media-retaining perforated plate to provide a smaller upper fixed bed portion and a larger fluidized bed portion therebeneath. The wastewater is subjected to initial treatment in the fluidized portion in the bed and to final treatment in the fixed portion of the bed. The

media-retaining perforated plate together with the filtering action of the fixed bed portion substantially prevents media loss and greatly reduces the bacteria loss. In addition, more complete removal of the organic contaminants is obtained without sacrificing the high-rate capacity of the fluidized bed.

The fixed bed section drives the reaction to completion because of the higher biomass concentration thereon. Viable bacteria cells escaping from the fluidized bed are trapped by the filtering and retention action of the fixed bed section. Further, the entering wastewater, which is high in contaminants, is first treated in a fluidized bed where intensive mixing occurs while the effluent from the fluidized portion, which is lean in contaminants, is next treated in a fixed bed where mixing is not intensive. This arrangement provides more efficient waste removal for given volume.

The method of this invention also facilitates cleaning of the reactor beds. Periodically, the treatment of the wasterwater is discontinued and the perforated plate is raised to a level out of contact with the bed when fully fluidized and above an outlet which is normally above the plate. Wash water is then passed upwardly through the bed at a velocity fully fluidizing the bed. The wash water is removed together with excess cellular material through the outlet, which is preferably provided in the side of the reactor. The fixed portion of the bed is broken up to release the cellular material including the bacterial floc. This may be promoted by the use of a mechanical agitator within within the fixed bed portion, such as a shearing mixer.

Another patent of the semifluidized bed bioreactor, also proposed by Fan and Wen (1982), suggests a new method for cleaning of the reactor beds. During the cleaning period, the perforated plate is raised to a level at which the bed can be fully fluidized but below a wash water outlet which

is normally above the plate. Wash water is then passed upwardly through the bed at a velocity fully fluidizing the bed. The wash water is removed together with excess cellular material through the outlet, which is preferably provided in the side of the reactor. The fixed portion of the bed is broken up to release the cellular material including the bacterial floc. This may be promoted by the use of concurrent gas introduction, such as combined flow of water and air under high turbulence.

POROUS MEDIA FILTER

The use of the semifluidized bed as a porous media filter was first patented by Wen and Fan (1979). The patent describes a method of operating a semifluidized bed filter in which the filter cake thickness is controlled by the fluidizing action of the porous media or grains instead of complicated mechanical devices such as cutting blades.

A conventional deep bed filter is composed of a fixed or packed bed of grains, usually sand or sand and anthracite. The suspended solids in the effluent are retained in the filter either by adhesion to the filter grains or by the straining process. The operation of a deep bed filter is typically characterized by shallow penetration, rendering much of the bed ineffective as a filtering medium. Furthermore, a layer of filtered solids will collect on the surface and within the first few layers of the grains, giving rise to a sharp increase in the pressure drop.

In a semifluidized-bed filter proposed by Wen and Fan (1979), the packed section of the bed functions as a deep bed filter whereas the fluidized section provides the turbulent scouring action in delaying clogging of the bed. The use of this apparatus for filtration purposes presented by them is shown in Figure II-7. Initially, the bed will be in a completely fixed configuration as the fluid stream containing suspended solids enters the bed.

The suspended solids upon entering the portion of the bed adjacent to the distributor zone will be unable to penetrate the bed to any great extent before being stopped by the grains. A "cake" of suspended solids will begin to be built up in this zone. The formation of the "cake" will produce an abrupt increase in the pressure drop. This rise in the pressure drop will activate a driving mechanism which will raise the upper sieve plate. The mechanical movement of the sieve plate in conjunction with the forces being exerted by the fluid stream will cause disruption of the formed "cake" of suspended solids into small fragments. Cake disruption will also be aided by the fluidized particles. Also the act of disruption of existent "cake" will cause more of the particles which are encased by the cake to become fluidized. Raising of the sieve plate will continue while small suspended solids in the stream are being trapped in the fixed bed. The amount of fixed bed will gradually decrease with successive disruption of the formed cakes. The filtration cycle is terminated when the suspended solids penetrate through the ever decreasing packed bed section.

A recent study of semifluidized-bed filters was presented by Hsu and Fan (1981; 1982), and Fan and Hsu (1984). In their work, the filtration cycle starts with the restraining plate in the proper position forming a semifluidized bed with 25%, 50% or 75% fluidization. Instead of forming the "cake" around the entrance section of the fixed bed, the suspended solids together with some of the fluidizing grains will begin to form a fixed bed in one side of the initially fluidized section, thus lowering the sharp increase in the pressure drop. With the filtration run, the newly-built fixed bed will extend gradually down to the distributor plate. Their results indicate that the filtration run duration can be increased up to 6 times that of a deep bed filter with the use of a semifluidized bed without sacrificing the filtrate quality.

HEAT TRANSFER

Purachander Rao and Kapathi (1969) studied the variation in the magnitude of wall heat-transfer coefficient with changes in the operating parameters in a semifluidized bed. Their experimental results show the values of the Nusselt number obtained for the semifluidized bed to be lower than those for the fixed bed and higher than those for the fluidized bed at a given Reynolds number. It was also shown that the values of the heat-transfer coefficient for the semifluidized bed can be calculated from the available correlations for the heat-transfer coefficients in packed beds and fluidized beds (see, e.g., Leva et al., 1948); the mean heat-transfer coefficient of the semifluidized bed was shown to be the sum of the heat-transfer coefficient of the packed and fluidized beds multiplied by the length fraction of the respective sections.

SEMIFLUIDIZATION WITHOUT RESTRAINING PLATE

The upper restraining plate is not essential to the formation of a semifluidized bed. A new type of solid-gas semifluidized bed contactor was proposed by Corella and Bilbao (1982). The contactor was constructed from a column with a considerable enlargement in the cross section of its upper zone. This enlargement in cross section caused a reduction in the gas velocity in that region. The inlet gas was introduced in such a way that the gas velocity was greater than the minimum fluidization velocity in the lower zone and lower than the minimum fluidization velocity in the upper zone, thus giving rise to the formation of a fluidized bed and a fixed bed in series. The fluid dynamics and bubble behavior in this type of contactor was also investigated.

SEMIFLUIDIZATION IN A GAS-LIQUID-SOLID SYSTEM

Fluidization in gas-liquid-solid systems where liquid is the continuous phase can be achieved with either cocurrent upflow of gas and liquid or

downflow of liquid counter to the upflow of gas. The downflowing, liquid-supported bed is termed an inverse gas-liquid-solid fluidized bed. A semi-fluidized bed is formed when a mass of fluidized particles is compressed from above with a porous restraining plate.

The hydrodynamics of inverse and cocurrent gas-liquid-solid semi-fluidization have been experimentally investigated by Chern *et al.* (1983; 1984). Their investigation was concerned with the behavior of the pressure drop, gas holdup, onset liquid velocity for semifluidization, and heights of the packed section and fluidized section.

NOMENCLATURE

A = cross-sectional area of the bed

C = correction factor defined in Eq. II-14

c_f = correction factor used in Eq. II-17

d_p = equivalent particle diameter

D_c = column diameter

g_c = conversion factor

G = mass flow rate of fluid per unit area of the empty bed

G_{mf} = onset velocity of fluidization

G_{osf} = onset velocity of semifluidization

G_{smf} = maximum semifluidization velocity

Ga = $d_p^3 \rho_f(\rho_s - \rho_f)g/\mu^2$, Galileo number

h = semifluidized bed height

h_o = height of initial static bed at the least dense condition

h_f = height of fully fluidized bed

h_{pa} = height of packed section in semifluidized bed

$k_{\ell m}$ = overall log mean mass-transfer coefficient

$(k_f)_{\ell m}$ = log mean mass-transfer coefficient of the fluidized section in the semifluidized bed

$(k_{pa})_{\ell m}$ = log mean mass-transfer coefficient of the packed section in the semifluidized bed

ΔP_t = overall pressure drop through semifluidized bed

$(\frac{\Delta P}{L})_f$ = pressure drop per unit length in the fluidized section of a semifluidized bed

$(\frac{\Delta P}{L})_{pa}$ = pressure drop per unit length in the packed section of a semifluidized bed

R = bed expansion ratio, semifluidized bed height divided by initial static bed height under the least dense condition

Re_{msf} = $(d_p G_{msf})/\mu$, Reynolds number at the maximum semifluidization velocity

Re_{osf} = $(d_p G_{osf})/\mu$, Reynolds number at the onset of semifluidization

Sf = $(W - W_{pa})/[(h - h_o)^3 \rho_s]$, semifluidization number

u = superficial fluid velocity

u_t = terminal velocity of the particle

u_{mf} = minimum fluidization velocity

W = total weight of particles

W_{pa} = weight of particles in the packed section of a semifluidized bed

X = weight fraction of particles in the packed section of a semifluidized bed

ε_o = porosity of the initial static bed under the least dense dense condition

ε_f = porosity of the fluidized section or the fully fluidized bed

ε_{pa} = porosity of the packed section

ϕ_s = sphericity of particles

μ = viscosity of fluid

Table II-1. Equations Describing the State of Semifluidization.

Reference	Form	System
Babu Rao and Doraiswamy (1967)	$\frac{G}{G_t} = \frac{4.62}{D^{-0.372}} (Ga)^{-0.15} (Sf)^{-0.186}$	gas-solid
Roy and Sarma (1973)	$\frac{G}{G_{msf}} = 0.684 \left(\frac{D_c}{d_p}\right)^{-0.11} \left(\frac{h_0}{D_c}\right)^{0.07} \left(\frac{\rho_s}{\rho_f}\right)^{-0.08} \left(\frac{h_{pa}}{h_0}\right)^{0.48} (R)^{0.42}$	liquid-spherical solids
	$\frac{G}{G_{msf}} = 0.945 \left(\frac{D_c}{d_p}\right)^{-0.15} \left(\frac{h_0}{D_c}\right)^{0.10} \left(\frac{\rho_s}{\rho_f}\right)^{-0.11} \left(\frac{h_{pa}}{h_0}\right)^{0.66} (R)^{0.57}$	liquid-non-spherical solids
Roy and Sen Gupta (1974)	$\frac{G}{G_{msf}} = 37.07 \left(\frac{D_c}{d_p}\right)^{0.23} \left(\frac{h_0}{D_c}\right)^{-0.89} \left(\frac{\rho_s}{\rho_f}\right)^{-0.11} \left(\frac{h_{pa}}{h_0}\right)^{0.32} (R)^{0.53}$	gas-spherical solids
	$\frac{G}{G_{msf}} = 35.16 \left(\frac{D_c}{d_p}\right)^{0.22} \left(\frac{h_0}{D_c}\right)^{-0.86} \left(\frac{\rho_s}{\rho_f}\right)^{-0.68} \left(\frac{h_{pa}}{h_0}\right)^{0.31} (R)^{0.51}$	gas-non-spherical solids
Roy (1971)	$\frac{G}{G_{msf}} = 4.80 \left(\frac{D_c}{d_p}\right)^{-0.18} \left(\frac{\rho_s}{\rho_f}\right)^{-0.32} \left(\frac{h_{pa}}{h_0}\right)^{0.59} (R)^{0.81}$	gas-solid
	$\frac{G}{G_{msf}} = 0.925 \left(\frac{D_c}{d_p}\right)^{-0.15} \left(\frac{\rho_s}{\rho_f}\right)^{-0.12} \left(\frac{h_{pa}}{h_0}\right)^{0.32} (R)^{0.43}$	liquid-solid

Table II-2. Equations for the Minimum Semifluidization Velocity.

Reference	Form	System
Roy and Sarma (1972)	$\frac{G_{osf}}{G_{mf}} = 1.875 \left(\frac{D_c}{d_p}\right)^{0.266} \left(\frac{\rho_s}{\rho_f}\right)^{-0.228} (R)^{0.585}$	liquid-spherical solids
	$\frac{G_{osf}}{G_{mf}} = 1.625 \left(\frac{D_c}{d_p}\right)^{0.266} \left(\frac{\rho_s}{\rho_f}\right)^{-0.228} (R)^{0.585}$	liquid-non-spherical solids
Roy (1971)	$\frac{G_{osf}}{G_{msf}} = 0.473 \left(\frac{D_c}{d_p}\right)^{-0.20} \left(\frac{\rho_s}{\rho_f}\right)^{0.17} (R)^{0.38}$	liquid-solid
	$\frac{G_{osf}}{G_{msf}} = 0.071 \left(\frac{D_c}{d_p}\right)^{-0.20} \left(\frac{\rho_s}{\rho_f}\right)^{0.17} (R)^{0.38}$	gas-solid
Roy and Sen Gupta (1975)	$\frac{G_{osf}}{G_{msf}} = 48.0 \left(\frac{D_c}{d_p}\right)^{0.38} \left(\frac{\rho_s}{\rho_f}\right)^{-1.05} (R)^{0.64}$	gas-solid

Table II-3. Equations for the Maximum Semifluidization Velocity.

Reference	Form	System
Roy and Sarma (1974a)	$\frac{G_{msf}}{G_{mf}} = 5.71\left(\frac{D_c}{d_p}\right)^{0.42}\left(\frac{\rho_s}{\rho_f}\right)^{-0.67}$	liquid-solid
Roy and Sen Gupta (1975)	$Re_{msf} = 1.15 \times 10^{-3}(Ga)^{0.676}$	gas-solid
Roy (1971)	$G_{msf} = \frac{1.85 \times 10^4 \, (d_p)^{0.65}[\rho_f(\rho_s - \rho_f)]^{0.55}}{\mu^{0.10}}$ $\left(\frac{kg}{hr\text{-}m^2}\right)$	liquid-solid
	$G_{msf} = \frac{1.37 \times 10^4 \, (d_p)^{0.65}[\rho_f(\rho_s - \rho_f)]^{0.55}}{\mu^{0.10}}$ $\left(\frac{kg}{hr\text{-}m^2}\right)$	gas-solid

Table II-4. Correlations for the Correction Factor.

Reference	Form	System
Roy and Sen Cupta (1973)	$C = 7.3 \times 10^{-3}[(\frac{D_c}{d_p})^{-0.53}(\frac{\rho_s}{\rho_f})^{1.18}(\frac{h_o}{D_c})^{-2.05}(R)^{1.56}(\frac{h_{pa}}{h_o})^{0.64}]$	gas-spherical solids
	$C = 1.95 \times 10^{-1}[(\frac{D_c}{d_p})^{-0.24}(\frac{\rho_s}{\rho_f})^{0.55}(\frac{h_o}{D_c})^{-0.94}(R)^{0.72}(\frac{h_{pa}}{h_o})^{0.24}]$	gas-non-spherical solids
Roy and Sarma (1974b)	$C = 16.7[(\frac{D_c}{d_p})^{-0.59}(\frac{\rho_s}{\rho_f})^{0.67}(\frac{h_o}{D_c})^{-0.43}(\frac{h_{pa}}{h_o})^{0.08}(R)^{0.08}]$	liquid-solids

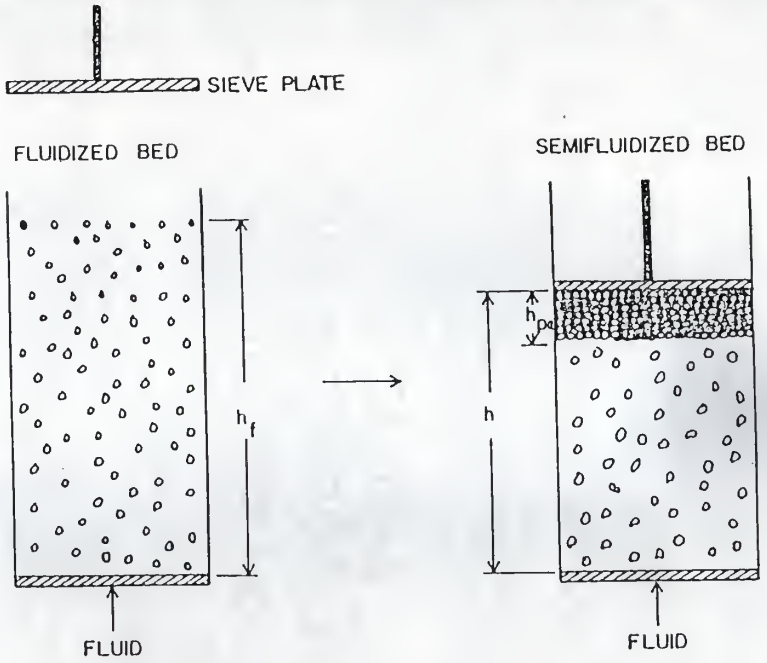

Figure II-1. Formation of a semifluidization bed ($\rho_s > \rho_f$).

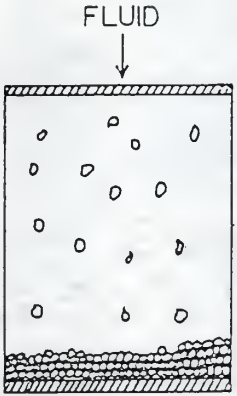

Figure II-2. A semifluidized bed in which the density of particles is less than that of the fluid.

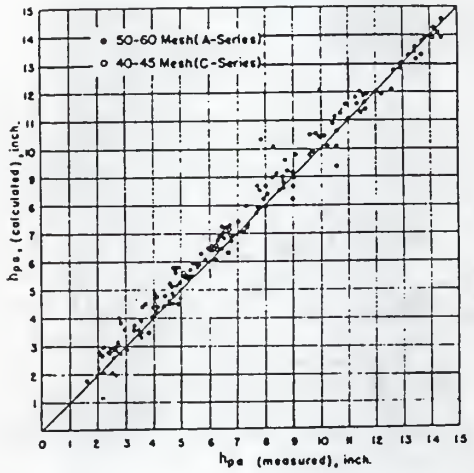

Figure II-3. Comparison of measured heights of packed section with theoretical values for 50x60 mesh and 40x45 mesh particles (Fan and Wen, 1961).

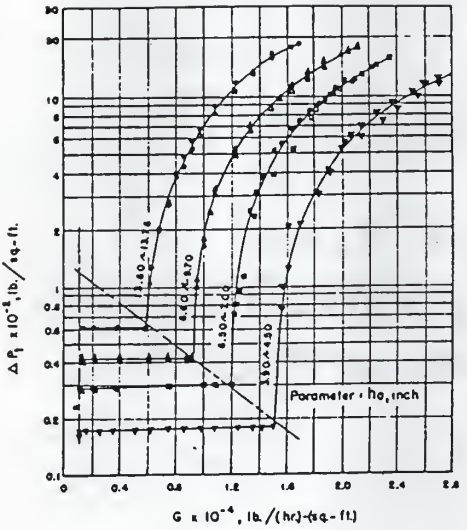

Figure II-4. Overall pressure drop through fully and semifluidized beds of 50x60 mesh particles (Fan and Wen, 1961).

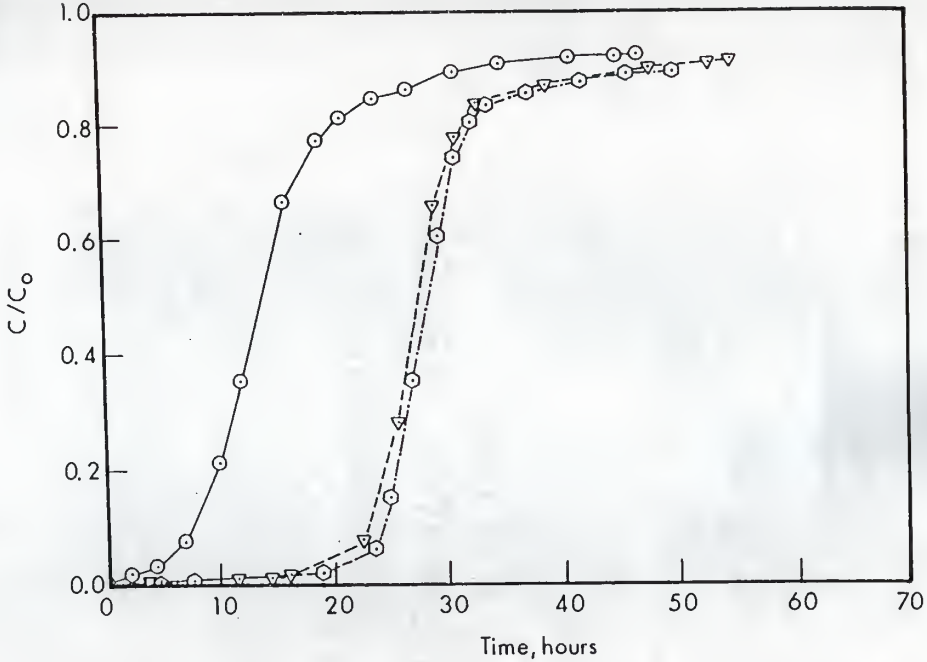

Figure II-5. Breakthrough profiles for (○) fluidized bed, (▽) semifluidized bed with 60% fluidization, (⬡) packed bed adsorbers: F-400 carbon (Mathews and Fan, 1983a).

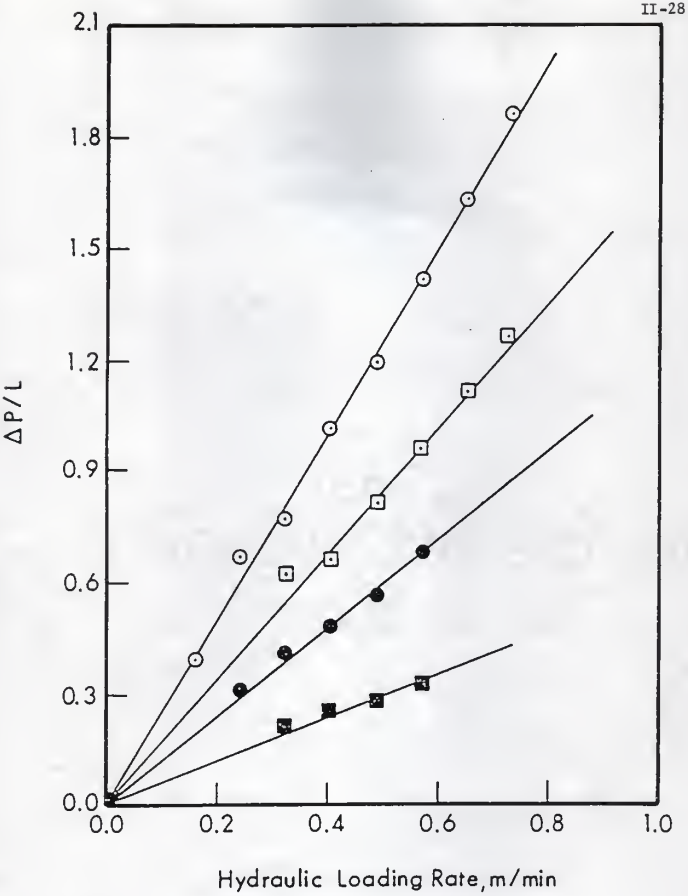

Figure II-6. Pressure drop data for F-400 carbon:
(○) packed bed and semifluidized beds with
(□) 25% fluidization, (●) 50% fluidization and
(■) 75% fluidization (Mathews and Fan, 1983a).

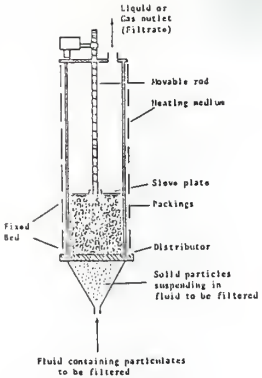

(a) Initial Stage.

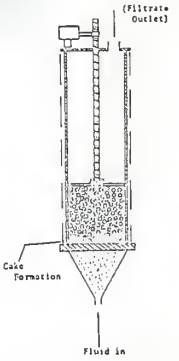

(b) Cake of Fines Start to Form at the Bottom of the Fixed Bed.

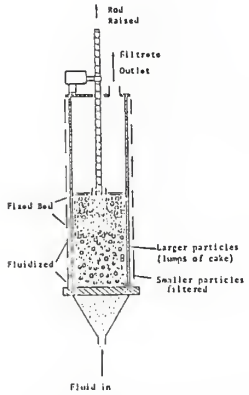

(c) Top Sieve Plate is Gradually Lifted and a Fluidized Bed is Formed Making Flow and Filtration Easier.

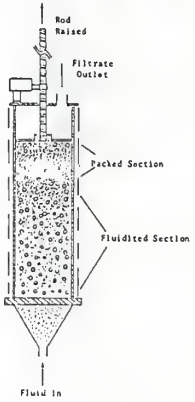

(d) Final Stage of Filtration. Fines Collected Can Be Purged by Lifting the Sieve Plate and Washed by Suitable Fluid.

Figure II-7. Use of the Semifluidized Bed for the Filtration Process (Wen and Fan, 1979)

CHAPTER III MASTER EQUATION AND ONE-STEP PROCESSES

Macroscopic physics deals with macroscopic quantities, such as the positions and velocities of bodies, electrical charges and currents, amounts or concentrations of chemical compounds. They obey macroscopic laws which can be derived from general principles such as conservation laws, together with some specific assumptions of phenomenological nature, for example, those of Fourier and Fick. The resultant differential equations are the macroscopic or deterministic equations; for instance, the rate equations for chemical reactions, the damped harmonic oscillator equation for a pendulum in air, the diffusion equation. They are approximate; in reality there are small deviations from them, which show up as fluctuations.

Of course, the fluctuations cannot be found exactly; that would be tantamount to solving the microscopic equations. In principle, all information is contained in the microscopic equations of motion of all particles, but it hardly needs saying that an exact solution of these equations is beyond human means. It is therefore necessary to embark upon a less ambitious program and develop a theory which goes beyond the macroscopic description in that it includes fluctuations, but shortcuts the connection with the microscopic equations. This is the so-called stochastic approach which views the macroscopic phenomena as the outcome of the collective behavior of numerous particles and includes fluctuations by means of the repeated randomness assumption; some call it the mesoscopic level of approach.

One popular stochastic approach starts out from the transition probability density, $\underline{P}$, and assumes that it obeys the Chapman-Kolmogorov equation with the type of

$$\frac{d}{dt}\underline{P} = \underline{P}\,\underline{U} \qquad \text{(III-1)}$$

where $\underline{U}$ is a matrix of intensities of transition.

MASTER EQUATION

The Master equation is an equivalent form of the Chapman-Kolmogorov equation for Markov processes, but it is easier to manipulate and more directly related to physical process to be modeled.

Consider a discrete set of states with labels, n, the Master equation can be written as (see, e.g., Van Kampen, 1981)

$$\frac{dp_n(t)}{dt} = \sum_{n'} [v_{n'n}\, p_{n'}(t) - v_{nn'}\, p_n(t)] \qquad \text{(III-2)}$$

where $v_{n'n}$ is the intensity of transition from state n' to state n. In this form the meaning becomes particularly clear. The Master equation is a gain-loss balance equation for the probability of being in state n; the first term in the right-hand side of this expression is the gain due to transitions from other states, and the second term is the loss due to transitions into other states.

As an example for demonstrating the usefulness of the Master equation, let's consider a simple one-step or birth-death process. For the birth-death process, it is assumed that in the state n; n = 0, 1, 2, ..., n_0, (see, e.g., Chiang, 1980)

1. The conditional probability that a birth event, which changes the state from n to (n+1), will occur during the time interval (t, t+Δt) is $\lambda_n\, t + o(\Delta t)$, where λ_n is the intensity of birth transition.
2. The conditional probability that a death event, which changes the state from n to (n-1), will occur during the time interval

$(t, t+\Delta t)$ is $\mu_n \, t + o(\Delta t)$, where μ_n is the intensity of death transition.

3. The conditional probability that more than one event will occur in this time interval is $o(\Delta t)$, where $o(\Delta t)$ signifies that

$$\lim_{\Delta t \to 0} \frac{o(\Delta t)}{\Delta t} = 0$$

Substituting the corresponding λ_n's and μ_n's into the Master equation, Eq. III-2, and neglecting the terms with the order of Δt, i.e., $o(\Delta t)$, give

$$\frac{dp_n(t)}{dt} = \lambda_{n-1} \, p_{n-1}(t) + \mu_{n+1} \, p_{n+1}(t) - (\lambda_n + \mu_n) \, p_n(t);$$

$$n = 1, 2, \ldots, (n_0-1), \qquad \text{(III-3)}$$

$$\frac{dp_0(t)}{dt} = -\lambda_0 \, p_0(t) + \mu_1 \, p_1(t) \qquad \text{(III-4)}$$

and

$$\frac{dp_{n_0}(t)}{dt} = \lambda_{n_0-1} \, p_{n_0-1}(t) - \mu_{n_0} \, p_{n_0}(t) \qquad \text{(III-5)}$$

For convenience, define μ_0, λ_{-1}, λ_{n_0} and μ_{n_0+1} to be zero. Equations III-3 through III-5 can therefore be combined as

$$\frac{dp_n(t)}{dt} = \lambda_{n-1} \, p_{n-1}(t) + \mu_{n+1} \, p_{n+1}(t) - (\lambda_n + \mu_n) \, p_n(t);$$

$$n = 0, 1, 2, \ldots, n_0 \qquad \text{(III-6)}$$

The solution of this expression gives the probability distribution of the process.

ONE-STEP PROCESSES AND ONE-STEP OPERATOR

The one-step or birth-death processes are a special class of stochastic processes, which occur in many applications and can be analyzed in some detail.

The one-step operator, $\mathbf{E}$, is defined by its effect on an arbitrary function f(n) as (see, e.g., Van Kampen, 1981)

$$\mathbf{E}f(n) = f(n+1) \text{ and } \mathbf{E}^{-1}f(n) = f(n-1) \tag{III-7}$$

If n ranges from $-\infty$ to $+\infty$, it is possible to regard $\mathbf{E}$ as an actual operator in function space, but if there are one or two boundaries, it is better to regard $\mathbf{E}$ simply as an abbreviating symbol. Most of its properties are immediately evident, but we note in particular

$$\sum_{n=0}^{n_0-1} g(n)\, \mathbf{E}f(n) = \sum_{n=1}^{n_0} f(n)\, \mathbf{E}^{-1}g(n) \tag{III-8}$$

for any pair of functions f and g. The difference in the limits of the summations in both members is inconvenient. Fortunately, it is often useful in practice, either because the terms are infinite (and f or g vanish sufficiently rapidly at infinity) or the missing terms may be added to the sum since they are zero. For instance, the term with n=0 may be added on the right-hand side of this equation if f(0) or g(-1) is defined to be zero. Therefore, this equation becomes

$$\sum_{n=0}^{n_0} g(n)\, \mathbf{E}f(n) = \sum_{n=0}^{n_0} f(n)\, \mathbf{E}^{-1}g(n) \tag{III-9}$$

Equation III-9 means that f and g in the summation can be exchanged by changing the sign of the one-step operator.

With the aid of the one-step operator, the Master equation for one-step processes, Eq. III-6, may be rewritten as

$$\frac{dp_n(t)}{dt} = (\mathbf{E} - 1)\, \mu_n\, p_n(t) + (\mathbf{E}^{-1} - 1)\, \lambda_n\, p_n(t); \tag{III-10}$$

$$n = 0,\ 1,\ 2, \ldots,\ n_0$$

With the aid of Eq. III-9, the mean and variance of n governed by this equation can be easily obtained. As an example, assume that intensities of transition take the form as

$$\lambda_n = \alpha(n_0 - n) \tag{III-11}$$

$$\mu_n = \beta n \tag{III-12}$$

Substitution of Eqs. III-11 and III-12 into Eq. III-10 yields

$$\frac{dp_n(t)}{dt} = (\mathbf{E} - 1)\beta n\, p_n(t) + (\mathbf{E}^{-1} - 1)\alpha(n_0 - n)\, p_n(t); \quad n = 0, 1, 2, \ldots, n_0 \tag{III-13}$$

Multiplying both sides of this expression by the respective n's and summing all resultant equations, we have

$$\frac{d\langle n\rangle}{dt} = \sum_{n=0}^{n_0} n(\mathbf{E} - 1)\beta n\, p_n(t) + \sum_{n=0}^{n_0} n(\mathbf{E}^{-1} - 1)\alpha(n_0 - n)\, p_n(t) \tag{III-14}$$

where $\langle n\rangle$ is the mean of n. From the property of the one-step operator as given in Eq. III-9, we see that Eq. III-14 is equivalent to

$$\frac{d\langle n\rangle}{dt} = \sum_{n=0}^{n_0} \beta n\, p_n(t)(\mathbf{E}^{-1} - 1)n + \sum_{n=0}^{n_0} \alpha(n_0 - n)\, p_n(t)(\mathbf{E} - 1)n \tag{III-15}$$

$$= -\beta\langle n\rangle + \alpha(n_0 - \langle n\rangle)$$

The solution of this equation subject to the initial condition,

$$\langle n\rangle = 0 \quad \text{at } t = 0,$$

gives

$$\langle n\rangle = \frac{\alpha n_0}{\alpha+\beta}\left[1 - e^{-(\alpha+\beta)t}\right] \tag{III-16}$$

The variance of n, $\langle\langle n \rangle\rangle$, defined as

$$\langle\langle n \rangle\rangle = \langle n^2 \rangle - \langle n \rangle^2$$

is also of interest. Multiplying both sides of Eq. III-13 by the respective n^2's and summing all resultant equations, we obtain

$$\frac{d\langle n^2 \rangle}{dt} = \sum_{n=0}^{n_0} n^2 (E - 1) \beta n \, p_n(t) + \sum_{n=0}^{n_0} n^2 (E^{-1} - 1) \alpha (n_0 - n) \, p_n(t) \qquad \text{(III-17)}$$

From Eq. III-9, the above equation reduces to

$$\frac{d\langle n^2 \rangle}{dt} = \sum_{n=0}^{n_0} \beta n \, p_n(t)(E^{-1} - 1)n^2 + \sum_{n=0}^{n_0} \alpha (n_0 - n) \, p_n(t)(E - 1)n^2$$

$$= -2(\alpha+\beta)\langle n^2 \rangle + [(2n_0 - 1)\alpha + \beta]\langle n \rangle + \alpha n_0 \qquad \text{(III-18)}$$

The solution of this expression subject to the initial condition,

$$\langle n^2 \rangle = 0 \quad \text{at } t = 0,$$

yields the variance, $\langle\langle n \rangle\rangle$, as

$$\langle\langle n \rangle\rangle = \frac{\alpha n_0}{\alpha+\beta} [1 - e^{-(\alpha+\beta)t}] \{1 - \frac{\alpha[1 - e^{-(\alpha+\beta)t}]}{\alpha+\beta}\} \qquad \text{(III-19)}$$

OTHER APPLICATION OF THE ONE-STEP OPERATOR TECHNIQUE

The one-step operator technique is not restricted to solve the linear, one-step processes; it can be used elsewhere. As an example consider a simple polymerization system (Fan, 1983). Let M be the monomer, $P_j^{\cdot}$ be the free radical with j chain length, P_j^{*} be the polymer with j chain length. The polymerization mechanism is assumed to be

$$M \xrightarrow{k_i} P_1^{\cdot} \qquad \text{; initiation}$$

$$P_j^{\cdot} + M \xrightarrow{k_p} P_{j+1}^{\cdot} \qquad \text{; propagation}$$

$$P_j^{\cdot} + M \xrightarrow{k_m} P_{j+1}^{*} \qquad \text{; termination}$$

The corresponding batch kinetic equations are

$$\frac{d[M]}{dt} = -k_i[M] - (k_p+k_m)[M][P_T^{\cdot}] \tag{III-20}$$

$$\frac{d[P_1^{\cdot}]}{dt} = k_i[M] - (k_p+k_m)[M][P_1^{\cdot}] \tag{III-21}$$

$$\frac{d[P_j^{\cdot}]}{dt} = k_p[M][P_{j-1}^{\cdot}] - (k_p+k_m)[P_j^{\cdot}] \quad ; \; j \geq 2 \tag{III-22}$$

and

$$\frac{d[P_j^{*}]}{dt} = k_m[M][P_{j-1}^{\cdot}] \quad ; \; j \geq 2 \tag{III-23}$$

where $[P_T^{\cdot}]$ is defined as

$$[P_T^{\cdot}] = \sum_{j=1}^{\infty} [P_j^{\cdot}]$$

By means of the eigenzeit transformation which defines

$$d\tau = [M]\, dt \,, \tag{III-24}$$

Eqs. III-20 through III-23 can be transformed, respectively, as

$$\frac{d[M]}{d\tau} = -k_i - (k_p+k_m)[P_T^{\cdot}] \tag{III-25}$$

$$\frac{d[P_1^{\cdot}]}{d\tau} = k_i - (k_p+k_m)[P_1^{\cdot}] \tag{III-26}$$

$$\frac{d[P_j^{\cdot}]}{d\tau} = k_p[P_{j-1}^{\cdot}] - (k_p+k_m)[P_j^{\cdot}] \quad ; \; j \geq 2 \tag{III-27}$$

and

$$\frac{d[P_j^{*}]}{d\tau} = k_m[P_{j-1}^{\cdot}] \quad ; \; j \geq 2 \tag{III-28}$$

Notice that these are the linear equations.

Addition of Eqs. III-26 and III-27 leads to

$$\frac{d[P_T^{\cdot}]}{d\tau} = k_i - k_m[P_T^{\cdot}] \tag{III-29}$$

The solution of this equation subject to the initial condition

$$[P_T^{\cdot}] = 0 \quad \text{at } \tau = 0,$$

yields

$$[P_T^{\cdot}] = \frac{k_i}{k_m}(1 - e^{-k_m\tau}) \tag{III-30}$$

The mean and variance of the chain length of polymer can be related to the first and second moments of the MWD (molecular weight distribution). The general expression is

$$E[j^n] = \sum_{j=1}^{\infty} j^n\{[P_j^{\cdot}] + [P_j^{*}]\} \tag{III-31}$$

where $E[j]$ is the first moment and $E[j^2]$ is the second moment. The technique used in the preceding section can also be employed here to obtain the moments defined by Eq. III-31. Multiplying both sides of Eqs. III-26 through III-28 by respective j's and summing all resultant equations result in

$$\frac{dE[j]}{d\tau} = k_i - (k_p+k_m) \sum_{j=1}^{\infty} j[P_j^*] + (k_p+k_m) \sum_{j=1}^{\infty} j[P_{j-1}^*] \quad \text{(III-32)}$$

Introducing the one-step operator, $\mathbf{E}$, this expression reduces to

$$\frac{dE[j]}{d\tau} = k_i - (k_p+k_m) \sum_{j=1}^{\infty} j(1 - \mathbf{E}^{-1})[P_j^*] \quad \text{(III-33)}$$

From Eq. III-9, we see that the above equation is equivalent to

$$\begin{aligned} \frac{dE[j]}{d\tau} &= k_i - (k_p+k_m) \sum_{j=1}^{\infty} [P_j^*](1 - \mathbf{E})j \\ &= k_i + (k_p+k_m) \sum_{j=1}^{\infty} [P_j^*] \\ &= k_i + (k_p+k_m)[P_T^*] \end{aligned} \quad \text{(III-34)}$$

Substituting Eq. III-30 into Eq. III-34, the solution of the resultant equation subject to the initial condition

$$E[j] = 0 \quad \text{at } \tau = 0,$$

gives

$$E[j] = \left[\frac{k_i(k_p+2k_m)}{k_m}\right]\tau + \left[\frac{k_i(k_p+k_m)}{k_m^2}\right] e^{-k_m\tau} - \frac{k_i(k_p+k_m)}{k_m^2} \quad \text{(III-35)}$$

The mean is equal to the first moment.

The derivation of the second moment follows the similar procedure. Multiplying both sides of Eqs. III-26 through III-28 by respective j^2's and summing all resultant equations give

$$\frac{dE[j^2]}{d\tau} = k_i - (k_p+k_m)\sum_{j=1}^{\infty} j^2[P_j^*] + (k_p+k_m)\sum_{j=1}^{\infty} j^2[P_{j-1}^*]$$

$$= k_i - (k_p+k_m)\sum_{j=1}^{\infty} j^2(1 - E^{-1})[P_j^*]$$

$$= k_i - (k_p+k_m)\sum_{j=1}^{\infty} [P_j^*](1 - E)j^2$$

$$= k_i + (k_p+k_m)\sum_{j=1}^{\infty} [P_j^*](2j+1)$$

$$= k_i + (k_p+k_m)\{2\sum_{j=1}^{\infty} j[P_j^*] + [P_T^*]\} \qquad \text{(III-36)}$$

To solve the above equation, $\sum_{j=1}^{\infty} j[P_j^*]$ has to be found. Multiplying both sides of Eqs. III-26 and III-27 by respective j's and summing all the resultant equations result in

$$\frac{d\sum_{j=1}^{\infty} j[P_j^*]}{d\tau} = k_i - (k_p+k_m)\sum_{j=1}^{\infty} j[P_j^*] + k_p\sum_{j=1}^{\infty} j[P_{j-1}^*]$$

$$= k_i - k_p[P_T^*] - k_m\sum_{j=1}^{\infty} j[P_j^*] \qquad \text{(III-37)}$$

Substituting the solution of this equation and Eq. III-30 into Eq. III-36, the solution of the resultant equation subject to the initial condition

$$E[j^2] = 0 \quad \text{at } \tau = 0,$$

yield

$$E[j^2] = [\frac{2k_i k_p(k_p+k_m)}{k_m^2}]\tau e^{-k_m\tau} + [\frac{k_i(k_p+k_m)(4k_p+3k_m)}{k_m^3}]e^{-k_m\tau} + [\frac{k_i(k_p+k_m)(2k_p+3k_m) + k_m^2}{k_m^2}]\tau - \frac{k_i(k_p+k_m)(4k_p+3k_m)}{k_m^3} \qquad \text{(III-38)}$$

The variance can be calculated from the first and second moments.

CHAPTER IV ANALYSIS OF DEEP BED FILTRATION DATA: Modeling as a Birth-Death Process

In this chapter, a fairly general stochastic model, namely, the linear, birth-death process, is employed in conjunction with the Carman-Kozeny equation to simulate the performance of the deep bed filter in terms of the pressure drop dynamics under a constant flow condition. The model takes into account both blockage of pores by suspended particles and scouring of deposited particles; the entire bed is assumed to be spatially lumped. In spite of this simplicity, the model appears to represent the majority of the available experimental data.

MODEL

A stochastic birth-death model was first employed by Litwiniszyn (1966) to describe pore blockage and scouring in a filtration process. By incorporating the Carman-Kozeny equation, this model has been developed to simulate the pressure drop dynamics through the deep bed filter under the constant flow condition.

Birth-Death Process

A stochastic process $\{N(t)\}$ is a family of random variables describing an empirical process whose development is governed by probabilistic laws. In considering the filtration process in a deep packed bed as a stochastic process, the number of blocked pores in a unit volume of the bed at time t, $N(t)$, can be taken as the random variable (Litwiniszyn, 1966); a specific value of $N(t)$ will be denoted by n. Given $N(t) = n$ it is assumed that for the birth-death process (Chiang, 1980),

1. The conditional probability that a birth event will occur, i.e., that an open pore will be blocked during the time interval

$(t, t + \Delta t)$, is $\lambda_n \Delta t + o(\Delta t)$, where λ_n is a function of n.

2. The conditional probability that a death event will occur, i.e., that a blocked pore will be scoured during the time interval $(t, t + \Delta t)$, is $\mu_n \Delta t + o(\Delta t)$, where μ_n is a function of n.

3. The conditional probability that more than one event will occur in this time interval is $o(\Delta t)$, where $o(\Delta t)$ signifies that

$$\lim_{\Delta t \to 0} \frac{o(\Delta t)}{\Delta t} = 0$$

Obviously the probability of no change in the time interval $(t, t + \Delta t)$ is $[1 - \lambda_n \Delta t - \mu_n \Delta t - o(\Delta t)]$. The probability that exactly n pores are blocked at the moment t will be denoted as $p_n(t) = \Pr[N(t) = n]$; $n = 0, 1, \ldots$ For the two adjacent intervals $(0, t)$ and $(t, t+\Delta t)$, the occurrence of exactly n pores being blocked during the time interval $(0, t+\Delta t)$ can be realized in the following mutually exclusive ways.

1. All n pores are blocked in $(0, t)$, and none in $(t, t+\Delta t)$, with probability $p_n(t)[1 - \lambda_n \Delta t - \mu_n \Delta t + o(\Delta t)]$.

2. Exactly $(n-1)$ pores are blocked in $(0, t)$, and one pore is blocked in $(t, t+\Delta t)$, with probability $p_{n-1}(t)[\lambda_{n-1} \Delta t + o(\Delta t)]$.

3. Exactly $(n+1)$ pores are blocked in $(0, t)$, and one pore is scoured in $(t, t+\Delta t)$, with probability $p_{n+1}(t)[\mu_{n+1} \Delta t + o(\Delta t)]$.

4. Exactly $(n-j)$ pores are blocked in $(0, t)$, and j pores are blocked in $(t, t+\Delta t)$, where $2 \leq j \leq n$, with probability $o(\Delta t)$.

5. Exactly $(n+j)$ pores are blocked in $(0, t)$, and j pores are scoured in $(t, t+\Delta t)$, where $2 \leq j \leq (n_0-n)$, with probability $o(\Delta t)$.

Considering all these possibilities and combining all quantities of $o(\Delta t)$ give

$$p_n(t+\Delta t) = p_n(t)[1 - \lambda_n \Delta t - \mu_n \Delta t] + p_{n-1}(t)\lambda_{n-1}\Delta t + p_{n+1}(t)\mu_{n+1}\Delta t + o(\Delta t), \quad n \geq 1 \tag{IV-1}$$

and

$$p_0(t+\Delta t) = p_0(t)[1 - \lambda_0 \Delta t] + p_1(t)\mu_1 \Delta t + o(\Delta t) \tag{IV-2}$$

Rearranging these equations and taking the limit as $\Delta t \to 0$ yield the following Master equations (see APPENDIX A)

$$\frac{dp_n(t)}{dt} = \lambda_{n-1}p_{n-1}(t) - (\lambda_n + \mu_n)p_n(t) + \mu_{n+1}p_{n+1}(t), \quad n \geq 1 \tag{IV-3}$$

and

$$\frac{dp_0(t)}{dt} = -\lambda_0 p_0(t) + \mu_1 p_1(t) \tag{IV-4}$$

Litwiniszyn (1966) has assumed that the intensities of transition, λ_n and μ_n, take the form

$$\lambda_n = \alpha(n_0 - n), \quad n = 0,1,2,\ldots,n_0 \tag{IV-5}$$

$$\mu_n = \beta n \tag{IV-6}$$

where n_0 is the total number of open pores susceptible to blockage at the moment $t = 0$, and α and β are the proportionality constants. The constants α and β may be called the blockage and scouring constants, respectively. Equation IV-5 implies that the rate of pore blockage is proportional to the number of open pores, and Eq. IV-6 implies that the rate of pore scouring is proportional to the number of blocked pores. Introducing Eqs.

IV-5 and IV-6 into Eqs. IV-3 and IV-4, respectively, the following equations are obtained;

$$\frac{dp_n(t)}{dt} = \alpha[n_0 - (n-1)]p_{n-1}(t) - [\alpha(n_0 - n) + \beta n]p_n(t) + \beta(n+1)p_{n+1}(t), \quad n \geq 1 \tag{IV-7}$$

and

$$\frac{dp_0(t)}{dt} = -\alpha n_0 p_0(t) + \beta p_1(t) \tag{IV-8}$$

At the start of the filtration process, all pores are open; thus, the initial conditions to Eqs. IV-7 and IV-8 may be expressed as

$$p_n(0) = 0 \qquad n = 1,2,\ldots,n_0 \tag{IV-9}$$

$$p_0(0) = 1$$

Solution of Eqs. IV-7 and IV-8, subject to initial conditions, Eq. IV-9, yields the distribution of the probabilities. However, such information has limited physical significance. Instead, the mean number of blocked pores at a given moment t, namely, E[N(t)], is determined; it is defined as

$$E[N(t)] = \sum_{n=0}^{n_0} n p_n(t) \tag{IV-10}$$

To evaluate this value, it is unnecessary to solve Eqs. IV-7 and IV-8. We can use the method of probability generating function defined as

$$G(s,t) = \sum_{n=0}^{n_0} s^n p_n(t) \tag{IV-11}$$

Multiplying both sides of Eq. IV-7 by the respective s^n's and Eq. IV-8 by s^0, and summing all resultant equations, the following expression is obtained upon rearrangement (see, e.g., Chiang, 1980; also see APPENDIX B).

$$\frac{\partial G(s,t)}{\partial t} = \frac{\partial G(s,t)}{\partial s}[\beta + (\alpha - \beta)s - \alpha s^2] + G(s,t)[\alpha n_0(s - 1)] \tag{IV-12}$$

The corresponding initial and boundary conditions are

$$G(s,0) = 1 \tag{IV-13}$$

$$G(1,t) = 1 \tag{IV-14}$$

The solution of Eq. IV-12 is

$$G(s,t) = \left[\frac{(\alpha s + \beta) - \alpha(s - 1)e^{-(\alpha + \beta)t}}{\alpha + \beta}\right]^{n_0} \tag{IV-15}$$

Examination of Eqs. IV-10 and IV-11 shows that

$$E[N(t)] = \left.\frac{\partial G(s,t)}{\partial s}\right|_{s = 1} \tag{IV-16}$$

Substitution of Eq. IV-15 into Eq. IV-16 gives

$$E[N(t)] = \alpha n_0\left[\frac{1 - e^{-(\alpha + \beta)t}}{\alpha + \beta}\right] \tag{IV-17}$$

The variance of the random variable, Var[N(t)], takes the form of

$$Var[N(t)] = \left\{\frac{\partial^2 G(s,t)}{\partial s^2} + \frac{\partial G(s,t)}{\partial s} - \left[\frac{\partial G(s,t)}{\partial s}\right]^2\right\}\Bigg|_{s = 1}$$

$$= \frac{\alpha n_0}{\alpha + \beta}[1 - e^{-(\alpha + \beta)t}]\left\{1 - \frac{\alpha[1 - e^{-(\alpha + \beta)t}]}{\alpha + \beta}\right\} \tag{IV-18}$$

Constant Flow Filtration

To utilize the results obtained in the preceding subsection, it is necessary to relate the mean of the number of blocked pores to measurable variables. In the present modeling, it is assumed that the "pore" refers to finite but small space within the filter bed, which is susceptible to the deposition of solid particles. Each "pore" may or may not have the clearly defined boundary, and the space surrounded by several grains or particles may be composed of more than one pore. Once occupied by the particles deposited from the flow, thus preventing additional suspension to pass through it, the pore is said to be "blocked" without regard to the nature of deposition. It is also assumed that all pores have the same radius, r. For the constant flow filtration, denoting the linear velocity of the suspension flowing through the pores at the moment t as v(t) and the linear velocity at the onset of filtration as v_0, we have

$$n_0 \pi r^2 v_0 = \{n_0 - E[N(t)]\} \pi r^2 v(t) \tag{IV-19}$$

or, upon rearrangement,

$$v(t) = \frac{n_0}{n_0 - E[N(t)]} v_0 \tag{IV-20}$$

The pressure drop for laminar flow through a small section of the packed bed can be adequately described by the Carman-Kozeny equation (see, e.g., Zenz and Othmer, 1960)

$$-\delta P = 150 \frac{(1-\varepsilon)^2}{\varepsilon^3} \frac{\mu u}{d_p^2} \delta z \tag{IV-21}$$

The superficial velocity, u, in this equation can be expressed in terms of linear velocity, v, as

$$u = \varepsilon v \tag{IV-22}$$

Substitution of Eq. IV-22 into Eq. IV-21 yields

$$-\delta P = 150 \left(\frac{1-\varepsilon}{\varepsilon}\right)^2 \frac{\mu v}{d_p^2} \delta z \tag{IV-23}$$

Thus, the pressure drop through the entire packed bed becomes

$$-\Delta P = \int_0^L 150 \left(\frac{1-\varepsilon}{\varepsilon}\right)^2 \frac{\mu v}{d_p^2} dz \tag{IV-24}$$

For simplicity, the entire bed is assumed to be spatially uniform and single set of values for ε and v is employed to represent the pressure drop characteristics of the entire bed. Therefore, Eq. IV-24 reduces to

$$-\frac{\Delta P}{L} = 150 \left(\frac{1-\varepsilon}{\varepsilon}\right)^2 \frac{\mu v}{d_p^2} \tag{IV-25}$$

Note that the change of fluid velocity in the pores during a filtration run is expressed by Eq. IV-20. Thus, substituting Eq. IV-20 into Eq. IV-25 results in (see, e.g., Hsu and Fan, 1984).

$$-\frac{\Delta P(t)}{L} = 150 \left(\frac{1-\varepsilon}{\varepsilon}\right)^2 \frac{\mu v_0}{d_p^2} \left\{\frac{n_0}{n_0 - E[N(t)]}\right\} \tag{IV-26}$$

The expression for $E[N(t)]$, Eq. IV-17, can now be substituted into the above equation to obtain

$$-\frac{\Delta P(t)}{L} = 150 \left(\frac{1-\varepsilon}{\varepsilon}\right)^2 \frac{\mu v_0}{d_p^2} \left[\frac{\alpha + \beta}{\beta + \alpha e^{-(\alpha+\beta)t}}\right] \tag{IV-27}$$

For simplicity, we attribute an increase in the pressure drop only to the increase in the linear velocity of flow; this is equivalent to assuming that the porosity term, $[(1-\varepsilon)/\varepsilon]^2$, in Eq. IV-27 remains unchanged. Equation IV-27, therefore, reduces to

$$-\frac{\Delta P(t)}{L} = \left(-\frac{\Delta P}{L}\right)_0 \left[\frac{\alpha + \beta}{\beta + \alpha e^{-(\alpha + \beta)t}}\right] \qquad \text{(IV-28)}$$

where $(-\Delta P/L)_0$ is a constant and reflects the initial pressure drop per unit length of the filter bed.

COMPARISON OF THE MODEL WITH THE EXPERIMENTAL DATA AND DISCUSSION

The experimental results by previous researchers (Eliassen, 1935; Ives, 1961; Rimer, 1968; Deb, 1969; Huang, 1972) have been analyzed based on the present model; the results are shown in Figures IV-1 through IV-11.

The values of α and β in the model equation, Eq. IV-28, have been determined by the following procedure. The preliminary value of α is first determined from the initial slope of the time dependent pressure drop curve. With this value in hand, the preliminary value of β is estimated from the entire set of the data. Finally, the values of α and β are recovered by using this set of preliminary values as a starting point of search for the minimum of sum of squares residual by means of a non-linear optimizing technique (see, e.g., Marquardt, 1963). The initial pressure drop per unit bed depth, $(-\Delta P/L)_0$, which is also contained in the equation, can be estimated by the Carman-Kozeny equation or, more accurately, can be measured at the onset of the experimental run. The measured values of the initial pressure drop have been used in the present work.

Deb (1969) conducted his experiment by allowing turbid water to flow through a deep sand bed with uniform grain size of 0.647 mm at a constant filtration rate. The concentration of Fuller's earth particles in turbid water was 45×10^{-4} vol%. The pressure drop were measured at various depths during the filtration run without disturbing the normal operation. The present model, in which the scouring effect is negligible, giving rise to

a pure birth process, appears to adequately explain the increase in the pressure drop (see Figure IV-1). The negligible scouring effect seemed to be due to the short operating time as well as the diluteness of influent concentration, for which the deposit accumulation within the bed was small so that the blockage mechanism became far more dominant than the scouring mechanism.

A rapid filter with a depth of 60 cm was used by Eliassen (1935) to remove suspended hydrous ferric floc particles from the water. The pressure drop reading was taken every ten hours; the results are shown in Figure IV-2. Each experimental run lasted sufficiently long to retain a large amount of deposits in the filter. Under such conditions, a significant scouring effect probably took place.

The present model shows a good fit with the data of Huang (1972), which appear in Figures IV-3 through IV-5; the only exception is run B-5-III in Figure IV-5. This deviation was probably caused by the shallow penetration of suspended particles along the bed. Huang measured the concentration of suspended particles at different depths of the bed under various flow rates as illustrated in Figure IV-6. Notice that when the flow rate was 4.9 m/h, the filter medium beyond a depth of 35 cm did not contribute to the further removal of suspended particles, rendering the lower 15.8 cm of the bed unutilized. Thus, we can postulate that the present model is only applicable to the first 35 cm of the bed, as illustrated in Figure IV-5.

The results of Rimer (1968) are shown in Figure IV-7 and IV-8, and those of Ives (1961) in Figure IV-9. The present model agrees well with the data of Rimer from the entire bed depth. However, the model can describe Ives' data only from the first portion of the bed. This is indicative of the shallow penetration discussed in the preceding paragraph. Ives measured

in detail the specific deposit as a function of time and bed positions by means of the radioactive algae technique and determined conclusively that the penetration was indeed shallow.

The data of Deb and Rimer show that the operating times in their experiments were roughly equal (see Figures IV-1 and IV-7). However, the pressure drop through Deb's filter was modeled as a pure birth process but that through Rimer's filters was modeled as the birth-death process, for which the scouring effect was taken into account. The need to incorporate the scouring effect in the model for Rimer's data can be justified in the light of measurement of effluent concentration. In Rimer's filter, the effluent concentration continued to increase with time as shown in Figure IV-10. This is indicative of the scouring phenomenon; recall that the scouring rate increase with an increase in the deposit accumulation as can be seen in Eq. IV-6. In contrast, Deb's effluent concentration data illustrated in Figure IV-11 do not exhibit such a monotonically increasing trend.

The present model equation, Eq. IV-28, contains two adjustable parameters, α and β. These two parameters are functions of many factors, among which are the size distributions of collector grains and suspended particles, properties of the liquid and involved surfaces, filtration rate, bed porosity, and suspension concentration.

The parameters, α and β, increase with an increase in the filtration rate as shown in Figure IV-4. A plausible reason is that at the same influent concentration, the filter with a higher flow rate is likely to retain more solid particles than that with a lower flow rate within the same time period.

The parameters are functions of the suspension concentration which decreases along the bed during a filtration run. Thus, these two parameters might also decrease with the bed depth as indicated in Figure IV-7. In contrast, α decreases monotonically with the bed depth while β varies irregularly as indicated in Figure IV-8. Notice that the bed in Figure IV-7 is of unisized sand while the bed in Figure IV-8 is of multimedia (anthracite, sand, and garnet). It appears that α depends strongly on the suspension concentration while β depends weakly on the suspension concentration; the latter is also highly dependent on the type of bed grains and bed structure, i.e., the spatial distribution of these grains.

The stochastic birth-death model considered here is assumed to be time-homogeneous, in which both parameters, α and β, are not functions of time because of the constant filtration rate and suspension concentration., i.e., the constant operating conditions. For the case where the filtration rate or suspension concentration varies with time during a filtration run, the birth-death model is still applicable, but both parameters will be functions of time; in other words, the process described by the model is the time-heterogeneous process.

NOMENCLATURE

d_a = diameter of the anthracite

d_p = average diameter of the grain particles

d_s = diameter of the sand

$E[N(t)]$ = mean value of the random variable $N(t)$

$G(s,t)$ = probability generating function

L = depth of the bed

n = number of pores clogged per unit volume of the bed

n_0 = total number of open pores susceptible to blockage per unit volume of the bed

$N(t)$ = a random variable which describes the number of blocked pores per unit volume of the bed at the moment t

$p_n(t)$ = probability that exactly n pores are blocked at the moment t

$(-\Delta P/L)$ = pressure drop per unit length of the filter

R^2 = fraction of variation

r = radius of pore

s = variable of the probability generating function

t = time

u = superficial velocity

v = linear velocity

$Var[N(t)]$ = variance of the random variable $N(t)$

z = height along the filter bed

λ_n = intensity of the birth transition

μ_n = intensity of the death transition

α = proportionality constant defined in Eq. IV-5, the blockage constant

β = proportionality constant defined in Eq. IV-6, the scouring constant

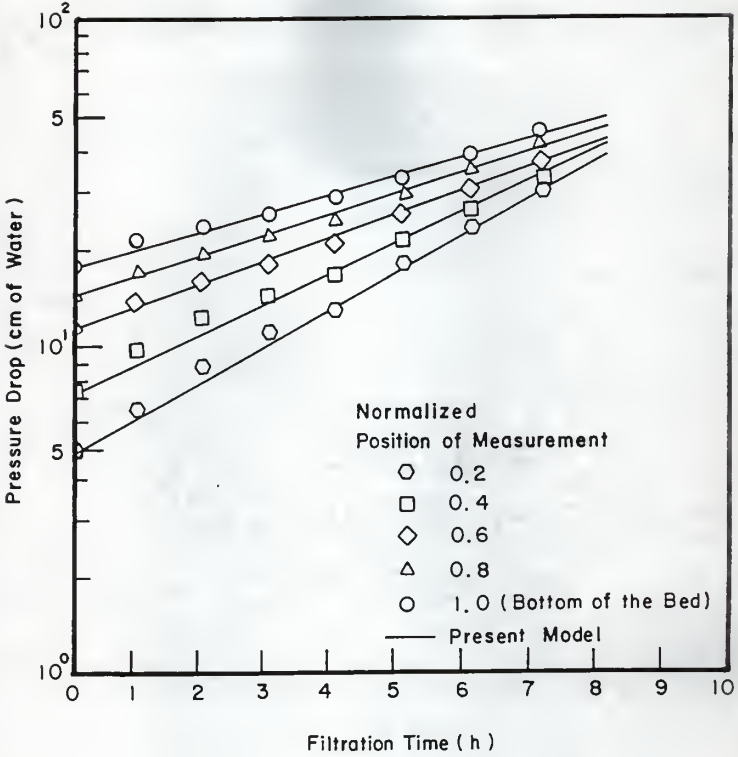

Figure IV-1. Fitting the present model to Deb's data (1969): sand size (0.0647 cm), bed depth (61 cm), flow rate (4.9 m/h), Fuller's earth suspension (45×10^{-4} vol%).

Run I; position 0.2 (α = 0.261 h^{-1}, β = 0.000 h^{-1}, R^2 = 0.993),
position 0.4 (α = 0.217 h^{-1}, β = 0.000 h^{-1}, R^2 = 0.992),
position 0.6 (α = 0.164 h^{-1}, β = 0.000 h^{-1}, R^2 = 0.990),
position 0.8 (α = 0.146 h^{-1}, β = 0.000 h^{-1}, R^2 = 0.986),
position 1.0 (α = 0.130 h^{-1}, β = 0.000 h^{-1}, R^2 = 0.987).

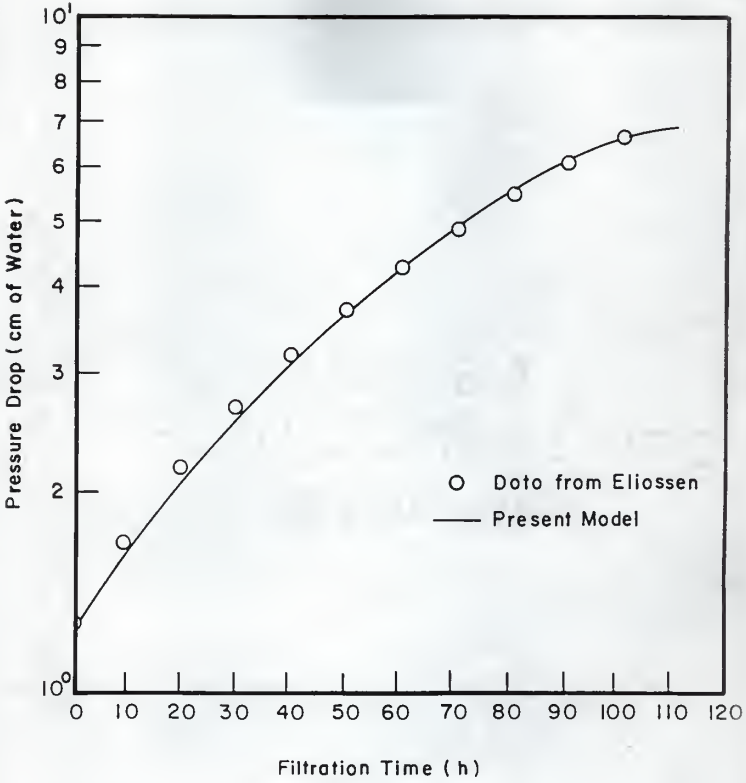

Figure IV-2. Fitting the present model to Eliassen's data (1935): sand size (0.061 cm), bed depth (60 cm), flow rate (4.9 m/h), hydrous ferric oxide floc suspension (concentration, 7.3×10^{-4} wt%).

Run 6; $\alpha = 0.0252\ h^{-1}$, $\beta = 0.0045\ h^{-1}$, $R^2 = 0.996$.

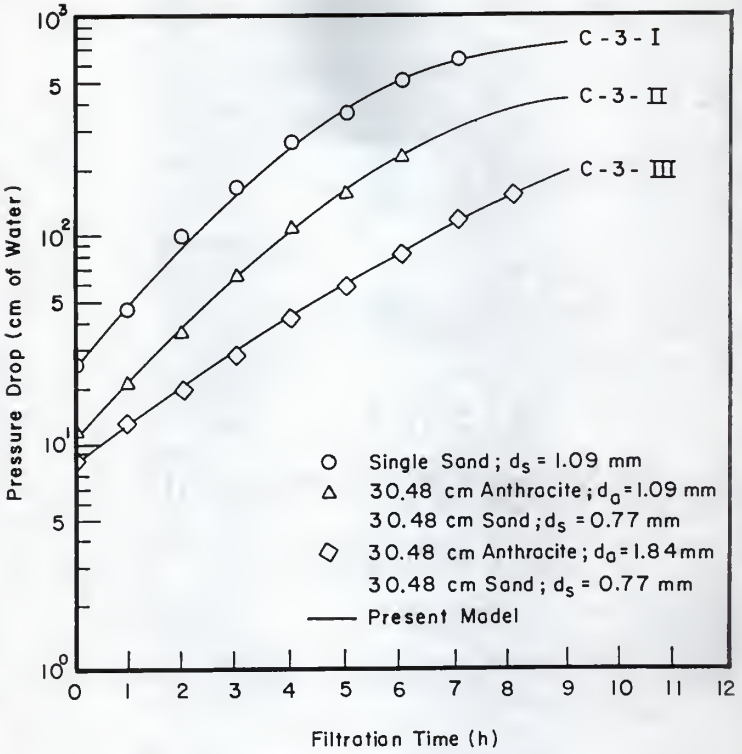

Figure IV-3. Fitting the present model to Huang's data (1972): bed depth (60.96 cm), flow rate (9.8 m/h), waste water suspension (12.5 mg/ℓ).

Runs; C-3-I (α = 0.645 h^{-1}, β = 0.0209 h^{-1}, R^2 = 0.995),

C-3-II (α = 0.578 h^{-1}, β = 0.0146 h^{-1}, R^2 = 0.997),

C-3-III (α = 0.382 h^{-1}, β = 0.0073 h^{-1}, R^2 = 0.998).

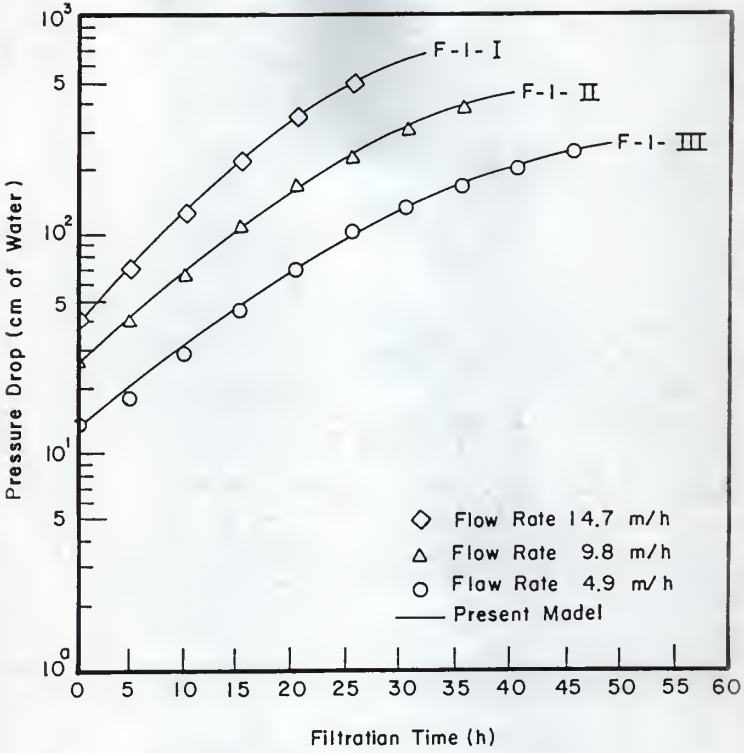

Figure IV-4. Fitting the present model to Huang's data (1972): bed depth (60.96 cm: anthracite, 30.48 cm, d_a = 0.184 cm; sand, 30.48 cm, d_s = 0.055 cm), waste water suspension (12.5 mg/ℓ).

Runs; F-1-I (α = 0.122 h^{-1}, β = 0.0054 h^{-1}, R^2 = 0.999),

F-1-II (α = 0.100 h^{-1}, β = 0.0045 h^{-1}, R^2 = 0.992),

F-1-III (α = 0.089 h^{-1}, β = 0.0040 h^{-1}, R^2 = 0.998).

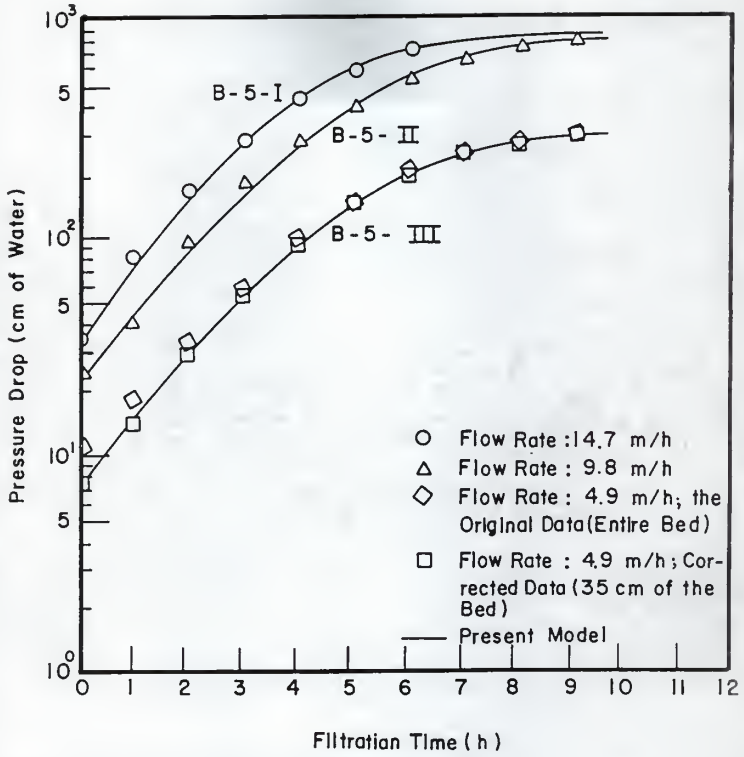

Figure IV-5. Fitting the present model to Huang's data (1972): sand size (0.092 cm), bed depth (50.8 cm), waste water suspension (12.5 mg/ℓ).

Runs; B-5-I (α = 0.787 h^{-1}, β = 0.033 h^{-1}, R^2 = 0.996),

B-5-II (α = 0.690 h^{-1}, β = 0.019 h^{-1}, R^2 = 0.997),

B-5-III (α = 0.698 h^{-1}, β = 0.017 h^{-1}, R^2 = 0.999).

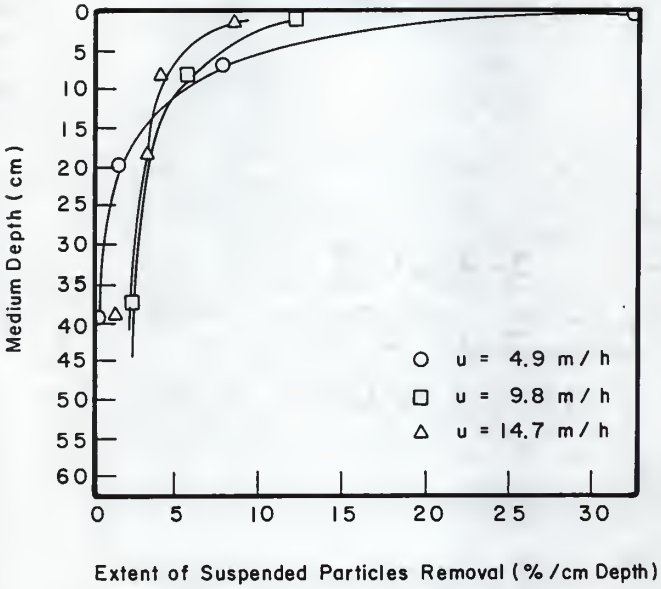

Figure IV-6. Extent of suspended particles removal per cm depth of a unisized sand filter;
sand size, 0.092 cm; filtration time, 1 h;

Runs; B-5-I, II, III (Huang, 1972).

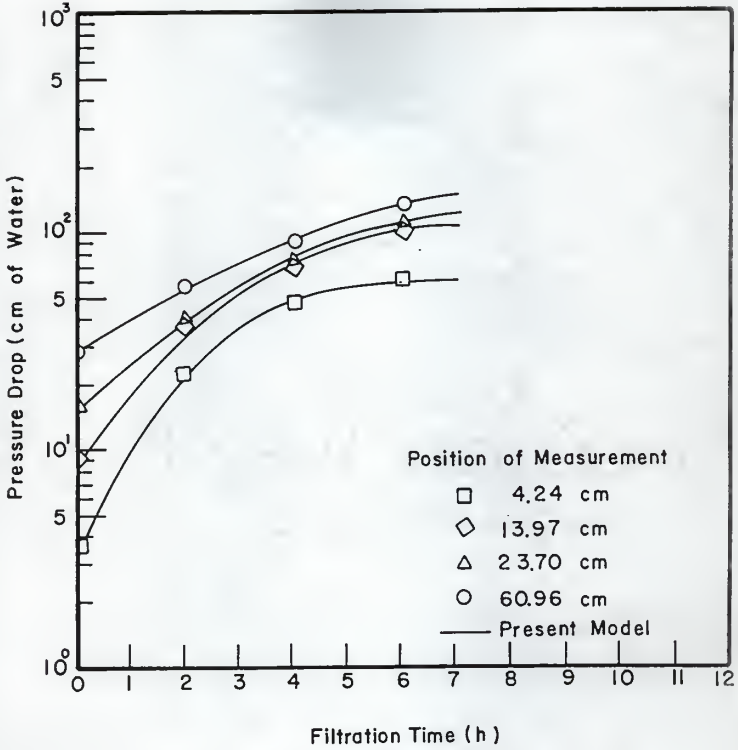

Figure IV-7. Fitting the present model to Rimer's data (1968): sand size (0.046 cm), bed depth (60.96 cm), flow rate (7.3 m/h), $FeCl_3$ suspension (5 mg/ℓ, pH = 8.3).

Run VII-2; position 4.24 cm ($\alpha = 1.035\ h^{-1}$, $\beta = 0.069\ h^{-1}$, $R^2 = 0.986$),

position 13.47 cm ($\alpha = 0.718\ h^{-1}$, $\beta = 0.066\ h^{-1}$, $R^2 = 0.981$),

position 23.70 cm ($\alpha = 0.511\ h^{-1}$, $\beta = 0.063\ h^{-1}$, $R^2 = 0.997$),

position 60.96 cm ($\alpha = 0.347\ h^{-1}$, $\beta = 0.060\ h^{-1}$, $R^2 = 0.998$).

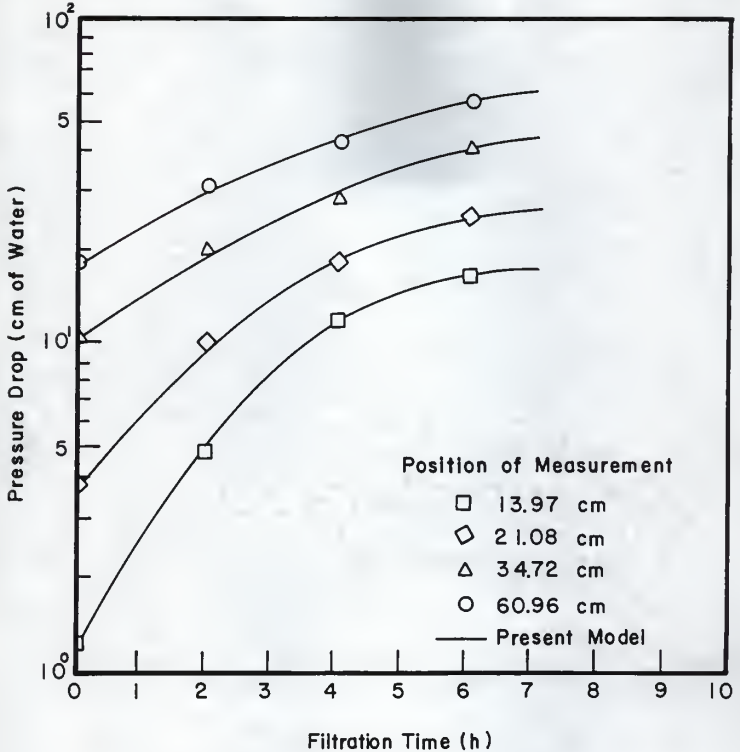

Figure IV-8. Fitting the present model to Rimer's data (1968): bed depth (60.96 cm: anthracite, 20.32 cm, d_a = 0.100 cm; sand, 20.32 cm, d_s = 0.071 cm; garnet, 20.32 cm, d_g = 0.059 cm), flow rate (7.3 m/h).

Run VII-2; position 13.97 cm (α = 0.778 h^{-1}, β = 0.055 h^{-1}, R^2 = 0.999),

position 21.08 cm (α = 0.558 h^{-1}, β = 0.081 h^{-1}, R^2 = 0.994),

position 34.72 cm (α = 0.319 h^{-1}, β = 0.071 h^{-1}, R^2 = 0.986),

position 60.96 cm (α = 0.276 h^{-1}, β = 0.088 h^{-1}, R^2 = 0.992).

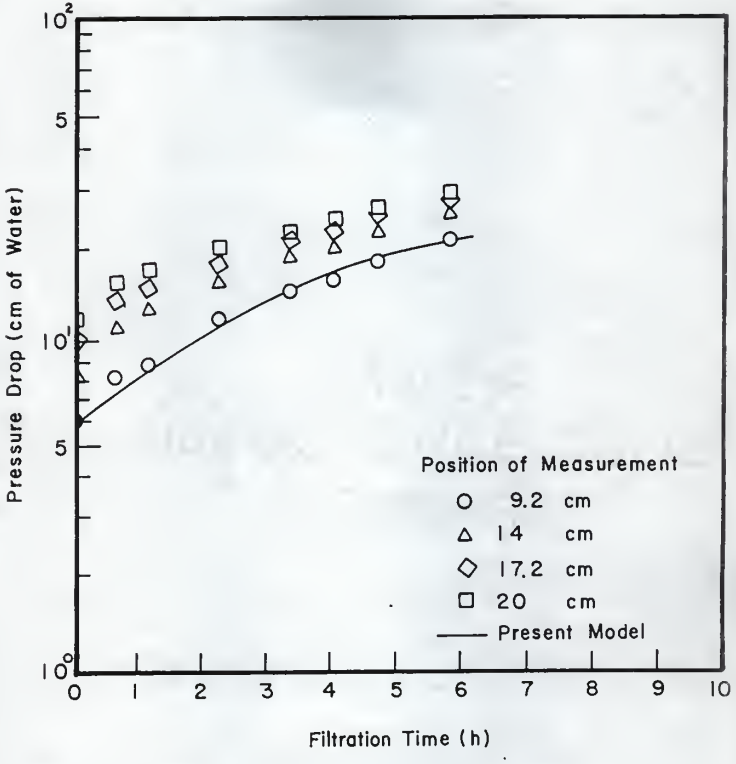

Figure IV-9. Fitting the present model to Ives' data (1961): sand size (0.0544 cm), bed depth (20 cm), flow rate (4.9 m/h), chlorella algae suspension (135×10^{-4} vol%).

Run 1B; position 9.2 cm ($\alpha = 0.359\ h^{-1}$, $\beta = 0.102\ h^{-1}$, $R^2 = 0.986$).

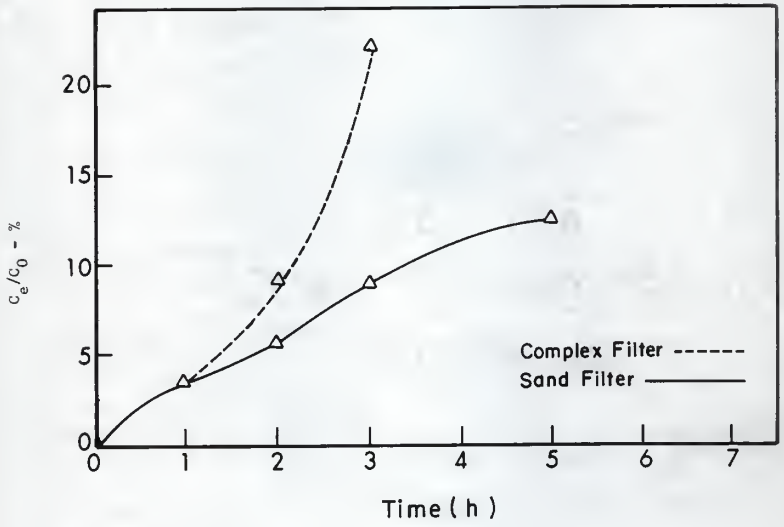

Figure IV-10. Ratio of the effluent to influent ferric iron concnetrations, C_e/C_0, as a function of time: Run VII-2 (Rimer, 1968).

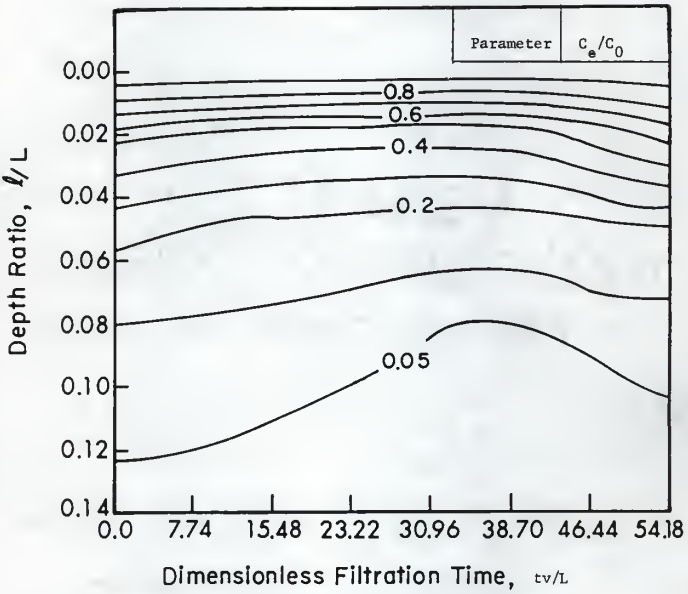

Figure IV-11. Isoconcentration ratio lines: Run 1 (Deb, 1969).

APPENDIX A: AN ALTERNATIVE DERIVATION OF THE MASTER EQUATIONS

The Master equations, Eqs. IV-3 and IV-4, in the text can also be derived through the consideration of a time homogeneous Markov process. Let $p_{ij}(\tau,t)$ denote the transition probability that the system in the state of i pores blocked at time τ will change to the state of j pores blocked at time t; $i,j = 0,1,2,\ldots,n_0$. It is assumed that within the small time invertal $(t,t+\Delta t)$

$$p_{ij}(t,t+\Delta t) = v_{ij}\Delta t + o(\Delta t) \ , \ i \neq j; \ i,j = 0,1,2,\ldots,n_0 \qquad \text{(A-1)}$$

$$1 - p_{ii}(t,t+\Delta t) = -v_{ii}\Delta t + o(\Delta t) \ , \ i = 0,1,2,\ldots,n_0 \qquad \text{(A-2)}$$

where v_{ij} and v_{ii} are the intensities of transition.

It can be shown that the transition probabilities, $\{p_{ij}(\tau,t)\}$ satisfy the following Kolmogorov forward differential equations (Chiang, 1980),

$$\frac{d}{dt} p_{ij}(\tau,t) = \sum_{k=0}^{n_0} p_{ik}(\tau,t) \, v_{kj} \ , \ i,j = 0,1,2,\ldots,n_0, \qquad \text{(A-3)}$$

with the initial condition

$$p_{ij}(\tau,\tau) = \begin{cases} 1, & i = j \\ 0, & i \neq j \end{cases} \qquad \text{(A-4)}$$

Let $p_{ij}(t)$ denote the transition probability from time 0 to time t. In matrix notation, Eqs. A-3 and A-4 can be written, respectively, as

$$\frac{d}{dt} \underline{P}(t) = \underline{P}(t) \, \underline{U} \qquad \text{(A-5)}$$

and

$$\underline{P}(0) = \underline{I} = \text{identity matrix} \tag{A-6}$$

where

$$\underline{P}(t) = \begin{bmatrix} P_{00}(t) & P_{01}(t) & \cdots & P_{0n_0}(t) \\ P_{10}(t) & P_{11}(t) & \cdots & P_{1n_0}(t) \\ \vdots & \vdots & & \vdots \\ P_{n_0 0}(t) & P_{n_0 1}(t) & \cdots & P_{n_0 n_0}(t) \end{bmatrix} \tag{A-7}$$

and

$$\underline{U} = \begin{bmatrix} v_{00} & v_{01} & \cdots & v_{0n_0} \\ v_{10} & v_{11} & \cdots & v_{1n_0} \\ \vdots & \vdots & & \vdots \\ v_{n_0 0} & v_{n_0 1} & \cdots & v_{n_0 n_0} \end{bmatrix} \tag{A-8}$$

In the present model, it is assumed that given $N(t) = n$

1. The transition probability that more than one pore will be blocked or scoured is $o(\Delta t)$, i.e.,

$$v_{ij} = 0 , \quad |j - i| \geq 2; \quad i,j = 0,1,\ldots,n_0. \tag{A-9}$$

2. The transition probability that an open pore will be blocked during the interval $(t, t+\Delta t)$ is $\lambda_n \Delta t + O(\Delta t)$, i.e.,

$$v_{ij} = \lambda_n , \quad i = n ; \quad n = 0,1,2,\ldots,n_0-1 \quad j = n + 1 \tag{A-10}$$

3. the transition probability that a blocked pore will be scoured during the interval $(t, t+\Delta t)$ is $\mu_n \Delta t + o(\Delta t)$, i.e.,

$$v_{ij} = \mu_n , \quad i = n ; \quad j = n - 1 \qquad n = 1,2,\ldots,n_0; \tag{A-11}$$

4. The transition probability of the no change in the interval $(t, t+\Delta t)$ is $[1 - \lambda_n \Delta t - \mu_n \Delta t - o(\Delta t)]$, i.e.,

$$v_{ii} = -(\lambda_n + \mu_n) , \quad i = n; \qquad n = 0,1,2,\ldots,n_0 \tag{A-12}$$

Then Eq. A-8 reduces to

$$\underline{U} = \begin{bmatrix} -\lambda_0 & \lambda_0 & 0 & 0 & \cdots & 0 \\ \mu_1 & -(\lambda_1+\mu_1) & \lambda_1 & 0 & \cdots & 0 \\ 0 & \mu_2 & -(\lambda_2+\mu_2) & \lambda_2 & \cdots & 0 \\ \cdot & \cdot & \cdot & \cdot & \cdot & \cdot \\ \cdot & \cdot & \cdot & \cdot & \cdot & \cdot \\ \cdot & \cdot & \cdot & \cdot & \cdot & \cdot \\ 0 & 0 & 0 & 0 & \cdots & -\mu_{n_0} \end{bmatrix} \tag{A-13}$$

Let $p_n(t)$ be the probability that exactly n pores are blocked at time t, and $\underline{P}(t)$ the vector of probabilties, i.e.,

$$\underline{P}(t) = [p_0(t)\ p_1(t)\ p_2(t)\ \ldots\ p_{n_0}(t)] \tag{A-14}$$

It can be seen that

$$\underline{P}(t) = \underline{P}(0)\,\underline{P}(t) \tag{A-15}$$

Multiplying both sides of Eq. A-5 with $\underline{P}(0)$, we obtain

$$\frac{d}{dt}\,\underline{P}(0)\underline{P}(t) = \underline{P}(0)\underline{P}(t)\underline{U} \tag{A-16}$$

or

$$\frac{d}{dt}\,\underline{P}\,(t) = \underline{P}(t)\underline{U} \tag{16a}$$

Expanding Eq. A-16a, we obtain

$$\frac{dp_n(t)}{dt} = \lambda_{n-1}P_{n-1}(t) - (\lambda_n + \mu_n)p_n(t) + \mu_{n+1}p_{n+1}(t)\ ,\ n \geq 1 \tag{A-17}$$

and

$$\frac{dp_0(t)}{dt} = -\lambda_0 P_0(t) + \mu_1 P_1(t) \tag{A-18}$$

which are the same as Eqs. IV-3 and IV-4, in the text.

APPENDIX B: SOLUTION OF THE PROBABILITY GENERATING FUNCTION OF THE MASTER EQUATIONS

The system of differential equations, Eqs. IV-7 and IV-8, in the text, describe the linear stochastic birth-death process as

$$\frac{dp_n(t)}{dt} = \alpha[n_0 - (n-1)]p_{n-1}(t) - [\alpha(n_0 - n) + \beta n]p_n(t) + \beta(n+1)p_{n+1}(t), \qquad n \geq 1 \tag{B-1}$$

and

$$\frac{dp_0(t)}{dt} = -\alpha n_0 p_0(t) + \beta p_1(t) \tag{B-2}$$

The mean number of the blocked pores at a given moment t is to be determined; it is

$$E[N(t)] = \sum_{n=0}^{n_0} n p_n(t) \tag{B-3}$$

To evaluate this value, we use the method of probability generating function which is defined as

$$G(s,t) = \sum_{n=0}^{n_0} s^n p_n(t) \tag{B-4}$$

Multiplying both sides of Eq. B-1 by the respective s^n's and Eq. B-2 by s^0, the following expression is obtained;

$$\sum_{n=0}^{n_0} s^n \frac{dp_n(t)}{dt} = [\beta + (\alpha - \beta)s - \alpha s^2][\sum_{n=0}^{n_0} n s^{n-1} p_n(t)] + [\alpha n_0 (s-1)][\sum_{n=0}^{n_0} s^n p_n(t)] \tag{B-5}$$

Since

$$\frac{\partial G(s,t)}{\partial t} = \sum_{n=0}^{n} s^n \frac{dP_n(t)}{dt} \tag{B-6}$$

and

$$\frac{\partial G(s,t)}{\partial s} = \sum_{n=0}^{n_0} n s^{n-1} p_n(t), \tag{B-7}$$

Equation B-5 reduces to

$$\frac{\partial G(s,t)}{\partial t} = \frac{\partial G(s,t)}{\partial s} [\beta + (\alpha - \beta)s - \alpha s^2] + G(s,t)[\alpha n_0 (s-1)] \tag{B-8}$$

The initial and boundary conditions can be expressed as

$$G(s,0) = 1 \tag{B-9}$$

$$G(1,t) = 1 \tag{B-10}$$

Assume that the solution of Eq. B-8 take the form of

$$G(s,t) = [f(s) + g(s,t)]^{n_0} \tag{B-11}$$

Substituting this into Eq. B-8 yeilds

$$\frac{\partial g(s,t)}{\partial t} = [\beta + (\alpha - \beta)s - \alpha s^2][\frac{df(s)}{ds} + \frac{\partial g(s,t)}{\partial s}]$$

$$+ [\alpha(s-1)][f(s) + g(s,t)] \tag{B-12}$$

Let f(s) and g(s,t) satisfy

$$[\beta + (\alpha - \beta)s - \alpha s^2]\frac{df}{ds} + [\alpha(s-1)]f(s) = 0 \tag{B-13}$$

and

$$\frac{\partial g(s,t)}{\partial t} = [\beta + (\alpha - \beta)s - \alpha s^2]\frac{\partial g(s,t)}{\partial s} + [\alpha(s-1)]g(s,t) \tag{B-14}$$

From Eqs. B-9 and B-11, we obtain

$$g(s,0) = 1 - f(s) \tag{B-15}$$

From Eqs. B-10 and B-11, we have

$$f(1) = 1 \tag{B-16}$$

$$g(1,t) = 0 \tag{B-17}$$

Subject to these boundary and initial conditions, Eqs. B-13 and B-14 are solved, respectively, as

$$f(s) = \frac{\alpha s + \beta}{\alpha + \beta} \tag{B-18}$$

$$g(s,t) = \frac{-\alpha(s - 1)e^{-(\alpha + \beta)t}}{\alpha + \beta} \tag{B-19}$$

Therefore, the solution of Eq. B-18 becomes

$$G(s,t) = \left[\frac{(\alpha s + \beta) - \alpha(s - 1)e^{-(\alpha + \beta)t}}{\alpha + \beta}\right]^{n_0} \tag{B-20}$$

which is the same as Eq. IV-15 in the text.

CHAPTER V BIRTH-DEATH MODELING OF DEEP BED FILTRATION: Sectional Analysis

In the stochastic modeling presented in Chapter IV, or more specifically birth-death modeling, it has been assumed that the intensity of birth or the blockage intensity, λ_n, and the intensity of death or the scouring intensity, μ_n, are linearly proportional to the number of open pores and the number of blocked pores in the bed, respectively (Litwiniszyn, 1968a; 1968b; 1969; Hsu and Fan, 1984). This assumption of linearity gives rise to

$$\lambda_n = \alpha(n_0 - n); \qquad n = 0, 1, 2, \ldots, n_0 \qquad \text{(V-1)}$$

$$\mu_n = \beta n; \qquad n = 0, 1, 2, \ldots, n_0 \qquad \text{(V-2)}$$

where n_0 is the total number of open pores susceptible to blockage in a unit volume of the bed, α is the blockage constant, and β is the scouring constant. Equation V-1 is based on the postulation that as the number of open pores susceptible to blockage becomes larger, the probability of an open pores being blocked will be proportionally greater, and Eq. V-2 on the postulation that as the number of blocked pores becomes larger, the probability of a blocked pore being scoured will be proportionally greater. The applicability of this modeling to the available experimental data has been amply demonstrated in Chapter IV.

It may be noted, however, that the linear velocity of flow through the bed, v, will increase when the number of open pores, (n_0-n), decreases; in fact, v is inversely proportional to (n_0-n). Furthermore, solid particles, suspended in faster moving fluid, will probably be less likely to be trapped

in the bed. Thus, we may also postulate that

$$\lambda_n \propto \frac{1}{v} \propto (n_0 - n) \tag{V-3}$$

Because of two effects of the number of open pores on λ_n, as characterized by Eqs. V-1 and V-3, it is highly probable that λ_n is proportional to the square of the number of open pores under some conditions. In other words, under this second-order approximation, λ_n assumes the form

$$\lambda_n = \alpha(n_0 - n)^2 \tag{V-4}$$

Similarly, μ_n assumes the form

$$\mu_n = \beta n^2 \tag{V-5}$$

MODEL

A second-order, birth-death model represented by Eqs. V-4 and V-5 is employed to describe both blockage of pores by suspended particles and scouring of deposited particles. This model, coupled with the Carman-Kozeny equation, simulate the pressure drop dynamics during a deep bed filtration.

Master Equation and One-step Operator

The number of blocked pores in a unit volume of the bed at time t, N(t), is taken as the random variable (Litwiniszyn, 1966); a specific value of N(t) will be denoted by n. For the birth-death process, representing the blockage-scouring process of pores in the filter bed, the following is assumed (Chiang, 1980).

1. The conditional (or transition) probability that a birth event, i.e., the blockage of an open pore, will occur during the time interval $(t, t+\Delta t)$ is $\lambda_n \Delta t + o(\Delta t)$, where λ_n is a function of n, (e.g., given by

Eq. V-1 or V-4).

2. The conditional probability that a death event, i.e., the scouring of a blocked pore, will occur during the time interval $(t, t+\Delta t)$ is $\mu_n \Delta t + o(\Delta t)$, where μ_n is also a function of n, (e.g., given by Eq. V-2 or V-5).

3. The conditional probability that more than one event will occur in this time interval is $o(\Delta t)$, which signifies that

$$\lim_{\Delta t \to 0} \frac{o(\Delta t)}{\Delta t} = 0$$

4. The conditional probability that no change occurs during the time interval $(t, t+\Delta t)$ is

$$[1 - \lambda_n \Delta t - \mu_n \Delta t + o(\Delta t)]$$

The relationship among these four conditional probabilities can be diagrammed as shown in Figure V-1. By denoting

$$p_n(t) = \Pr\{N(t) = n\}; \quad n = 0, 1, 2, \ldots, n_0$$

as the probability that n pores are blocked at time t, the probability balance around $N(t) = n$ yields (Chiang, 1980)

$$\frac{dp_n(t)}{dt} = \lambda_{n-1} p_{n-1}(t) + \mu_{n+1} p_{n+1}(t) - (\lambda_n + \mu_n) p_n(t);$$

$$n = 1, 2, \ldots, (n_0 - 1), \tag{V-6}$$

$$\frac{dp_0(t)}{dt} = -\lambda_0 p_0(t) + \mu_1 p_1(t) \tag{V-7}$$

and

$$\frac{dp_{n_0}(t)}{dt} = \lambda_{n_0-1} p_{n_0-1}(t) - \mu_{n_0} p_{n_0}(t) \tag{V-8}$$

Letting

$$\mu_0 = \lambda_{-1} = \lambda_{n_0} = \mu_{n_0+1} = 0,$$

Eqs. V-6 through V-8 can be combined as

$$\frac{dp_n(t)}{dt} = \lambda_{n-1} p_{n-1}(t) + \mu_{n+1} p_{n+1}(t) - (\lambda_n + \mu_n) p_n(t);$$

$$n = 0, 1, 2, \ldots, n_0 \qquad \text{(V-9)}$$

Equation V-9 is the so-called probability balance equation or Master equation (see, e.g., Van Kampen, 1981).

The one-step operator, $\mathbf{E}$, is defined by its effect on an arbitrary function f(n) as (see, e.g., Van Kampen, 1981)

$$\mathbf{E}\, f(n) = f(n+1) \text{ and } \mathbf{E}^{-1} f(n) = f(n-1) \qquad \text{(V-10)}$$

With the aid of this operator, the Master equation for the birth-death process, Eq. V-9, reduces to

$$\frac{\partial p(n,t)}{\partial t} = (\mathbf{E} - 1)\mu_n p(n,t) + (\mathbf{E}^{-1} - 1)\lambda_n p(n,t) \qquad \text{(V-11)}$$

where $p_n(t)$ has been rewritten as $p(n,t)$ for convenience.

Expansion of Master Equation

λ_n and μ_n, defined by Eqs. V-4 and V-5, respectively, are nonlinear, and thus, the analytical solution of Eq. V-11 is extremely difficult, if not impossible. It has been shown, however, that this difficulty can be circumvented by resorting to approximation based on the Taylor's expansion (see, e.g., Van Kampen, 1981).

For linear λ_n and μ_n defined by Eqs. V-1 and V-2, respectively, the mean of N(t), <n>, obtainable from the Master equation, Eq. V-11, is also obtainable from the corresponding deterministic governing equation given below (also see APPENDIX A).

$$\frac{d\bar{n}(t)}{dt} = \alpha[n_0 - \bar{n}(t)] - \beta\bar{n}(t) \tag{V-12}$$

where $\bar{n}(t)$ represents the deterministic value of n at the moment t. Accordingly, the corresponding deterministic governing equation with the second-order approximation becomes

$$\frac{d\bar{n}(t)}{dt} = \alpha[n_0 - \bar{n}(t)]^2 - \beta\bar{n}^2(t) \tag{V-13}$$

Letting

$$\phi(t) = \frac{\bar{n}(t)}{n_0} \quad ,$$

Eq. V-13 reduces to

$$\frac{d\phi(t)}{dt} = \alpha n_0[1 - \phi(t)]^2 - \beta n_0\phi^2(t) \tag{V-14}$$

Knowing that n has a maximum value of n_0, we expect that n consists of the macroscopic term, $n_0\phi(t)$, and the fluctuating term of order $n_0^{1/2}$, that is, p(n,t) will have a sharp peak located roughly at $n_0\phi(t)$ and a width of order $n_0^{1/2}$ (see Figure V-2). Hence, we set

$$n = n_0\phi(t) + n_0^{1/2}\zeta \tag{V-15}$$

where ζ is a new variable. Notice that $\phi(t)$ satisfies the deterministic governing equation as will be elaborated later. Accordingly, the probability distribution p of n now becomes the probability distribution π of ζ. Thus,

$$p(n,t)\Delta n = \pi(\zeta,t)\Delta\zeta$$

This in conjunction with Eq. V-15 yields

$$\pi(\zeta,t) = n_0^{1/2} p(n,t) \tag{V-16}$$

The time derivative in Eq. V-11 is taken with constant n; This means that this derivative is taken in the ζ-t plane along the direction given by (see Eq. V-15)

$$\frac{d\zeta}{dt} = -n_0^{1/2} \frac{d\phi}{dt}$$

Hence,

$$n_0^{1/2} \frac{\partial p(n,t)}{\partial t} = \frac{\partial \pi}{\partial t} - n_0^{1/2} \frac{d\phi}{dt} \frac{\partial \pi}{\partial \zeta} \tag{V-17}$$

The operator $\mathbf{E}$ changes n into n+1, and therefore, ζ into $\zeta+n_0^{-1/2}$, so that (see APPENDIX B)

$$\mathbf{E} = 1 + n_0^{-1/2} \frac{\partial}{\partial \zeta} + \frac{1}{2} n_0^{-1} \frac{\partial^2}{\partial \zeta^2} + \cdots \tag{V-18}$$

and

$$\mathbf{E}^{-1} = 1 - n_0^{-1/2} \frac{\partial}{\partial \zeta} + \frac{1}{2} n_0^{-1} \frac{\partial^2}{\partial \zeta^2} + \cdots \tag{V-19}$$

Substituting Eqs. V-16 through V-19 into the Master equation, Eq. V-11, and cancelling the common factor $n_0^{-1/2}$ in each term, we have

$$\frac{\partial \pi}{\partial t} - n_0^{1/2} \frac{d\phi}{dt} \frac{\partial \pi}{\partial \zeta}$$

$$= \beta n_0^2 \left(n_0^{-1/2} \frac{\partial}{\partial \zeta} + \frac{1}{2} n_0^{-1} \frac{\partial^2}{\partial \zeta^2} + \ldots\right)(\phi + n_0^{-1/2}\zeta)^2 \pi$$

$$+ \alpha n_0^2 \left(-n_0^{-1/2} \frac{\partial}{\partial \zeta} + \frac{1}{2} n_0^{-1} \frac{\partial^2}{\partial \zeta^2} - \ldots\right)(1 - \phi - n_0^{-1/2}\zeta)^2 \pi \tag{V-20}$$

By absorbing the factor n_0 into the time variable as

$$n_0 t = \tau \tag{V-21}$$

Eq. V-14 is simplified as

$$\frac{d\phi}{d\tau} = \alpha(1-\phi)^2 - \beta\,\phi^2 \tag{V-22}$$

The transformation given by Eq. V-21 together with the truncation of the terms after the second derivative for large n_0 gives

$$\frac{\partial \pi}{\partial \tau} \sim n_0^{1/2} \frac{d\phi}{d\tau} \frac{\partial \pi}{\partial \zeta}$$

$$= \beta\, n_0 \left(n_0^{-1/2} \frac{\partial}{\partial \zeta} + \frac{1}{2} n_0^{-1} \frac{\partial^2}{\partial \zeta^2}\right) (\phi + n_0^{-1/2}\zeta)^2 \pi$$

$$+ \alpha\, n_0 \left(-n_0^{-1/2} \frac{\partial}{\partial \zeta} + \frac{1}{2} n_0^{-1} \frac{\partial^2}{\partial \zeta^2}\right) (1-\phi- n_0^{-1/2}\zeta)^2 \pi \tag{V-23}$$

Expanding the right-hand side of Eq. V-23 and collecting the resultant terms of order of $n_0^{1/2}$ and n_0^0 separately, we have

$$\frac{d\phi}{d\tau} = \alpha(1-\phi)^2 - \beta\phi^2 \tag{V-24}$$

and

$$\frac{\partial \pi}{\partial \tau} = 2[\beta\phi - \alpha(1-\phi)] \frac{\partial}{\partial \zeta} (\zeta\pi) + \frac{1}{2} [\beta\phi^2 + \alpha(1-\phi)^2] \frac{\partial^2}{\partial \zeta^2} \pi \tag{V-25}$$

That Eq. V-24 is the same as the deterministic governing equation, Eq. V-22, satisfies our postulation that ϕ is governed by the deterministic governing equation. Equation V-25 suffices for determining the first and second moments of ζ, $\langle\zeta\rangle$ and $\langle\zeta^2\rangle$, respectively, which contain the significant information on the random variable. Upon transformation of Eq. V-25, we

obtain (see APPENDIX C)

$$\frac{\partial \langle \zeta \rangle}{\partial \tau} = [2\alpha(1-\phi) - 2\beta\phi] \langle \zeta \rangle \tag{V-26}$$

$$\frac{\partial \langle \zeta^2 \rangle}{\partial \tau} = [4\alpha(1-\phi) - 4\beta\phi] \langle \zeta^2 \rangle + \alpha(1-\phi)^2 + \beta\phi^2 \tag{V-27}$$

Since

$$n = n_0\phi + n_0^{1/2}\zeta$$

as indicated by Eq. V-15, we have

$$\langle n \rangle = n_0\phi + n_0^{1/2}\langle \zeta \rangle \tag{V-28}$$

$$\langle\langle n^2 \rangle\rangle = \langle n^2 \rangle - \langle n \rangle^2$$

$$= n_0[\langle \zeta^2 \rangle - \langle \zeta \rangle^2] \tag{V-29}$$

where $\langle n \rangle$ is the first moment of n, $\langle n^2 \rangle$ is the second moment of n, and $\langle\langle n^2 \rangle\rangle$ is the variance of n.

For a pure birth process where $\beta = 0$, Eq. V-22 reduces to

$$\frac{d\phi}{d\tau} = \alpha(1-\phi)^2 \tag{V-30}$$

Solving this equation, subject to the initial condition

$$\phi = 0 \quad \text{at} \quad \tau = 0, \tag{V-31}$$

gives

$$\phi = \frac{\alpha\tau}{1+\alpha\tau} \tag{V-32}$$

Substituting this expression into Eq. V-26 and setting $\beta = 0$ in the resultant expression, we obtain

$$\frac{\partial \langle \zeta \rangle}{\partial \tau} = \frac{2\alpha}{1 + \alpha\tau} \langle \zeta \rangle \tag{V-33}$$

The general solution of this equation is

$$\langle \zeta \rangle = c(1 + \alpha\tau)^2 \tag{V-34}$$

To satisfy the initial condition

$$\langle \zeta \rangle = 0 \quad \text{at} \quad \tau = 0, \tag{V-35}$$

the constant c must be zero; hence (see APPENDIX D),

$$\langle \zeta \rangle = 0 \tag{V-36}$$

Substitution of Eqs. V-32 and V-35 into Eq. V-28 gives

$$\langle n \rangle = \frac{\alpha n_0 \tau}{1 + \alpha\tau} \tag{V-37}$$

Knowing that

$$n_0 t = \tau$$

as indicated by Eq. V-21 and letting

$$\alpha n_0 = k \tag{V-38}$$

Eq. V-37 reduces to

$$\langle n \rangle = n_0 \frac{kt}{1 + kt} \tag{V-39}$$

The expression is a reasonable approximation to $\langle n \rangle$ for a large n_0, where the terms after the second derivative in Eq. V-20 are negligible, and therefore, it is valid for the deep bed filtration process. The variance of n can also be obtained by solving Eqs. V-27 and V-29. For a sufficiently large n_0, the variance tends to become insignificant in simulating the filtration process.

Constant Flow Filtration

Denoting the linear velocity of the suspension flowing through the pores at time t as v(t) and the linear velocity at the onset of filtration as v_0, we have

$$v(t) = \frac{n_0}{n_0 - \langle n \rangle} v_0 \qquad \text{(V-40)}$$

under the assumption that all pores have the same radius.

For the second-order, pure birth process, substitution of Eq. V-39 into Eq. V-40 yields

$$v(t) = v_0(1 + kt) \qquad \text{(V-41)}$$

Under the simplifying assumption that an increase in the pressure drop can be attributed only to the increase in the linear velocity of flow, substituting Eq. V-41 into the Carman-Kozeny equation,

$$-\frac{\Delta P(t)}{L} = 150 \left(\frac{1-\varepsilon}{\varepsilon}\right)^2 \frac{\mu v(t)}{d_p^2} \quad , \qquad \text{(V-42)}$$

yields

$$-\frac{\Delta P(t)}{L} = 150\left(\frac{1-\varepsilon}{\varepsilon}\right)^2 \frac{\mu v_0}{d_p^2}(1+kt)$$

$$= \left(-\frac{\Delta P}{L}\right)_0 (1+kt) \qquad \text{(V-43)}$$

where $\left[-(\Delta P/L)_0\right]$ represents the initial pressure drop per unit length of the bed. For the linear, birth-death modeling presented in Chapter IV, the pressure drop through the filter bed has been shown to change as (also see APPENDIX E)

$$-\frac{\Delta P(t)}{L} = \left(-\frac{\Delta P}{L}\right)_0 \left\{\frac{\alpha+\beta}{\beta+\alpha e^{-(\alpha+\beta)t}}\right\} \qquad \text{(V-44)}$$

ANALYSIS OF AVAILABLE EXPERIMENTAL DATA AND DISCUSSION

Many factors may affect the blockage and scouring constants, α and β; they include the properties and concentration of suspension, filtration rate and bed characteristics. Within certain ranges, it is possible to manipulate independently all these factors except the suspension concentration which will decrease along the bed due to the trapping of solid particles. It is entirely conceivable, therefore, that under some situations, a lumped model treating the entire bed as a single compartment will fail to represent the deep bed filtration. Thus, it may be desirable to divide the bed along its axis into more than one compartment and to measure the increase in the pressure drop through each compartment under such situation. The experimental results of previous researchers (Eliassen, 1935; Ives, 1961; Rimer, 1968; Deb, 1969; Huang, 1972) have been analyzed in this light based on the present models; the results are shown in Figures V-3

through V-9.

In Eliassen's experiments, a rapid filter with a depth of 60 cm was used to remove suspended particles of hydrous ferric oxide floc from suspension. The pressure readings were taken every ten hours from different bed heights (4.27 cm, 11.89 cm, 42.36 cm, and 60 cm). For convenience, therefore, the bed has been divided into four compartments, and the pressure drop through each compartment and its changes have been simulated according to the present models. The results of runs 6 and 8 are shown in Figures V-3 and V-4, respectively. These figures show that the change in the pressure drop through the first compartment (0 ~ 4.27 cm) obeys essentially the second-order, pure birth process (Eq. V-43), that through the second compartment (4.27 ~ 11.89 cm) reflects the linear, birth-death behavior (Eq. V-44), and that through the third compartment (11.89 ~ 42.36 cm) follows the linear, pure birth model (Eq. V-44 with $\beta = 0$). These figures also show that the change in the total pressure drop through these three compartments (0 ~ 42.36 cm) can be satisfactorily simulated by the lumped, linear, birth-death model for which λ_n and μ_n are given by Eqs. V-1 and V-2, respectively. Notice that the pressure drop through the last compartment (42.36 ~ 60 cm) remained essentially constant during each filtration run. This implies that the last compartment was not utilized because of the relatively shallow penetration of the suspended particles; naturally, the present models are not applicable to the last compartment where no filtration occured.

The data of Huang (1972) are shown in Figure V-5 and those of Rimer are shown in Figures V-6 and V-7; they both measured the pressure drops at different bed heights. These figures demonstrate that compartmentalization of each filter leads to successful simulation of its dynamic behavior by the present models. The change in the pressure drop through the compartments

around the entrance section follows the linear, birth-death model and that through the compartments away from the entrance section reflects the linear, pure birth characteristics. These figures also show that the change in the overall pressure drop exhibits the linear, birth-death behavior. Notice that in Figure V-6 the pressure drop remained constant through the last compartment of Rimer's filter (44.45 ~ 69.96 cm), thus indicating that this portion was not utilized.

The results obtained by Deb (1969) and Ives (1961) are plotted in Figure V-8 and V-9, respectively. The penetration through their filters was indeed shallow. It can be seen in these figures that in each case the pressure drop remained constant through more than 50% of the bed away from the entrance section. However, in Deb's filter, the pressure drop through the remainder of the bed exhibited the linear, pure birth behavior, and in Ives' filter, the pressure drop through the remainder of the filter reflected the linear, birth-death characteristics.

In this work both sectional analysis and lumped analysis have been performed and the results are compared. The sectional analysis gives an insight into the performance of the deep bed filter but the lumped analysis provides a convenient way to simulate dynamics of the overall pressure drop variation.

According to Eliassen's data plotted in Figures V-3 and V-4, the second-order, pure birth behavior is found to occur in the compartment around the entrance section (0 ~ 4.27 cm) of his filter bed. Although only 7% of the bed exhibits this behavior, its contribution to the increase in the overall pressure drop is almost 30%

The blockage and scouring constants, α and β, are functions of the suspension concentration which decreases along the bed during a filtration

run. Thus, if the bed characteristics are uniform throughout the bed, these two constants are expected to decrease with the bed depth as indicated in Figures V-5 and V-6. While α decreases momotonically with bed depth, β varies irregularly as seen in Figure V-7. Notice that the bed in Figure V-7 is of multimedia (anthracite, sand, and garnet). It appears that α depends strongly on the suspension concentration while β depends weakly on it; however, the latter is highly dependent on the type of bed grains and the bed structure, i.e., the spatial distribution of these grains.

As mentioned earlier, the pressure drop dynamics in the section of the filter beds away from the entrance section tend to obey the linear, pure birth process as shown in Figures V-3 through V-7. A plausible interpretation is that in these sections, the suspension concentrations hecnee sufficiently dillute so that the blockage mechanism predominates over the scouring mechanism. This is equivalent to the situation seen in Figure V-8; the influent suspension concentration was only 45×10^{-4} volume% so that the scouring effect was negligible, which gave rise to the linear, pure birth process.

NOMENCLATURE

d_a = diameter of the anthracite

d_p = average diameter of the grain particles

d_s = diameter of the sand

L = depth of the bed

n = number of pores clogged per unit volume of the bed

n_0 = total number of open pores susceptible to blockage per unit volume of the bed

$N(t)$ = a random variable describing the number of blocked pores per unit volume of the bed at the moment t

$\langle n \rangle$ = mean or first moment of n

$\langle n^2 \rangle$ = second moment of n

$\langle\langle n^2 \rangle\rangle$ = variance of n

$p_n(t)$ = probability that exactly n pores are blocked at the moment t

$p(n,t)$ = same as $p_n(t)$

$(-\frac{\Delta P}{L})$ = pressure drop per unit length of the filter

r = radius of pore

t = time

u = superficial velocity

v = linear velocity

$\mathbb{E}$ = symbol of one-step operator

ζ = variable representing the fluctuating term

$\pi(\zeta,t)$ = probability density function

λ_n = intensity of the birth transition

μ_n = intensity of the death transition

α = proportionality constant defined in Eq. V-1 or V-4, the blockage constant

β = proportionality constant defined in Eq. V-2 or V-5, the scouring constant

τ = new variable defined in Eq. V-21

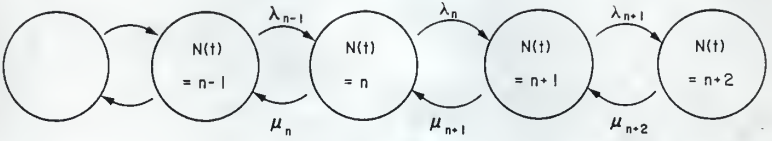

Figure V-1. Birth-death process and its conditional probabilities.

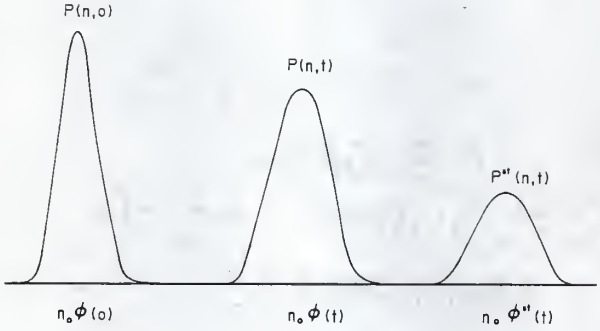

Figure V-2. Evolution of the probability density.

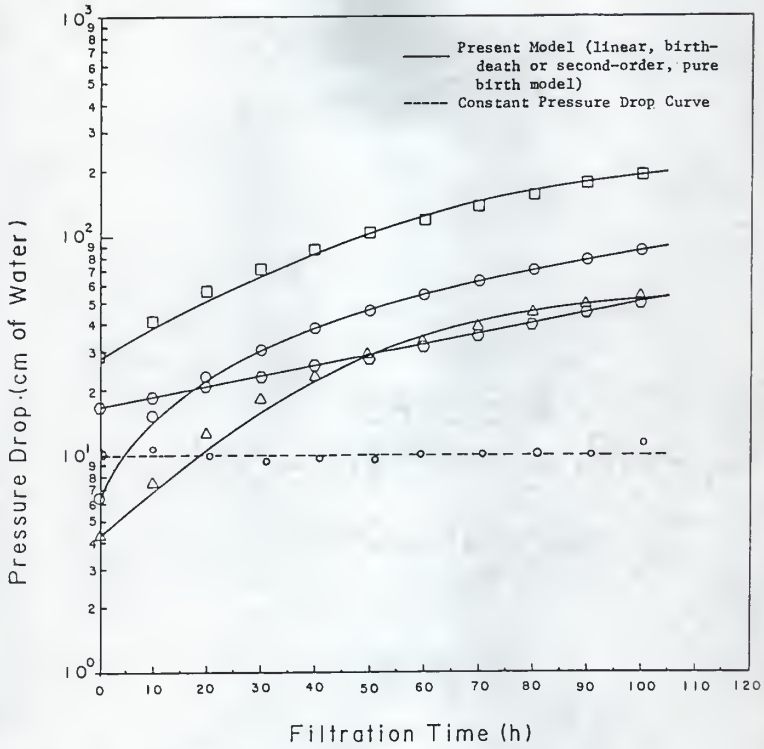

Figure V-3. Fitting the present model to Eliassen's data (1935): sand size (0.061 cm), bed depth (60 cm), flow rate (4.9 m/h), hydrous ferric oxide floc suspension (concentration, 7.3×10^{-4} wt%).

Run 6; O : first compartment (0 ∿ 4.27 cm), $k=0.123\ h^{-1}$,

Δ : second compartment (4.27 ∿ 11.89 cm), $\alpha=0.047\ h^{-1}$, $\beta=0.004\ h^{-1}$

O : third compartment (11.89 ∿ 42.36 cm), $\alpha=0.011\ h^{-1}$, $\beta=0$,

□ : lumped model (0 ∿ 42.36 cm), $\alpha=0.032\ h^{-1}$, $\beta=0.0045\ h^{-1}$,

o : fourth compartment (42.36 ∿ 60 cm).

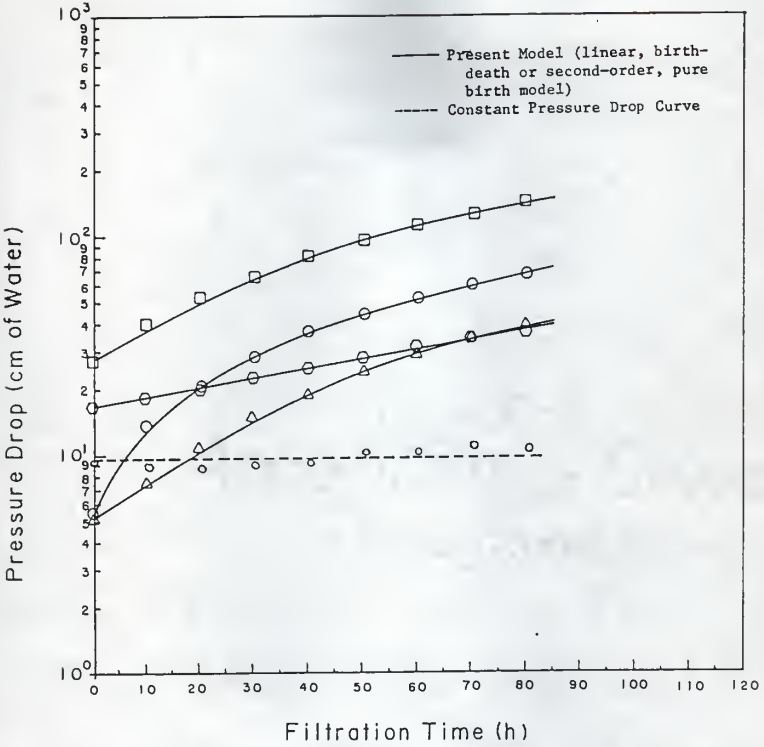

Figure V-4. Fitting the present model to Eliassen's data (1935): sand size (0.061 cm), bed depth (60 cm), flow rate (4.9 m/h), hydrous ferric oxide floc suspension (concentration, 7.3×10^{-4} wt%).

Run 8; ○ : first compartment (0 ∿ 4.27 cm), $k=0.14\ h^{-1}$,

△ : second compartment (4.27 ∿ 11.89 cm), $\alpha=0.0373\ h^{-1}$, $\beta=0.0043\ h^{-1}$,

○ : third compartment (11.89 ∿ 42.36 cm), $\alpha=0.01\ h^{-1}$, $\beta=0$,

□ : lumped model (0 ∿ 42.36 cm), $\alpha=0.032\ h^{-1}$, $\beta=0.0058\ h^{-1}$,

∘ : fourth compartment (42.36 ∿ 60 cm).

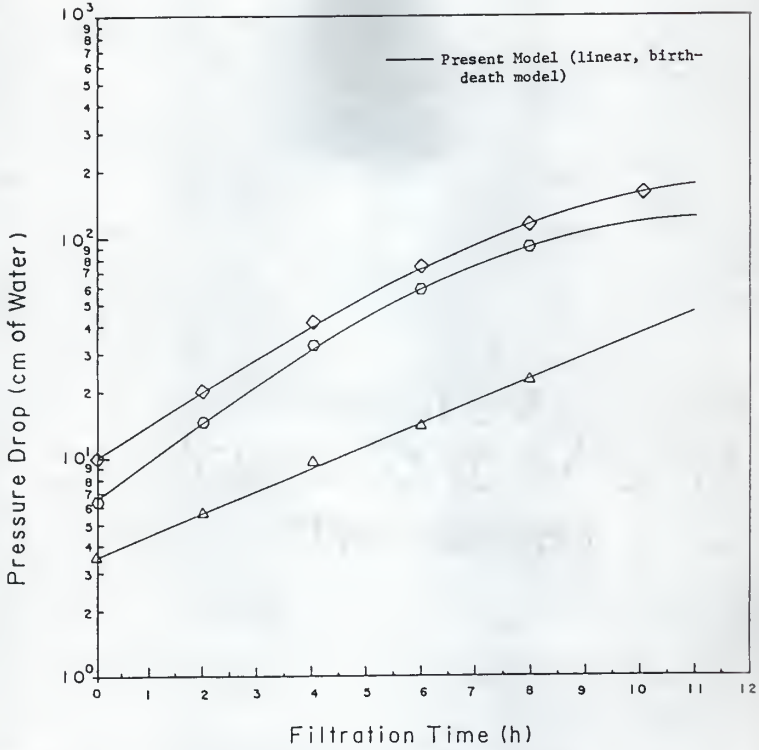

Figure V-5. Fitting the present model to Huang's data (1972): sand size (0.065 cm), bed depth (33.35 cm), flow rate(4.9 m/h), waste water suspension (12.5 mg/ℓ).

Run A-2-II; ○ : first compartment (0 ∿ 12.7 cm), α=0.429 h^{-1}, β=0.02 h^{-1},

△ : second compartment (12.7 ∿ 33.35 cm), α=0.232 h^{-1}, β=0,

◇ : lumped model (0 ∿ 33.35 cm), α=0.368 h^{-1}, β=0.016 h^{-1}.

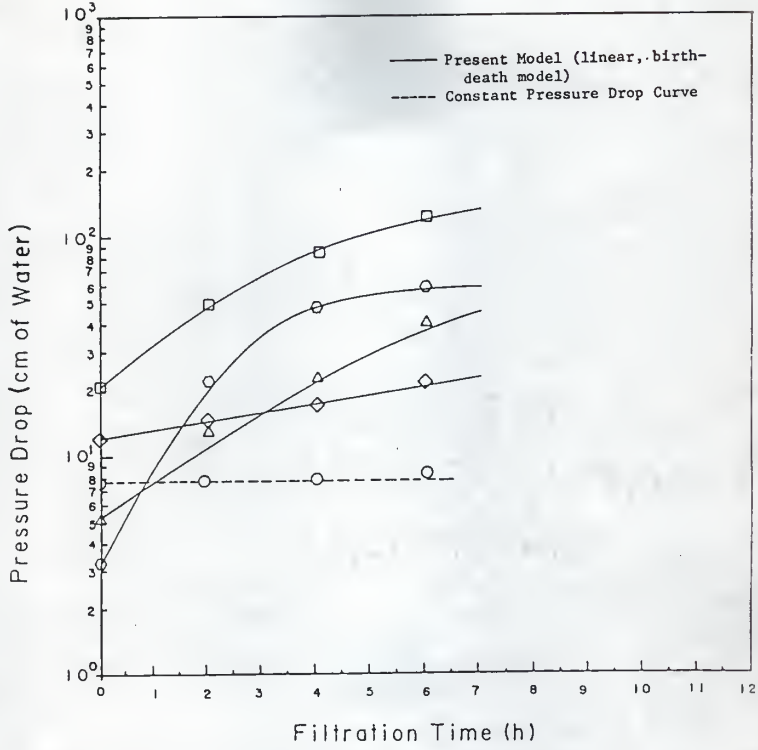

Figure V-6. Fitting the present model to Rimer's data (1968): sand size (0.046 cm), bed depth (60.96 cm), flow rate (7.3 m/h), $FeCl_3$ suspension (5 mg/ℓ, pH=8.3).

Run VII-2 ○: first compartment (0 ∿ 4.24 cm), α=1.035 h^{-1}, β=0.06 h^{-1},

△: second compartment (4.24 ∿ 13.97 cm), α=0.4133 h^{-1}, β=0.0286 h^{-1},

◇: third compartment (13.97 ∿ 44.45 cm), α=0.089 h^{-1}, β=0,

□: lumped model (0 ∿ 44.45 cm), α=0.469 h^{-1}, β=0.076 h^{-1},

○: fourth compartment (44.45 ∿ 60.96 cm).

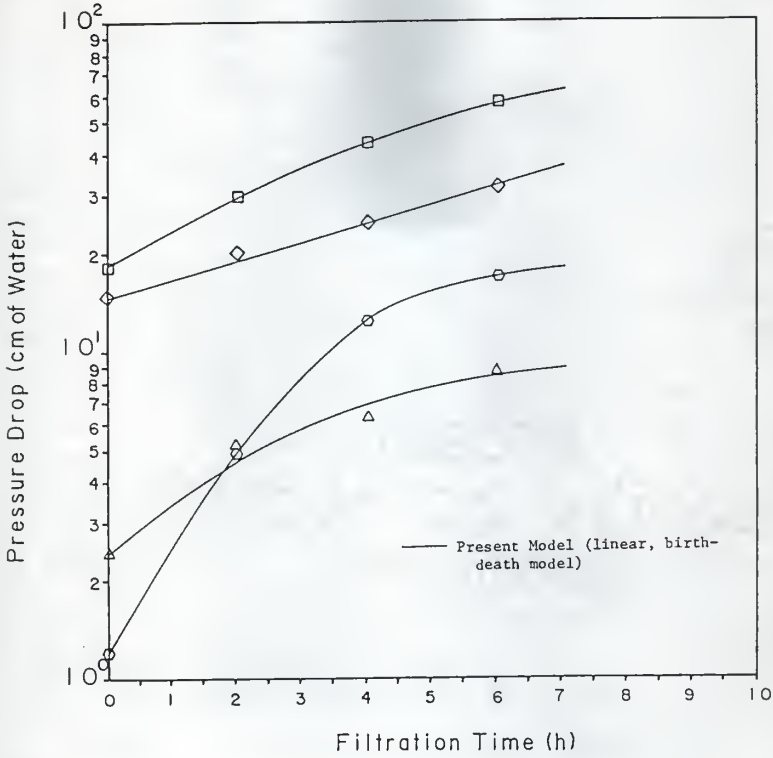

Figure V-7. Fitting the present model to Rimer's data (1968): bed depth (60.96 cm: anthracite, 20.32 cm, d_a: 0.100 cm; sand, 20.32 cm, d_s=0.071 cm, garnet 20.32 cm, d_g=0.059 cm), flow rate (7.3 m/h). Run VII-2; ○: first compartment (0 ∿ 13.97 cm), α=0.778 h^{-1}, β=0.055 h^{-1}, △: second compartment (13.97 ∿ 21.08 cm), α=0.367 h^{-1}, β=0.126 h^{-1}, ◇: third compartment (21.08 ∿ 60.96 cm), α=0.129 h^{-1}, β=0, □: lumped model (0 ∿ 60.96 cm), α=0.263 h^{-1}, β=0.076 h^{-1}.

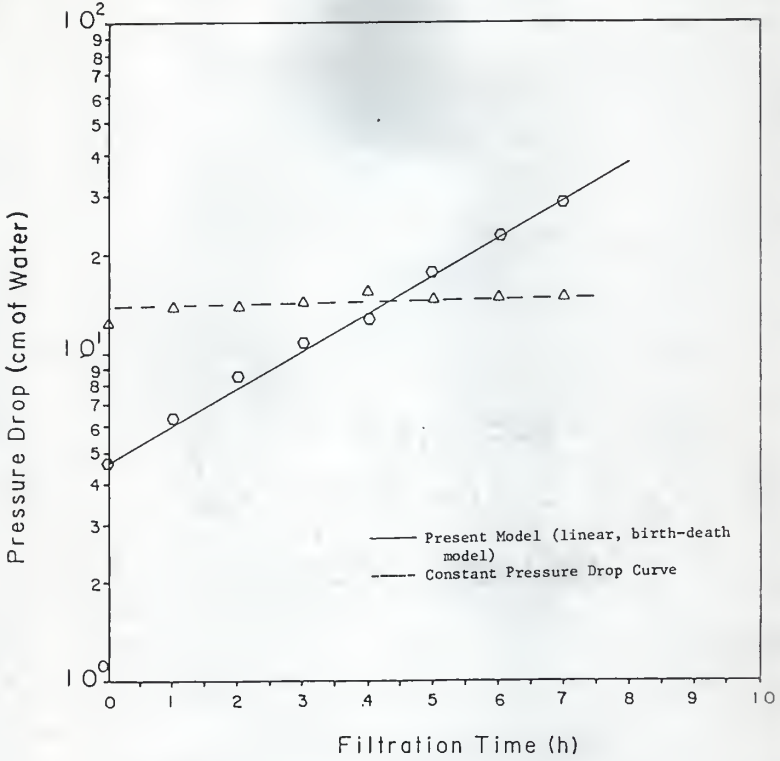

Figure V-8. Fitting the present model to Deb's data (1969): sand size (0.0647 cm), bed depth (61 cm), flow rate (4.9 m/h), Fuller's earth suspension (45×10^{-4} vol%).

Run I; ○: first compartment (0 ∿ 12.2 cm), α=0.261 h^{-1}, β=0,

△: second compartment (12.2 ∿ 60 cm).

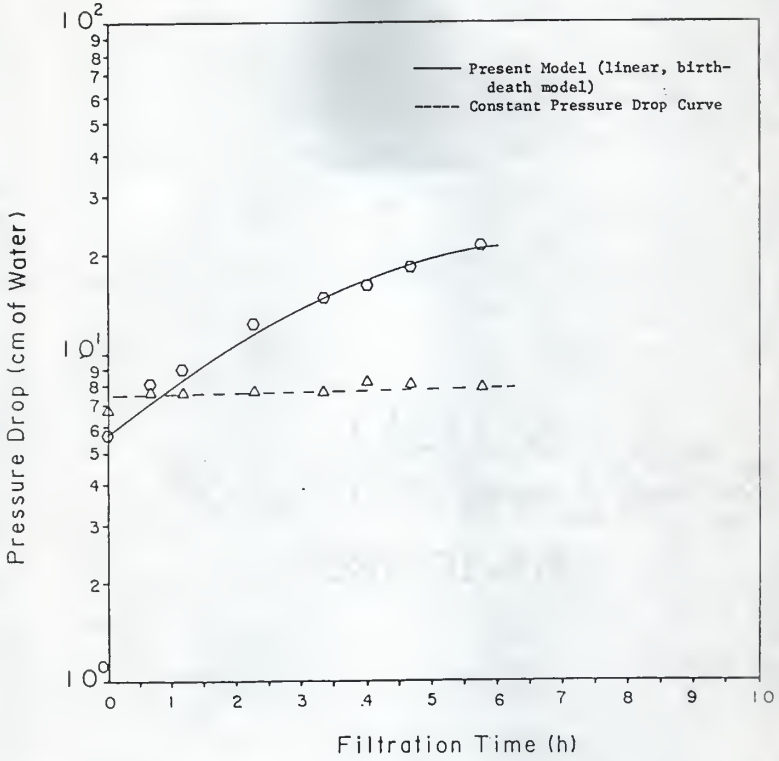

Figure V-9. Fitting the present model to Ives' data (1961): sand size (0.0544 cm), bed depth (20 cm), flow rate (4.9 m/h), chlorella algae suspension (135×10^{-4} vol%).

Run 1B; ○: first compartment (0 ∿ 9.2 cm), α=0.359 h^{-1}, β=0.102 h^{-1},

△: second compartment (9.2 cm ∿ 20 cm).

APPENDIX A. DERIVATION OF THE DETERMINISTIC GOVERNING EQUATION, EQ. V-12, IN THE TEXT

For any arbitrary functions f and g, the following expression holds (see, e.g., Van Kampen, 1981):

$$\sum_{n=0}^{N-1} g(n)\ \mathbb{E} f(n) = \sum_{n=1}^{N} f(n)\ \mathbb{E}^{-1} g(n) \tag{A-1}$$

For the case where

$$g(-1) = f(0) = g(N) = f(N+1) = 0,$$

Eq. A-1 becomes

$$\sum_{n=0}^{N} g(n)\ \mathbb{E} f(n) = \sum_{n=0}^{N} f(n)\ \mathbb{E}^{-1} g(n) \tag{A-2}$$

From Eq. V-11 in the text, the Master equation for the birth-death process is expressed as

$$\frac{dp_n(t)}{dt} = (\mathbb{E} - 1)\mu_n p_n(t) + (\mathbb{E}^{-1} - 1)\lambda_n p_n(t) \tag{A-3}$$

$$n = 0, 1, 2, \ldots, n_o$$

with

$$\lambda_{-1} = \mu_0 = \lambda_{n_0} = \mu_{n_0+1} = 0$$

Multiplying both sides of Eq. A-3 by the respective n's and summing all resultant equations from n=0 to $n=n_0$, we obtain

$$\frac{d\langle n\rangle}{dt} = \sum_{n=0}^{n_0} n(\mathbb{E} - 1)\mu_n p_n(t) + \sum_{n=0}^{n_0} n(\mathbb{E}^{-1} - 1)\lambda_n p_n(t) \tag{A-4}$$

From the property of the one-step operator as given in Eq. A-2, we see that Eq. A-4 is equivalent to

$$\frac{d\langle n\rangle}{dt} = \sum_{n=0}^{n_0} \mu_n p_n(t)(\mathbb{E}^{-1} - 1)n + \sum_{n=0}^{n_0} \lambda_n p_n(t)(\mathbb{E} - 1)n \qquad \text{(A-5)}$$

For the linear, birth-death process, the intensities of transition, λ_n and μ_n, take the following forms;

$$\lambda_n = \alpha(n_0 - n) \qquad \text{(A-6)}$$

and

$$\mu_n = \beta n \qquad \text{(A-7)}$$

Substitution of Eqs. A-6 and A-7 into Eq. A-5 yields

$$\frac{d\langle n\rangle}{dt} = -\beta\langle n\rangle + \alpha[n_0 - \langle n\rangle] \qquad \text{(A-8)}$$

This expression is the same as the deterministic governing equation, Eq. V-12, in the text, if $\langle n\rangle$ is replaced with $\bar{n}(t)$.

APPENDIX B. EXPANSION OF ONE-STEP OPERATOR, EQS. V-18 AND V-19, IN THE TEXT

Since

$$n = n_0\phi(t) + n_0^{1/2}\zeta$$

as indicated by Eq.

one is equivalent to the increase of ζ by $n_0^{-1/2}$. Expanding $\pi(\zeta+n_0^{-1/2},t)$ in the Taylor's series form, we obtain

$$\pi(\zeta+n_0^{-1/2},t) = \pi(\zeta,t) + n_0^{-1/2}\frac{\partial}{\partial\zeta}\pi(\zeta,t) + \frac{1}{2}n_0^{-1}\frac{\partial^2}{\partial\zeta^2}\pi(\zeta,t) + \ldots$$

$$= (1 + n_0^{-1/2}\frac{\partial}{\partial\zeta} + \frac{1}{2}n_0^{-1}\frac{\partial^2}{\partial\zeta^2} + \ldots)\pi(\zeta,t) \qquad \text{(B-1)}$$

This in conjunction with Eq. V-16 in the text,

$$\pi(\zeta,t) = n_0^{1/2}\,p(n,t),$$

yields

$$n_0^{-1/2}\,p(n+1,t) = (1 + n_0^{-1/2}\frac{\partial}{\partial\zeta} + \frac{1}{2}n_0^{-1}\frac{\partial^2}{\partial\zeta^2} + \ldots)n_0^{-1/2}p(n,t)$$

or

$$p(n+1,t) = (1 + n_0^{-1/2}\frac{\partial}{\partial\zeta} + \frac{1}{2}n_0^{-1}\frac{\partial^2}{\partial\zeta^2} + \ldots)p(n,t) \qquad \text{(B-2)}$$

Since

$$\mathbb{E}\,p(n,t) = p(n+1,\,t)$$

$$= (1 + n_0^{-1/2}\frac{\partial}{\partial\zeta} + \frac{1}{2}n_0^{-1}\frac{\partial^2}{\partial\zeta^2} + \ldots)\,p(n,t), \qquad \text{(B-3)}$$

we have

$$\mathbb{E} = 1 + n_0^{-1/2}\frac{\partial}{\partial\zeta} + \frac{1}{2}n_0^{-1}\frac{\partial^2}{\partial\zeta^2} + \ldots \qquad \text{(B-4)}$$

Similarly,

$$E^{-1} = 1 - n_0^{-1/2} \frac{\partial}{\partial \zeta} + \frac{1}{2} n_0^{-1} \frac{\partial^2}{\partial \zeta^2} - \cdots \qquad \text{(B-5)}$$

APPENDIX C. TRANSFORMATION METHOD USED IN EQUATION V-26 IN THE TEXT

The central-difference approximation gives

$$\frac{\partial}{\partial \zeta} f(\zeta) = \frac{f(\zeta + \Delta\zeta) - f(\zeta)}{\Delta\zeta} \tag{C-1}$$

and

$$\frac{\partial^2}{\partial \zeta^2} f(\zeta) = \frac{f(\zeta + \Delta\zeta) - 2f(\zeta) + f(\zeta - \Delta\zeta)}{(\Delta\zeta)^2} \tag{C-2}$$

Hence,

$$\Sigma g(\zeta) \frac{\partial}{\partial \zeta} f(\zeta) = g(\zeta)\left[\frac{f(\zeta + \Delta\zeta) - f(\zeta)}{\Delta\zeta}\right]$$

$$= \frac{1}{\Delta\zeta} \left[\Sigma g(\zeta) f(\zeta + \Delta\zeta) - \Sigma g(\zeta) f(\zeta)\right] \tag{C-3}$$

From the property of the one-step operator as indicated in Eq. A-2, we obtain

$$\frac{1}{\Delta\zeta}\left[\Sigma g(\zeta) f(\zeta + \Delta\zeta) - \Sigma g(\zeta) f(\zeta)\right]$$

$$= \frac{1}{\Delta\zeta}\left[\Sigma f(\zeta) g(\zeta - \Delta\zeta) - \Sigma f(\zeta) g(\zeta)\right]$$

$$= -\Sigma f(\zeta) \frac{\partial}{\partial \zeta} g(\zeta) \tag{C-4}$$

Eqs. C-3 and C-4 yield

$$\Sigma g(\zeta) \frac{\partial}{\partial \zeta} f(\zeta) = -\Sigma f(\zeta) \frac{\partial}{\partial \zeta} g(\zeta) \tag{C-5}$$

Similarly, we have

$$\Sigma g(\zeta) \frac{\partial^2}{\partial \zeta^2} f(\zeta) = \Sigma f(\zeta) \frac{\partial^2}{\partial \zeta^2} g(\zeta) \tag{C-6}$$

APPENDIX D. JUSTIFICATION OF THE INSTABILITY OF EQ. V-34 IN THE TEXT

The general solution of Eq. V-33 in the text takes the form

$$\langle\zeta\rangle = c(1 + \alpha\tau)^2 \qquad \text{(D-1)}$$

To satisfy the initial condition

$$\langle\zeta\rangle = 0 \quad \text{at } \tau = 0,$$

c must be zero. However, it is postulated that since the solution is an approximation; a slight variation possibly will exist in the initial value of $\langle\zeta\rangle$ so that c may take a small value other than zero. Notice that for a nonzero c, $\langle\zeta\rangle$ grows with time as indicated in Eq. D-1. Thus, a nonzero c implies that as the time elapses, $\langle\zeta\rangle$ will increase to such a large value that the assumption of the fluctuating term being of order $n_0^{1/2}$, as given in Eq. V-15 in the text, is no longer valid. It is worth noting, therefore, that if c is not zero, the expansion technique employed in the text need be further justified for a large time.

The applicability of the second-order, pure birth model developed in the text is examined here. For the filtration process, only the initial operating period is of interest; the operation need be terminated by the time the pressure drop buildup becomes too high or the filter fails to achieve the required quality of filtrate. Furthermore, the number of open pores, n_0, is very large, which substantially minimizes the fluctuations. To estimate the deviation involved in the model by assuming that c=0.01, let us consider the pressure drop data from the first compartment (0 $\sim$ 4.27 cm) of the filter of Eliassen (1935). The filter bed had a cross-sectional area of 1876.64 cm^2. The porosity of grains packed in the bed has been determined to be 0.41. The diameter of suspended solids is 0.00124 cm. By assuming that the size of the pores is 5 times that of the suspended solids, the number of open pores, n_0, is then calculated as

$$\frac{(4.27)(1876.64)(0.41)}{5\pi(0.00124)^3/6} = 6.58 \times 10^{11}$$

Obviously, n_0 is indeed a large number with an order of 10^{11}. The duration of Run 6, expressed in terms of dimensionless time, $\alpha\tau$, is 12.3 as given in Figure V-3 in the text. The mean number of blocked pores, $\langle n \rangle$, consists of the macroscopic and fluctuating terms as given in Eq. V-28 in the text, i.e.,

$$\langle n \rangle = n_0\phi + n_0^{1/2}\langle\zeta\rangle \tag{D-2}$$

Substituting the solution for ϕ and $\langle\zeta\rangle$ as given in Eqs. V-32 and V-36, respectively, in the text into this expression gives

$$\langle n \rangle = \frac{n_0\alpha\tau}{1 + \alpha\tau} + cn_0^{1/2}(1 + \alpha\tau)^2 \tag{D-3}$$

Substitution of the values of n_0, $\alpha\tau$, and c into this expression yields the mean number of blocked pores at the end of filtration as

$$\langle n \rangle = \frac{(6.58 \times 10^{11})(12.3)}{(1 + 12.3)} + (0.01)(6.58 \times 10^{11})^{1/2}(1 + 12.3)^2$$

$$= 6.058 \times 10^{11} + 1.435 \times 10^6$$

Notice that the fluctuating term (second term) is merely 2.36×10^{-4}% of the macroscopic term (first term). It is conceivable, therefore, that even toward the end of filtration, the fluctuating term is still negligible compared with the macroscopic term. Based on these observations, we believe that the second-order, pure birth model is indeed applicable.

APPENDIX E. DERIVATION OF EQUATION V-44 IN THE TEXT

The differential equation, Eq. A-8, describes the linear, birth-death process as

$$\frac{d\langle n\rangle}{dt} = -\beta\langle n\rangle + \alpha[n_0 - \langle n\rangle] \tag{E-1}$$

Solution of this equation subject to the initial condition

$$\langle n\rangle = 0 \quad \text{at} \quad t = 0 \tag{E-2}$$

gives

$$\langle n\rangle = \alpha n_0 \{\frac{1 - e^{-(\alpha+\beta)t}}{\alpha + \beta}\} \tag{E-3}$$

Substitution of this expression into Eq. V-40 in the text yields

$$v(t) = v_0 \{\frac{\alpha + \beta}{\beta + \alpha e^{-(\alpha+\beta)t}}\} \tag{E-4}$$

This equation in conjunction with Eq. V-42 in the text results in

$$-\frac{\Delta P(t)}{L} = 150(\frac{1 - \varepsilon}{\varepsilon})^2 \frac{\mu v_0}{d_p^2} \{\frac{\alpha + \beta}{\beta + \alpha e^{-(\alpha+\beta)t}}\}$$

$$= (-\frac{\Delta P}{L})_0 \{\frac{\alpha + \beta}{\beta + \alpha e^{-(\alpha+\beta)t}}\} \tag{E-5}$$

CHAPTER VI EXPERIMENTAL STUDY OF DEEP BED FILTRATION: Stochastic Analysis

In Chapters IV and V, stochastic models, namely, the linear, birth-death and second-order, pure birth processes, coupled with the Carman-Kozeny equation, have been employed to simulate the pressure drop and its temporal change during a filtration run.

Performance of a deep bed filter depends on a large number of variables including the size distribution of suspended solids, suspension concentration, filtration rate, and bed characteristics. The latter two variables have been widely investigated by numerous researchers (Rimer, 1968; Deb, 1969; Tchobanoglous, 1970; Tchobanoglous and Eliassen, 1970; Huang, 1972). The primary concern of the work presented in this chapter is to investigate experimentally the effect of the size distribution and concentration of suspended solids on the pressure drop dynamics within the filter bed; the results are treated stochastically.

EXPERIMENTAL FACILITIES AND METHODS

A schematic of the experimental set-up is shown in Figure VI-1. The set-up comprised an upflow deep bed filter, a suspension tank, a water tank, two pumps, a differential pressure transducer, a transducer indicator, and a strip chart recorder. The plexiglass filter had an inside diameter of 0.132 m and a length of 0.406 m between the bottom distributor plate and the outlet. The filtering medium consisted of - #20 to + #30 (20x30) mesh silica sand with an average diameter of approximately 0.710 mm and a density of 2600 kg/m^3. The bed of sand, 5 cm in depth, was supported between a bottom distributor plate and a top movable porous plate. These plates retained the sand particles but allowed the suspension to flow through.

The suspension was composed of coal particles dispersed in water.

Five different size ranges of coal particles, which were carefully sieved at least three times, were used in this work; these size ranges are outlined in Table VI-1. For each specific size range of coal particles, the suspension concentration ranged approximately from 0.001 to 0.015 weight percent (wt%). The coal particles were maintained in water in the suspension tank by agitating it with a 1/4 HP twin propeller mixer.

The porosity of the bed was dependent on the packing conditions; it ranged from 0.43 under the least dense static condition to 0.35. Prior to a filtration run, the sand was allowed to settle and form a bed with a porosity of around 0.38 with the top porous plate placed and maintained at a position immediately above the sand. The influent concentration, pH and temperature of the suspension were measured before each filtration run. Suspension from the suspension tank was introduced at a constant rate of 48.8 m/h to the bottom of the filter by a HYPRO piston pump. The suspension was then allowed to flow upward through the filter.

The pressure drop increase in the filter bed was monitored with a variable reluctance pressure transducer which was connected to pressure taps positioned below the bottom distributor plate and near the outlet of the filter, as shown in Figure VI-1. A strip chart recorder connected to the pressure transducer continuously recorded the change in the pressure drop during a filtration run. The pressure drop attributable to the column wall and porous plates was measured by passing water through the empty column at the same rate of 48.8 m/h; it was determined to be 1.73 cm H_2O. This amount was subtracted from the recorded pressure drop to obtain the pressure drop through the filter bed. Samples of the filtrate were collected intermittently from the effluent flowing through the outlet without disturbing the performance of the filter. These samples were then filtered in a 200 ml pressure filter to determine the solids content.

The filter was cleaned by fluidizing the entire bed with water to remove the deposited solids. During this period, the upper porous plate was raised to a position well above the fluidized sand particles. The coal particles were easily flushed from the filter in this manner. With the bed regenerated, the filtration cycle could be reinitiated.

RESULTS AND DISCUSSION

Five sets of filtration runs, namely, runs of series A, B, C, D, and E, were conducted with suspended solids of various sizes, size distributions, and concentrations. For each run, the pressure drop and the effluent concentration were measured as functions of filtration time.

Modeling of Pressure Drop Dynamics

Stochastic models which simulate the pressure drop dynamics within the filter bed under the constant flow condition are categorized into two classes, the linear, birth-death and second-order, pure birth processes, as presented in Chapters IV and V, respectively.

Models. The linear, birth-death model assumes that the blockage intensity, λ_n, and the scouring intensity, μ_n, are linearly proportional to the number of open pores and the number of blocked pores in the bed, respectively (Litwiniszyn, 1968a; 1968b; 1969). This assumption of linearity gives rise to

$$\lambda_n = \alpha(n_0 - n); \qquad n = 0, 1, 2, \ldots, n_0 \qquad \text{(VI-1)}$$

$$\mu_n = \beta n; \qquad n = 0, 1, 2, \ldots, n_0 \qquad \text{(VI-2)}$$

where n_0 is the total number of open pores susceptible to blockage in the bed, α is the blockage constant, and β is the scouring constant. As presented in Chapter IV, the mean number of blocked pores at the moment t, $\langle n \rangle$, can be solved based on the assumption given in Eqs. VI-1 and VI-2. Relating the mean number of blocked pores to the linear or interstitial velocity of the flow and incorporating the resultant expression into the Carman-Kozeny

equation give

$$(-\frac{\Delta P(t)}{L}) = 150(\frac{1-\varepsilon}{\varepsilon})^2 \frac{\mu V_0}{d_p^2} \{\frac{\alpha+\beta}{\beta+\alpha e^{-(\alpha+\beta)t}}\} \qquad \text{(VI-3)}$$

Under the simplifying assumption that the increase in the pressure drop can be attributed to that of the linear velocity of the flow, we have

$$(-\frac{\Delta P(t)}{L}) = (-\frac{\Delta P_0}{L}) \{\frac{\alpha+\beta}{\beta+\alpha e^{-(\alpha+\beta)t}}\} \qquad \text{(VI-4)}$$

or

$$\frac{[-\Delta P(t)]}{[-\Delta P_0]} = \frac{\alpha+\beta}{\beta+\alpha e^{-(\alpha+\beta)t}} \qquad \text{(VI-5)}$$

where $[-\Delta P(t)]$ represents the pressure drop through the bed at moment, t, and $[-\Delta P_0]$ that at the onset of filtration. Notice that if the scouring is negligible, i.e.,

$$\mu_n = 0$$

or

$$\beta = 0$$

the linear, birth-death process reduces to the linear, pure birth process (Litwiniszyn, 1963; Hsu and Fan, 1984). The resultant equation is

$$\frac{[-\Delta P(t)]}{[-\Delta P_0]} = e^{\alpha t} \qquad \text{(VI-6)}$$

The second-order, pure birth model assumes that λ_n is proportional to the square of the number of open pores in the bed, and μ_n is negligible. This assumption gives rise to

$$\lambda_n = (n_0 - n)^2; \qquad n = 0, 1, 2, \ldots, n_0 \qquad \text{(VI-7)}$$

$$\mu_n = 0; \qquad n = 0, 1, 2, \ldots, n_0 \qquad \text{(VI-8)}$$

As presented in Chapter V, the Master equation governing the probability

balance can be solved approximately by means of the so-called expansion technique. This technique yields the mean number of blocked pores and subsequently results in the following equation;

$$\frac{[-\Delta P(t)]}{[-\Delta P_0]} = 1 + kt \qquad \text{(VI-9)}$$

where

$$k = \alpha n_0 \qquad \text{(VI-10)}$$

Comparison of pressure drop data with models. The present models consider the entire bed as a single spatially-lumped compartment. For the filter bed with a depth of merely 5 cm, it is conceivable that such lumped models are satisfactory.

In Runs A-1 through A-9, the suspension filtered was composed of - #270 to + #400 (270x400) mesh coal particles with an average diameter of approximately 0.044 mm. The pressure drop was measured as a function of filtration time for each run; the results of Run A-1, A-4, and A-8 are shown in Figure VI-2. This figure shows that the change in the pressure drop through the bed can be described reasonably well by the linear, birth-death model (Eq. VI-5).

The suspension, used in Runs B-1 through B-9, comprised - #250 to + #270 (250x270) mesh coal particles with an average diameter of approximately 0.058 mm. The pressure drop data from Runs B-2, B-5, and B-9 are plotted against the filtration time in Figure VI-3. This figure demonstrates that the change in the pressure drop through the bed also exhibits the linear, birth-death behavior.

The suspension, filtered in Runs C-1 through C-6, consisted of - #140 to + #200 (140x200) mesh coal particles with an average diameter of approximately 0.090 mm. The pressure drop data from Runs C-1, C-4, and C-6 are

plotted in Figure VI-4. This figure indicates that the change in the pressure drop through the bed obeys essentially the second-order, pure birth process (Eq. VI-9).

In Runs D-1 through D-6, the suspension filtered was composed of - #100 to + #140 (100x140) mesh coal particles with an average diameter of approximately 0.127 mm. The pressure drop was measured as a function of filtration time for each run; the results of Runs D-1, D-4, and D-6 are shown in Figure VI-5. This figure shows that the change in the pressure drop during the initial period of a filtration run reflects the linear, pure birth behavior (Eq. VI-6). However, it also shows a departure from the predicted behavior in the later stage of the filtration run. Note that the diameter ratio of coal particles to grains is up to 0.18, indicating that a surface mat of deposit will form on the bottom of the filter during the later stage of a filtration run. This implies that the deep bed filtration will tend to resemble the cake filtration; the entire bed simply serves as the medium for the cake formation of coal particles during this period. Therefore, the pressure drop increase will certainly be greater that predicted for the deep bed filtration. Naturally, this phenomenon of cake formation is undesirable and should be avoided in the design of the deep bed filter.

In Runs E-1 through E-13, the suspension filtered consisted of - #100 to + #270 (100x270) mesh coal particles with an average diameter of approximately 0.101 mm; that is, a wider size range of coal particles was employed in the filtration runs to observe the combined effect of all possible mechanisms predicted by the present models. It appears that the combined mechanism of the linear, pure birth process and cake filtration predominates over either the linear, birth-death or second-order, pure birth mechanism as shown in Figure VI-6. Notice that the pressure drop increase in the

filter bed tends to be larger than that in any of the previous runs for the same suspension concentration. Similarly, the capacity of the filter with unisized grains is greater than that with grains varying widely in size; that is, the pressure drop increase in the former is smaller than that in the latter (Streander, 1940). These results imply that the size uniformity of grains or suspended solids may reduce the tendency of suspended solids to clog the bed, thus reducing the rate of pressure drop increase.

Analysis of Effluent Concentration Data

The effluent concentrations of suspended solids for Runs A-1, A-2, A-5, and A-8 are plotted as functions of filtration time in Figure VI-7. Note that the effluent concentrations increase with filtration time. This is indeed indicative of the existence of the scouring phenomenon within the bed; recall that the scouring rate increases with an increase in the deposit as indicated in Eq. VI-2. This monotonically increasing trend is also observed in the effluent concentration data for Run B-1 as shown in Figure VI-8. Therefore, the use of the linear, birth-death model is more than adequate for representing the pressure drop dynamics in Runs A and B.

For Run C-1, the effluent concentration of suspended solids was measured as a function of filtration time as shown in Figure VI-9. Notice that the data do not show the monotonically increasing trend; they seem to be independent of filtration time. Thus, the second-order, pure birth model, for which the scouring mechanism is assumed to be negligible, need be employed to depict the pressure drop dynamics in Runs C-1 through C-6.

The effluent or filtrate obtained from each of Runs D-1 through D-6 was essentially clean water. This implies that during a filtration run the rapid clogging of suspended solids around the entrance section of the bed will be significant. It is plausible, therefore, that the cake filtration dominated in these filtration runs.

Effect of Suspension Concentration

The pressure drop dynamics in Runs A-1 through A-9 and in Runs B-1 through B-9 can be depicted by the linear, birth-death model with two parameters, namely, the blockage constant, α, and the scouring constant, β. The suspension concentration ranged from 0.0147 wt% for Run A-1 to 0.0015 wt% for Run A-9, and it ranged from 0.0084 wt% for Run B-1 to 0.0013 wt% for Run B-9. The dependence of α and β on the suspension concentration for the runs of series A is illustrated in Figure VI-10 and that for the runs of series B is shown in Figure VI-11. Both figures indicate that α and β increase with an increase in the suspension concentration. Notice that β drops sharply to approach zero. This implies that the blockage mechanism will predominate over the scouring mechanism while the suspension becomes sufficiently dillute, thus giving rise to the linear, pure birth process.

The second-order, pure birth model is employed to simulate the pressure drop characteristics in Runs C-1 through C-6. The suspension concentration employed ranged from 0.0101 wt% for Run C-1 to 0.0018 wt% for Run C-6. The dependence of the constant, k, defined in Eq. VI-10, on the suspension concentration is shown in Figure VI-12. It appears that k also increases with an increase in the suspension concentration.

The linear, pure birth model can be employed to describe the change in the pressure drop during the earlier period of a filtration run in Runs D-1 through D-6 and in Runs E-1 through E-13. The suspension concentration ranged from 0.0104 wt% for Run D-1 to 0.0036 wt% for Run D-6, and it ranged from 0.0122 wt% for Run E-1 to 0.0031 wt% for Run E-13. The dependence of the blockage constant, α, on the suspension concentration for the runs in series D is depicted in Figure VI-13, and that for the runs of series E is shown in Figure VI-14. Both figures show that α increases with an increase in the suspension concentration.

Effect of Size and Size Distribution of Suspended Solids

Figure VI-15 illustrates the effect of the size distribution of suspended solids on the dynamic behavior of pressure drop through the bed for the same suspension concentration of 0.0073 wt%. As the particle size increases, the pressure drop dynamics undergo transition from the linear, birth-death behavior, through the second-order, pure birth behavior, to the linear, pure birth behavior; they eventually exhibit the characteristics of the cake filtration. Notice that the smaller the size of suspended particles, the easier they escape from the bed. It can be postulated that relatively speaking, the small particles, once deposited in the bed, will tend to be easily scoured by the forces acting on them. On the contrary, the large suspended particles tend to be trapped within the bed. This implies that as the size of suspended particles increases to a certain degree, the particles will be unable to penetrate into the bed to any great extent before being captured by the grains. And thus, a "cake" of suspended particles will begin to build up, and a sharp increase in the pressure drop will be observed as can be seen in Figures VI-5 and VI-6.

Table VI-1. Size of suspended coal particles employed in the experiments.

Runs	size mesh	mean particle diameter mm
series A	- #270 to + #400	0.044
series B	- #250 to + #270	0.058
series C	- #140 to + #200	0.090
series D	- #100 to + #140	0.127
series E	- #100 to + #270	0.101

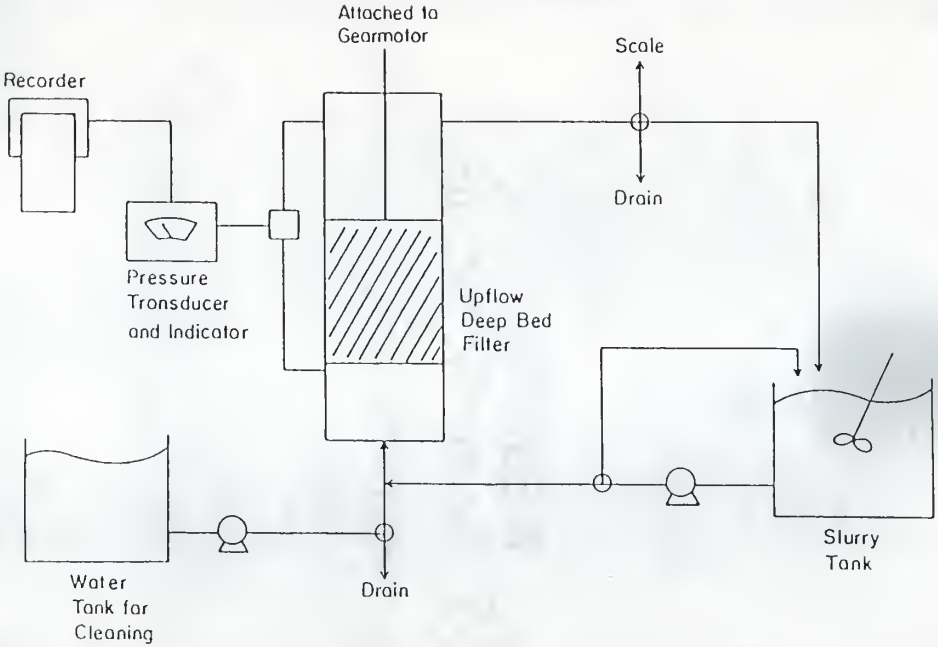

Figure VI-1. Schematic diagram of the experimental set-up.

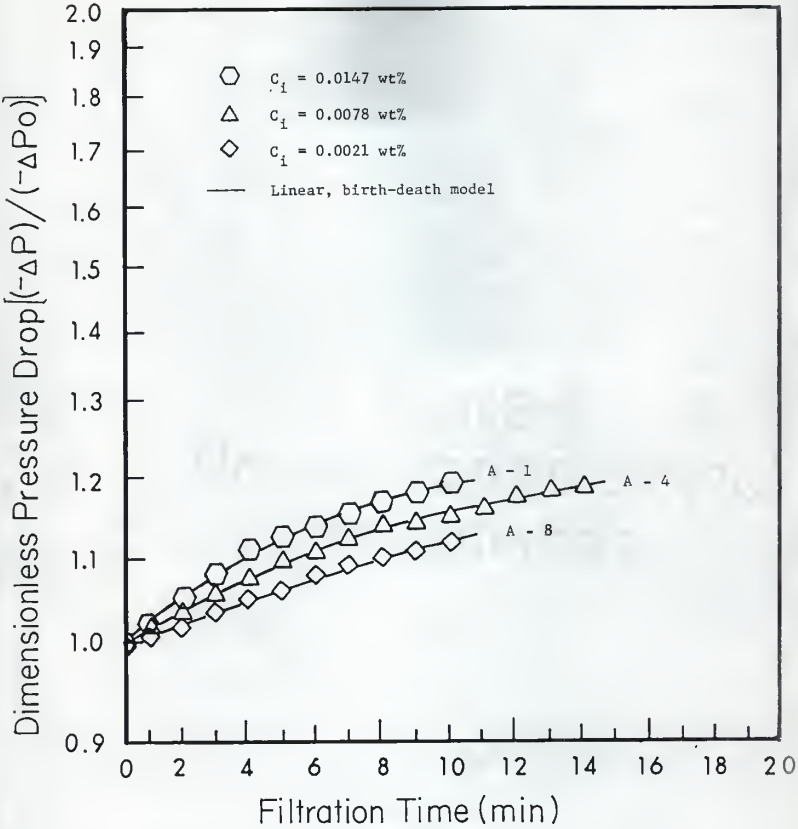

Figure VI-2. Increase in the pressure drop as a function of filtration time :
Runs; A-1 (α = 0.0324 min^{-1}, β = 0.1277 min^{-1}, pH = 9.1, T = 20.6°C),
A-4 (α = 0.0237 min^{-1}, β = 0.0953 min^{-1}, pH = 9.0, T = 20.8°C),
A-8 (α = 0.0142 min^{-1}, β = 0.0374 min^{-1}, pH = 9.1, T = 20.7°C).

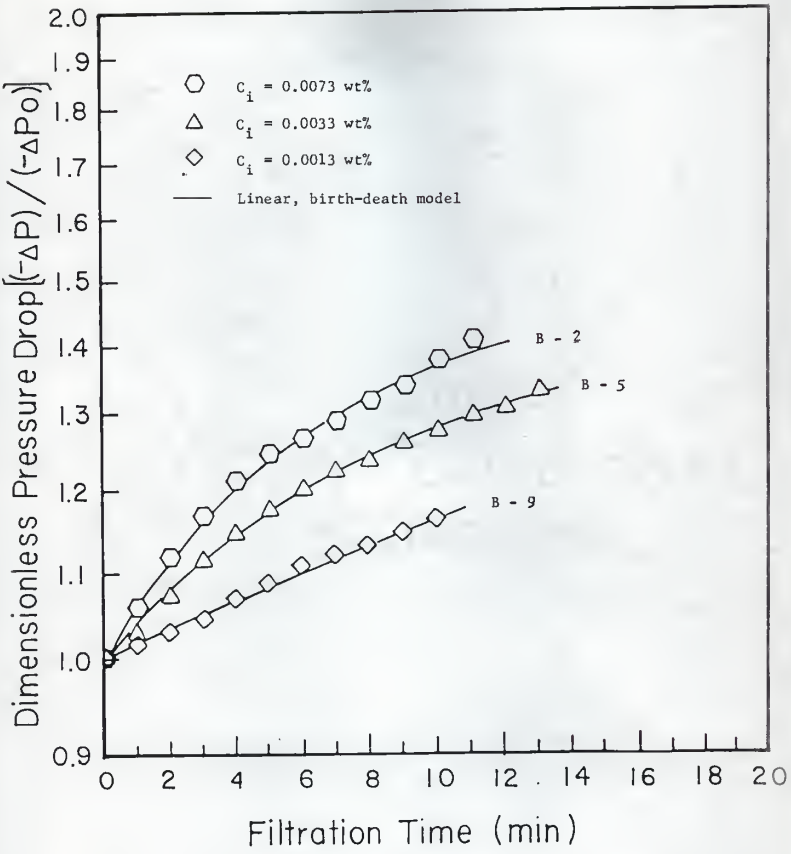

Figure VI-3. Increase in the pressure drop as a function of filtration time :
Runs; B-2 (α = 0.0593 min^{-1}, β = 0.1256 min^{-1}, pH = 9.0, T = 20.6 °C),
B-5 (α = 0.0409 min^{-1}, β = 0.0985 min^{-1}, pH = 9.1, T = 20.8 °C),
B-9 (α = 0.0159 min^{-1}, β = 0.0102 min^{-1}, pH = 9.1, T = 20.9 °C).

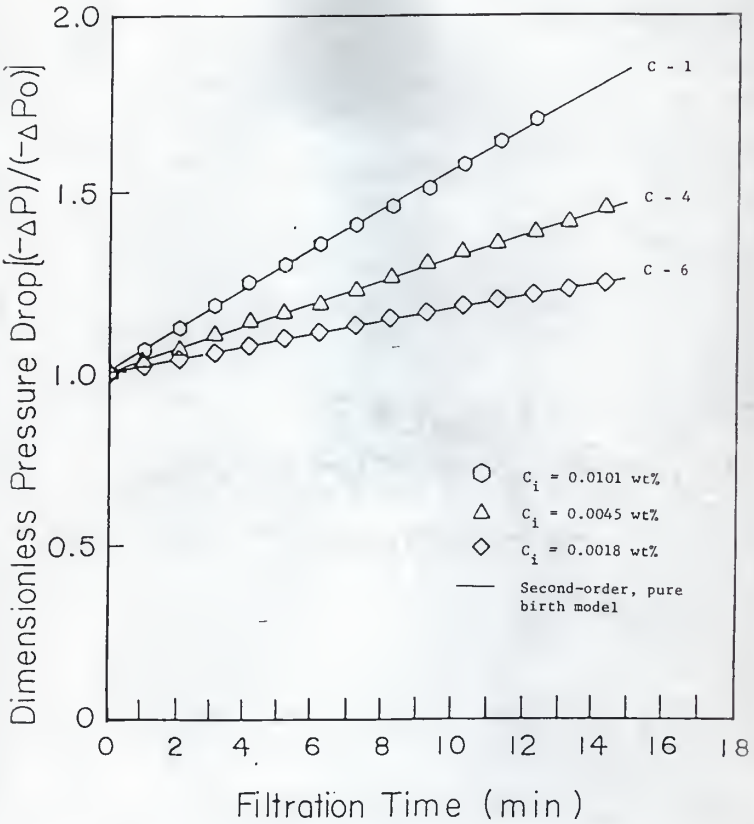

Figure VI-4. Increase in the pressure drop as a function of filtration time :
Runs; C-1 ($k = 0.0575\ min^{-1}$, pH = 8.5, T = 21.0°C),
C-4 ($k = 0.0321\ min^{-1}$, pH = 9.0, T = 19.6°C),
C-6 ($k = 0.0174\ min^{-1}$, pH = 9.1, T = 18.7°C).

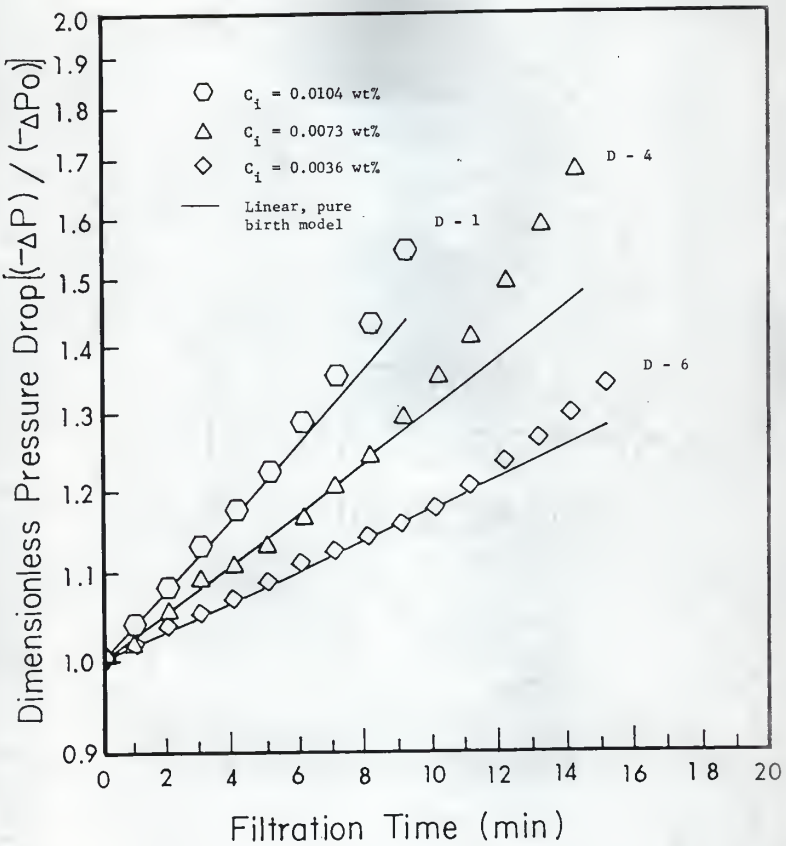

Figure VI-5. Increase in the pressure drop as a function of filtration time :
Runs; D-1 (α = 0.040 min^{-1}, pH = 8.7; T = 16.5 °C),
D-4 (α = 0.027 min^{-1}, pH = 8.9; T = 16.3 °C),
D-6 (α = 0.0162 min^{-1}, pH = 8.8; T = 16.3 °C).

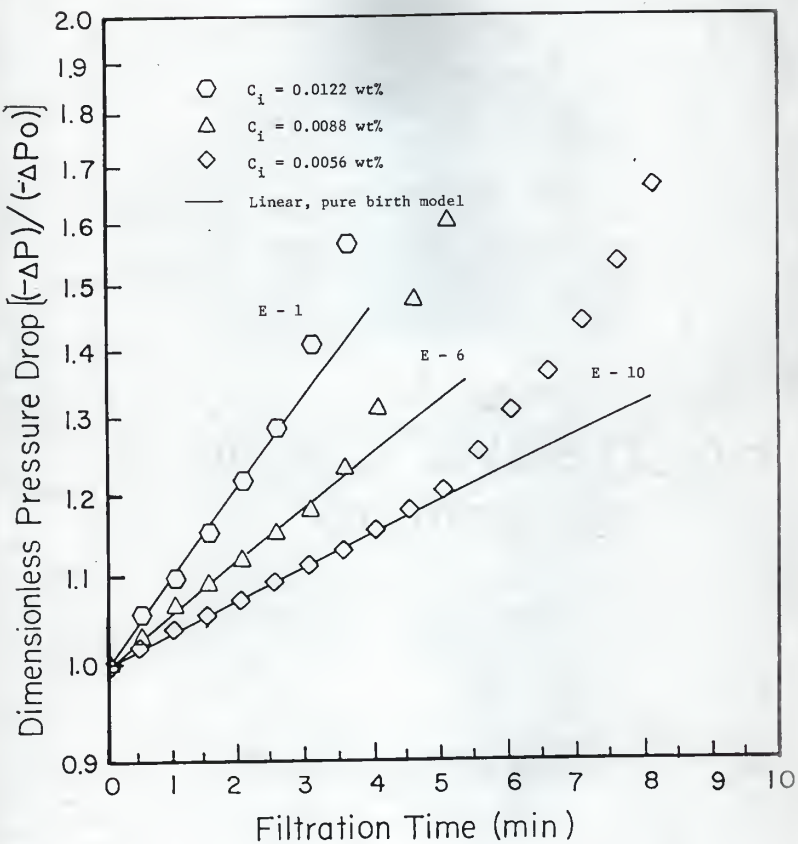

Figure VI-6. Increase in the pressure drop as a function of filtration time :
Runs; E-1 (α = 0.1000 min^{-1}, pH = 8.3, T = 21.9 °C),
E-6 (α = 0.0579 min^{-1}, pH = 8.6, T = 21.7 °C),
E-10 (α = 0.0357 min^{-1}, pH = 9.2, T = 22.3 °C).

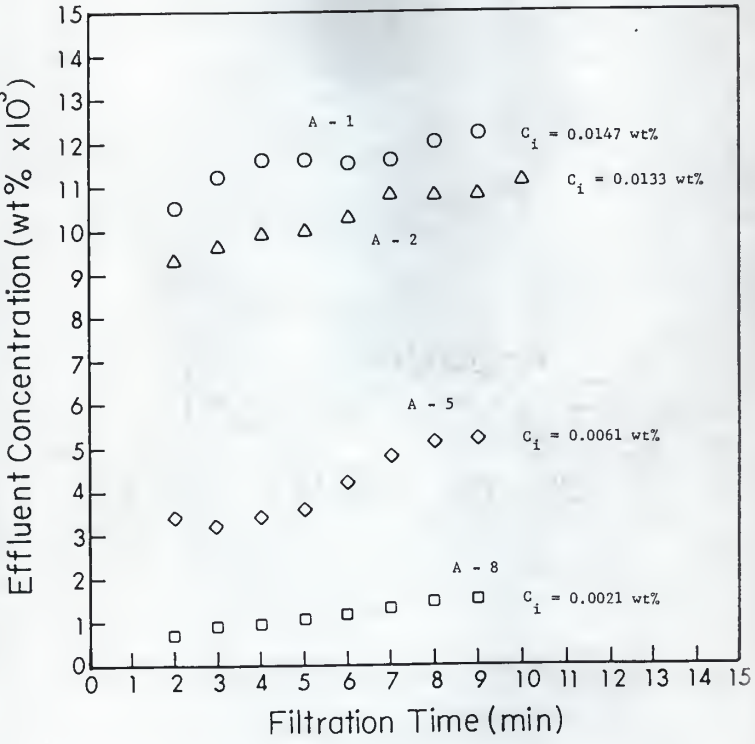

Figure VI-7. Effluent concentration of suspended particles as a function of filtration time : Runs A.

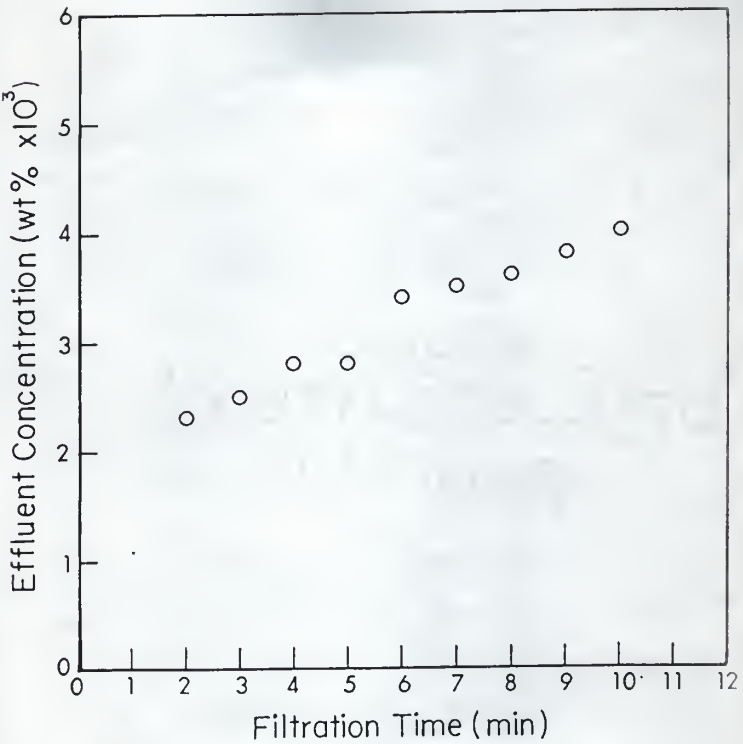

Figure VI-8. Effluent concentration of suspended particles as a function of filtration time : suspension concentration, 0.0084 wt%; Runs B-1.

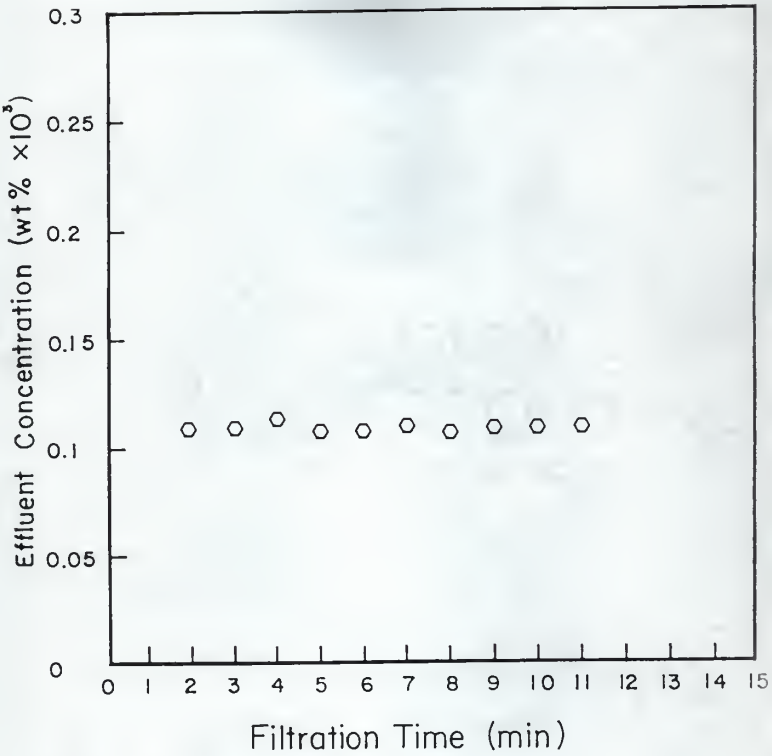

Figure VI-9. Effluent concentration of suspended particles as a function of filtration time : suspension concentration, 0.0101 wt%; Runs C-1.

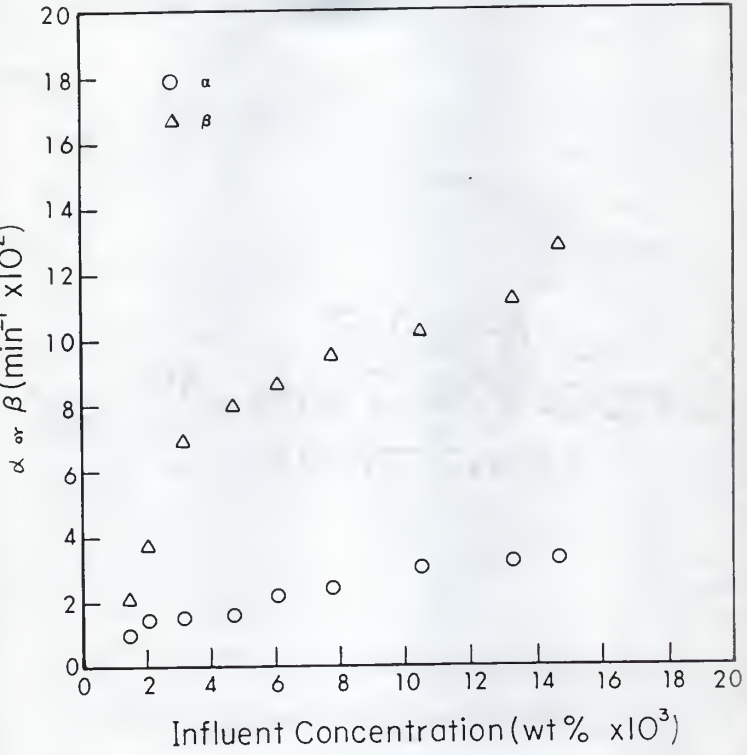

Figure VI-10. Dependence of the blockage constant, α, and the scouring constant, β, on the suspension concentration : Runs A-1 through A-9.

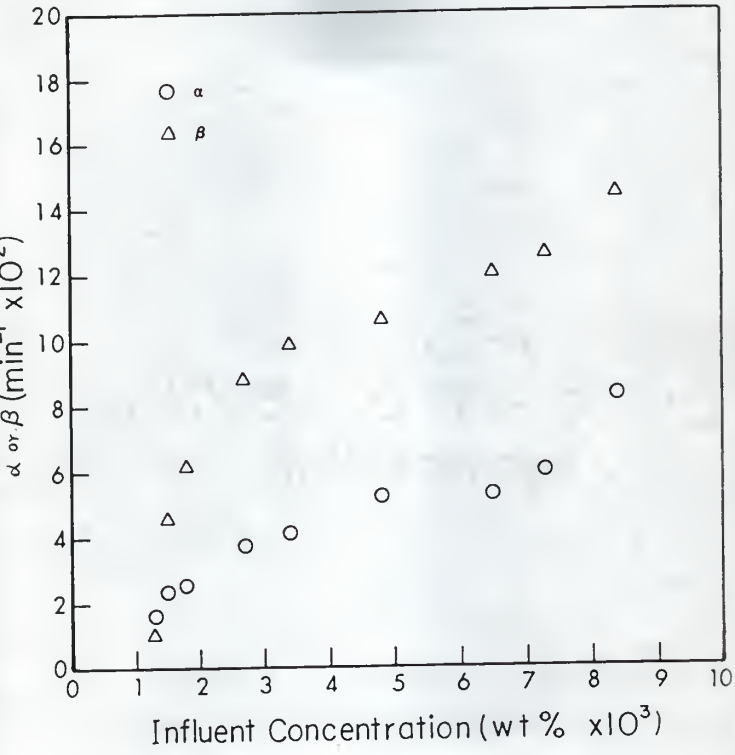

Figure VI-11. Dependence of the blockage constant, α, and the scouring constant, β, on the suspension concentration : Runs B-1 through B-9.

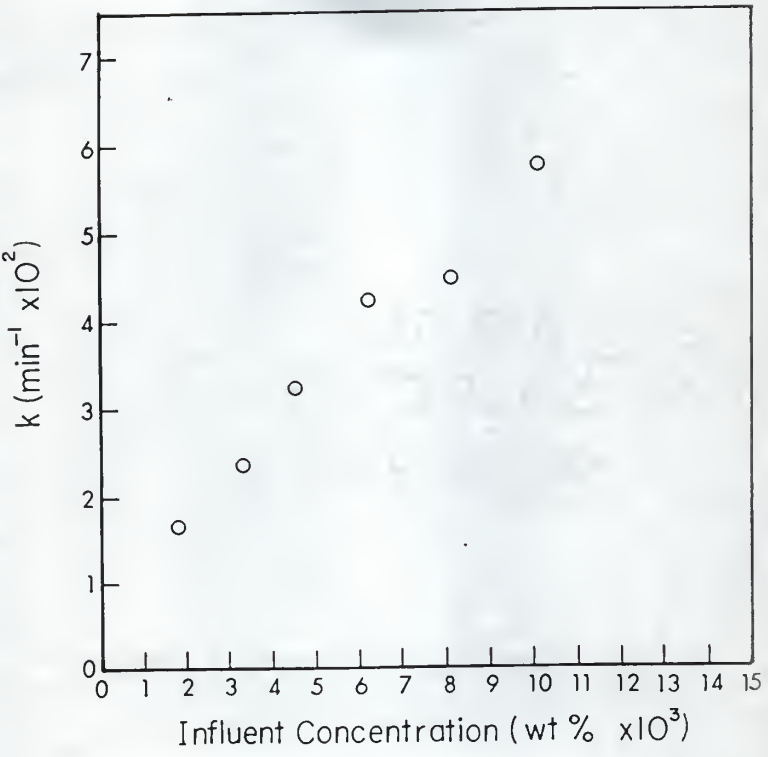

Figure VI-12. Dependence of the constant, k, on the suspension concentration : Runs C-1 through C-6.

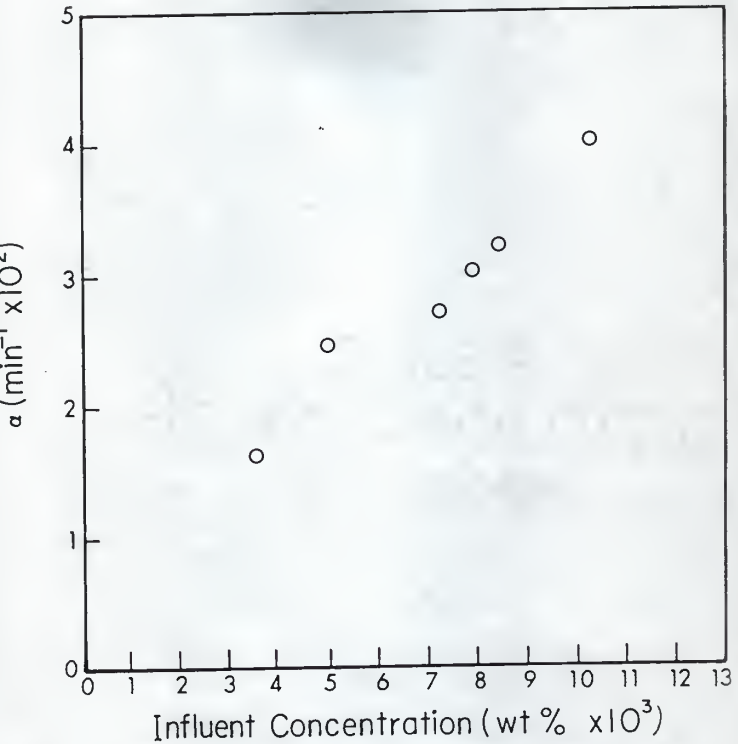

Figure VI-13. Dependence of the blockage constant, α, on the suspension concentration : Runs D-1 through D-6.

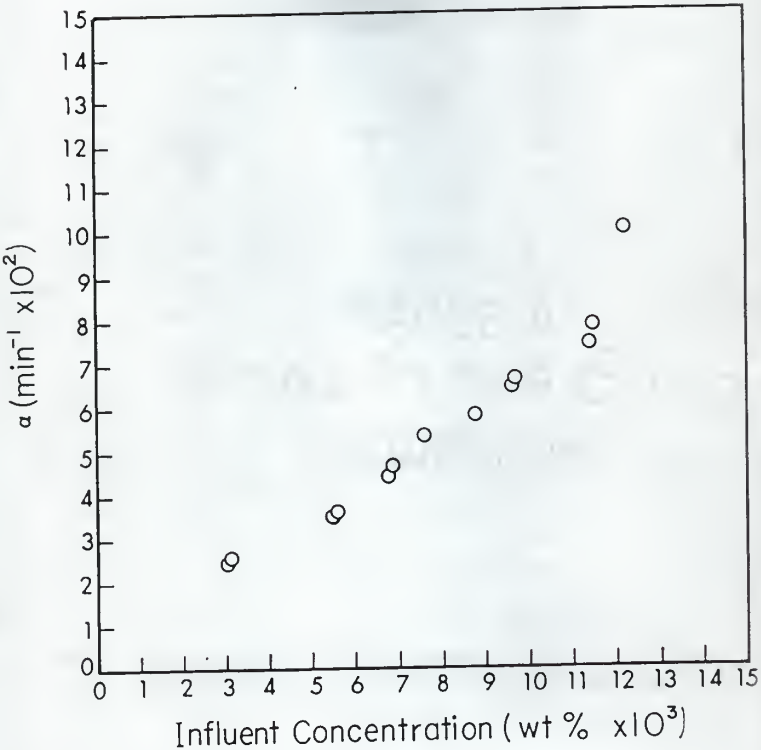

Figure VI-14. Dependence of the blockage constant, α, on the suspension concentration : Runs E-1 through E-13.

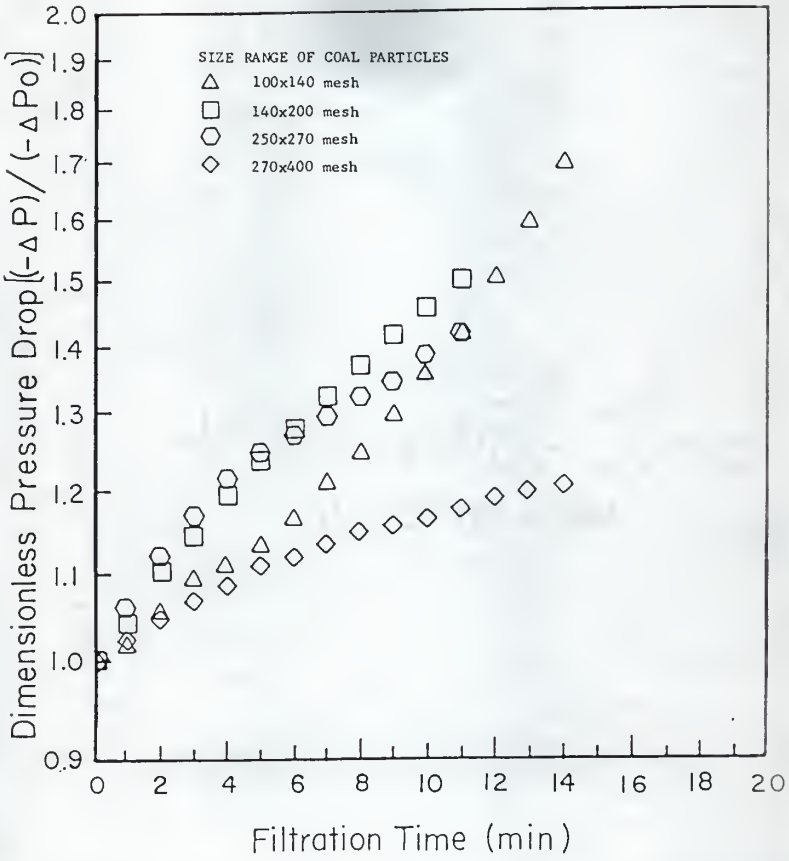

Figure VI-15. Increase in the pressure drop as a function of filtration time with the size of coal particles as the parameter : suspension concentration, 0.0073 wt%.

CHAPTER VII AN EXPERIMENTAL STUDY OF SEMIFLUIDIZED-BED FILTERS: Filtration of Suspended Solids with Narrow Size Ranges

Deep bed filters, also known as granular filters, are used extensively in purification of potable water and in treatment of waste water. The operation of deep bed filters is inefficient, however; it is typically characterized by the shallow penetration of suspended solids. As discussed in Chapter IV, Ives (1961) measured in detail the specific deposit as a function of time and bed position by means of the radioactive algae technique and concluded that the penetration of suspended solids through his deep bed filter was indeed shallow. The sectional analysis of the pressure drop dynamics within the deep bed filter presented in Chapter V indicates that the pressure drop through the last portion of the filter bed usually remains invariant with time and this unutilized portion can be as much as 80% of the entire bed as illustrated in Figure V-8 (Deb, 1969). Furthermore, a layer of filtered solids will usually collect on the surface and within the first few layers of the grains; that is, a "cake" of suspended solids will be formed around the entrance section of the bed, thus giving rise to an abrupt increase in the pressure drop. This phenomenon of "cake" formation has been discussed in Chapter VI (see Figures VI-11 and VI-13). The shallow penetration and "cake" formation lead to inefficient and short operation of the deep bed filters, thus requiring frequent backwashing (see, e.g., Diaper and Ives, 1965; Rimer, 1968; Huang, 1972).

To enhance the penetration of suspended solids into the filter, the size-graded sand filter was introduced to replace the unisized granular filter. The down-flow filter comprises sand of decreasing size in the direction of flow. The clean filter performs well; however, during the backwash cycle, the larger grains tend to settle to the bottom of the bed while the smaller ones tend to rise to the top, resulting in a reverse stratification in the filter. This eventually causes the filter performance to deteriorate (Diaper and Ives, 1965).

Reverse stratification of collector grains can be prevented by employing a multimedia filter. The multimedia filter is composed of layers of filtering media; the particle size of each succeeding layer decreases similar to the size graded filter, while the density of the media increases with each succeeding layer. The larger but lighter particles remain at the top of the bed and the smaller but heavier particles remain at the bottom during and after the backwash cycle. A typical multimedia filter consists of anthracite, sand, and garnet particles (Diaper and Ives, 1965; Rimer, 1968). Huang (1972) showed that filtration runs with a dual media filter of anthracite and sand were 60 to 160% longer than those obtained with a unisized sand filter were attainable. Similarly, Rimer (1968) showed that the average net yield was approximately 50% higher for water processed in the anthracite-sand-garnet filter than in the conventional sand filter. The results of these studies indicate that the performance of the sand filter is improved when a greater portion of the bed is utilized through the deeper penetration of solids.

The semifluidized-bed filter proposed by Wen and Fan (1979) has been employed to overcome the problem of the rapid clogging around the entrance section of the bed or the phenomenon of "cake" formation, which is usually experienced in the deep bed filtration. Unlike the multimedia filters, only a single medium, sand, is necessary. Initially, the bed will be in a completely fixed configuration as the fluid stream containing suspended solids enters the bed. The suspended solids, upon entering the portion of the bed around the entrance section, will be unable to penetrate the bed to any great extent before being stopped by the grains of sand. A "cake" of suspended solids will begin to be built up in this zone. The "cake" formation will produce a sharp increase in the pressure drop. This rise in the pressure drop will activate a driving mechanism which will raise the upper restraining plate. The mechanical movement of the restraining plate in conjunction with the forces being

exerted by the fluid stream will cause disruption of the formed "cake" of suspended solids into small fragments. Cake disruption will also be aided by the fluidized particles. Raising of the restraining plate and the disruption of the formed "cake" will continue until the breakthrough of the suspended solids occurs, which means the ever decreasing fixed bed can no longer achieve the required removal of the suspended solids from the suspension.

Another type of the semifluidized-bed filter has been proposed by Hsu and Fan (1981; 1982) and Fan and Hsu (1984) to overcome the problems of shallow solids penetration and rapid clogging simultaneously. In operating this filter, the filtration cycle starts with the restraining plate in a position forming the desired proportion of fixed to fluidized beds. During the filtration run, the fixed section functions as a deep bed filter in the capture of suspended solids. The fluidized section, on the other hand, provides the necessary turbulence in scouring the deposited solids, thus delaying the pressure drop increase.

The present work aimed to continue the investigation on the semifluidized-bed filter proposed by Hsu and Fan (1981; 1982) and Fan and Hsu (1984). However, instead of using suspended solids varying widely in size, such as sub #50 mesh coal particles used in their work, coal particles with several narrow size ranges were employed; these include - #270 to + #400 (270x400) mesh, - #250 to + #270 (250x270) mesh, - #140 to + #200 (140x200) mesh, and - #100 to + #140 (100x140) mesh coal particles. The primary interest was to investigate the effects of both the size of suspended solids and the "cake" formation on the performance of semifluidized-bed filters.

EXPERIMENTAL FACILITIES AND METHODS

A schematic of the experimental set-up is shown in Figure VII-1. The set-up consisted of a semifluidized-bed filter, a suspension tank, a water tank, two pumps, a differential pressure transducer, a transducer indicator,

and a strip chart recorder. The semifluidized-bed filter was constructed from a plexiglass column with an inside diameter of 0.132 m and a length of 0.406 m between the bottom distributor plate and the outlet. The filtering medium was composed of - #20 to + #30 (20x30) mesh silica sand with an average diameter of spproximately 0.710 mm and a density of 2600 kg/m^3.

The minimum fluidization velocity was determined experimentally to be 13.1 m/h. During a filtration run, suspension from the suspension tank was introduced at a constant rate of 48.8 m/h to the bottom of the filter by a HYPRO piston pump. For the operation of the deep bed filtration, the sand, 20 cm in depth (between 0.149 m and 0.349 m of the column) with the porosity of around 0.40, were supported between a bottom distributor plate and an upper movable restraining plate. These porous plates retained the sand but permitted the suspension to pass. This same amount of sand also served as the filtering medium for the operation of semifluidized-bed filters.

The suspension comprised coal particles dispersed in water. Coal particles of four different size ranges, which were carefully sieved at least three times, were employed; these size ranges are listed in Table VII-1. During a filtration run, the concentration of suspension was maintained constant in the suspension tank with agitation provided by a 1/4 HP propeller mixer.

By positioning the restraining plate at various heights, different ratios of the fixed-bed to fluidized-bed heights could be obtained. Prior to starting a filtration run under the constant influent concentration snd flow condition, the upper restraining plate was moved to a predetermined position, which would result in a desired degree of fluidization with the introduction of suspension. During s filtration run, the upper restraining plate was maintained at this position. For each suspension containing coal particles of specific size range, filtration with the semifluidized bed was performed with 75% or 50% fluidization, i.e., h_{pa}/h = 25% or 50%, respectively, in which h_{pa} represents the initial

fixed-bed height and h the entire bed height. Filtration runs with a completely fixed bed, namely, a 20 cm conventional deep bed filter, were also conducted under the same influent concentration and flow condition to provide a basis for comparison and evaluation.

The pressure drop increase through the filter bed was monitored with a variable reluctance pressure transducer which was connected to pressure taps positioned below the bottom distributor plate and near the outlet of the filter, as shown in Figure VII-1. A strip chart recorder connected to the pressure transducer indicator continuously recorded the change in the pressure drop during a filtration run. The pressure drop attributable to the column wall and porous plates was measured by passing water through the empty column at a constant rate of 48.8 m/h; it was determined to be 1.73 cm H_2O. This amount was subtracted from the recorded pressure drop to obtain the pressure drop through the filter bed. Samples of the filtrate were collected intermittently from the effluent flowing through the outlet without disturbing the performance of the filter. These samples were then filtered in a 20 mℓ pressure filter to determine the solids content.

The exhausted filter was cleaned by fluidizing the entire bed with water to remove the deposited solids. During this period, the upper restraining plate was raised to a poaition well above the fluidized sand as seen in Figure VII-2. The coal particles were easily flushed from the filter. With the bed regenerated, the filtration cycle could be re-activated.

RESULTS AND DISCUSSION

The results obtained with the semifluidized-bed filters, namely, the results from runs of series F, G, H, and I, are presented and compared to those obtained with the equivalent deep bed filters in Figure VII-3 through VII-14. Also presented are two sets of photographs taken during runs with two semifluidized-bed filters. One set, including Figures VII-9 and VII-11, is for the

filter with h_{pa}/h = 25% (Run I-2), and the other, including Figures VII-12 and VII-14, for the filter with h_{pa}/h = 50% (Run I-3).

Filtration of Relatively Small Particles

In Runs F-1 through F-3, the suspension was composed of - #270 to + #400 (270x400) mesh coal particles with an average diameter of approximately 0.044 mm. The influent concentration was maintained at 0.0227 wt% for each filtration run. The increase in the pressure drop across the entire bed was the largest for the deep bed filter (h_{pa}/h = 100%; Run F-1), and the smallest for the semifluidized-bed filter with 75% fluidization (h_{pa}/h = 25%; Run F-2) as seen in Figure VII-3.

The effluent concentration for all runs are plotted against the filtration time in Figure VII-4. The steadily increasing effluent concentrations are apparently indicative of the significant scouring effect in these runs; the only exception is Run F-2, in which the effluent concentration varies irregularly and tends to be smaller than that obtained by the deep bed filter. This exception was surprising in that the shortest fixed bed (25% of the entire bed height) tended to remove the largest amount of suspended solids. However, it was observed that during this run, the initial fixed bed was unstable; some of the sand detached from the bottom of the fixed bed into the fluidized portion of the bed, and as compensation, some of the fluidized sand deposited and filled these cavities. This detschment-deposition phenomenon continued throughout the filtration run. It is conceivable that this phenomenon induces a turbulent retarding action on the suspended solids, thus improving the removal efficiency. No phenomenon of "cake" formation was observed, and the operstion of the semifluidized-bed filters did not show distinct advsntage over that of the deep bed filter.

The suspension in Runs G-1 through G-3 contained - #250 to + #270 (250x270) mesh coal particles with an average diameter of approximately 0.058 mm. The influent concentration was kept at 0.0164 wt% for each run. The results of this set of runs, as shown in Figures VII-5 and VII-6, are quite similar to those

obtained in Runs F-1 through F-3. Again, for the particles of this size no "cake" formation was observed, and the operation of the semifluidized-bed filters did not show distinct advantage over that of the deep bed filter.

Filtration of Relatively Large Particles

In Runs H-1 through H-3, the suspension comprised - #140 to + #200 (140x200) mesh coal particles with an aversge diameter of approximately 0.090 mm. The influent concentration was maintained at 0.0149 wt% for each run. As indicated in Chapter VI, around 99% of the suspended solids with this size was removed with the 5 cm deep bed filter (see Figure VI-10), inferring that the shallow penetration of suspended solids will be significant in the operation of the 20 cm deep bed filter. Filtration runs were performed with the deep bed filter (Run H-1), the semifluidized-bed filter with h_{pa}/h = 25% (Run H-2), and the semifluidized-bed filter with h_{pa}/h = 50% (Run H-3). The change in the pressure drop for each run is plotted in Figure VII-7. In operating the deep bed filter (Run H-1), a sharp increase in the pressure drop was observed around 5 minutes after the onset of filtration. This is obviously indicative of the rapid clogging around the entrance section of the filter bed, that is, "cake" formation becoming significant. The results plotted in Figure VII-7 show that the capacity of the semifluidized-bed filters, reflected in the duration of filtration runs, was substantially higher than that of the deep bed filter; the duration of the semifluidized-bed filter with h_{pa}/h = 25% (Run H-2) was 2 times that of the deep bed filter (Run H-1), and a duration 3 times that of the deep bed filter was attained with the semifluidized-bed filter with h_{pa}/h = 50% (Run H-3). All the filters achieved essentially 100% removal of suspended solids except the semifluidized-bed filter with h_{pa}/h = 25% which yielded around 99% removal of suspended solids. This result is reasonable in that the thinner the fixed section, the lower the removal efficiency. Note, however, that this result is different from that observed in runs of series F; in these runs, the

semifluidized-bed filter with the shortest fixed section tended to remove the largest amount of suspended solids because of the detachment-deposition phenomenon discussed previously. It appears that the semifluidized-bed filter with h_{pa}/h = 50% had the best performance; the pressure drop buildup was the smallest without deterioration in the quility of the filtrate.

The suspension in Run I-1 through I-3 consisted of - #100 to + #140 (100x140) mesh coal particles with an average diameter of approximately 0.127 mm. The influent concentration was kept at 0.0140 wt% for each run. The results shown in Figure VII-8 resemble those in Figure VII-7. For the run with the deep bed filter (Run I-1), a sharp increase in the pressure drop was observed around 3 minutes after onset of the run. All the filters achieved essentially 100% removal of suspended solids. The duration of the semifluidized-bed filter with h_{pa}/h = 25% (Run I-2) was 3 times that of the deep bed filter (Run I-1), and a duration 5 times that of the deep bed filter was attained with the semifluidized-bed filter with h_{pa}/h = 50% (Run I-3). Again, the semifluidized-bed filter with h_{pa}/h = 50% exhibited the best performance.

Effect of the Size of Suspended Solids

Note that the size ratio of suspended solids to sand is an important parameter affecting the performance of a semifluidized-bed filter. As discussed in the previous sections, the larger the ratio, the more significant the shallow penetration and "cake" formation of suspended solids. It can concluded, therefore, that when the size ratio exceeds a certain value, the shallow penetration and "cake" formation of suspended solids become significant, and the use of the semifluidized-bed filters can substantially improve the efficiency of the operation as illustrated in Figures VII-7 and VII-8.

Structural Evolution of the Semifluidized-bed Filters

The photographic study, presented in Figures VII-9 through VII-14, depict clearly the structural evolution of the semifluidized-bed filters during operation.

Semifluidized-bed filter with $h_{pa}/h = 25\%$. Prior to a filtration run, the semifluidized-bed filter with $h_{pa}/h = 25\%$ had the configuration as seen in Figure VII-9. At the onset of operation, a fixed section and a fluidized section were formed in series in the semifluidized bed, in which the fixed-bed height was approximately 25% of the entire bed height. Initially, the entire bed acted like a deep bed filter with the fluidized section exerting relatively little effect on the operation. As the clogging in the fixed section became appreciable, the suspended solids could no longer penetrate into the fixed section. With the accumulation of the suspended solids in the fluidized section, the porosity of the fluidized section was reduced, rendering the linear velocity of flow in this section to increase. This, in turn, caused an increase in the drag forces exerted on the fluidized particles, forcing the suspended solids and fluidized sand to form an extended fixed section because the fluidized section could not expand. Notice that a predominant particles circulation pattern is often observed during the operation of a fluidized bed (see, e.g., Kunii and Levensipiel, 1977). Furthermore, this circulation pattern often skews to one side of the fluidized bed because of the difficulty in maintaining the completely uniform flow condition within the bed; the flow through the distributor plate is seldom totally uniformly distributed or the suspended solids are not uniformly captured in the fixed section. This nonsymmetrical flow pattern in the fluidized section resulted in a higher linear velocity of flow in one side of this section [see Figure VII-10(a)]. The flow with a higher linear velocity delivered an additional amount of particles to the interface between the fixed and fluidized sections, thereby extending the fixed section along this side [see Figure VII-10(a), 10(b)]. This increased the resistance to the flow and reduced the flow passing through it [see Figure VII-10(b)], which, in turn, altered the flow path, thereby causing the local linear velocity of flow along the extended fixed section to increase further and promoting the

continuous extension of the fixed section [see Figure VII-10(b), 10(c)]. This process continued during the run until the fixed section extended to the bottom distributor plate. It appears that instead of forming a layer of "cake" in the fixed section, most of the suspended solids distributes throughout the extended fixed section, thus reducing the rate of the pressure drop increase. The structural evolution of the semifluidized bed during the filtration run (Run I-2) is shown in Figure VII-11. These phenomena are similar to those observed by Hsu and Fan (1981).

Semifluidized-bed filter with $h_{pa}/h = 50\%$. Prior to a filtration run, the semifluidized-bed filter with $h_{pa}/h = 50\%$ had the configuration as seen in Figure VII-12 or Figure VII-13(a). The initial stage of the run was similar to that observed in the operation of the semifluidized-bed filter with $h_{pa}/h = 25\%$. However, instead of extending gradually, the fixed section extended rather rapidly along one side down to the bottom distributor plate [see Figure VII-13(b)]. Because of the high resistance to the flow on this side of the completely fixed section, almost all the flow began to pass through the fluidized section. Because of this flow bypassing, the extended fixed section barely contributed to the pressure drop. As the filtration run continued, an increasing amount of suspended solids and fluidized sand deposited themselves on the interface between the extended fixed section and fluidized section; subsequently, this action thickened the extended fixed section along the horizontal direction [see Figure VII-13(c)]. This lateral growth of the extended fixed section seemed to be due to the uneven flow motion in the fluidized section as elaborated in the following. Referring to Figure VII-13(c), the left side of the fixed section was highly resistant to the flow because of a large amount of deposition of suspended solids. Furthermore, the right side of the fixed section was also highly resistant to the flow because of the formation of the completely fixed section. Therefore, the flow in the fluidized section tended to pass through

the corner formed by the initial fixed section and the extended fixed section as illustrated in Figure VII-13(c); this was the direction the least resistant to the flow. The lateral component of this flow would constantly deliver both the suspended solids and fluidized sand to the interface between the extended fixed section anf the fluidized section, thus resulting in the continuous growth of the extended fixed section. It appears that this lateral growth of the extended fixed section captures continuously both the suspended solids and fluidized sand; simultaneously, the flow tends to bypass this growing fixed section, thus preventing a significant increase in the pressure drop. A structural evolution of the semifluidized bed during a filtration run (Run I-3) is illustrated in Figure VII-14.

Table VII-1. Size of suspended coal particles employed in the experiments.

Runs	size mesh	mean particle diameter mm
series F	- #270 to + #400	0.044
series G	- #250 to + #270	0.058
series H	- #140 to + #200	0.090
series I	- #100 to + #140	0.127

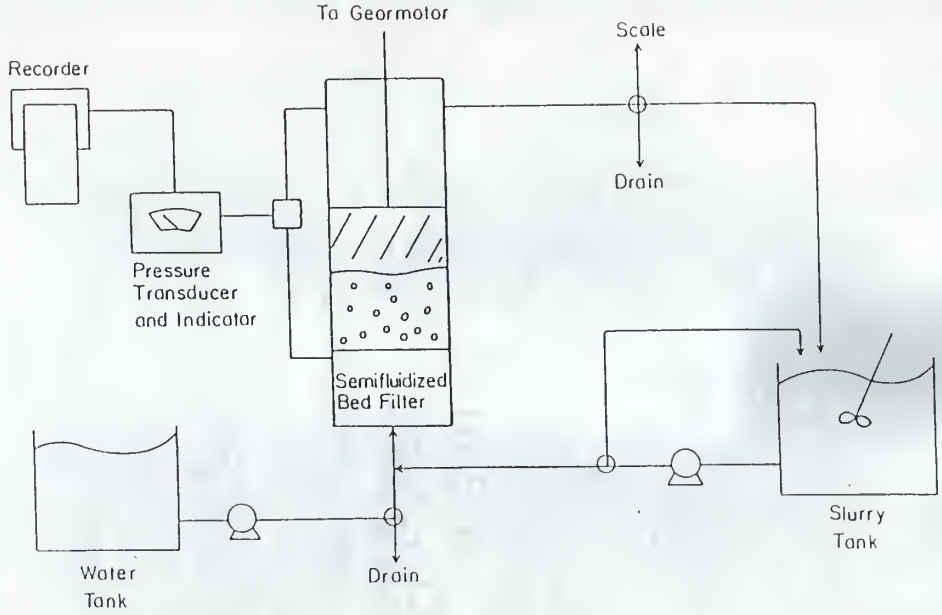

Figure VII-1. Schematic diagram of the experimental set-up.

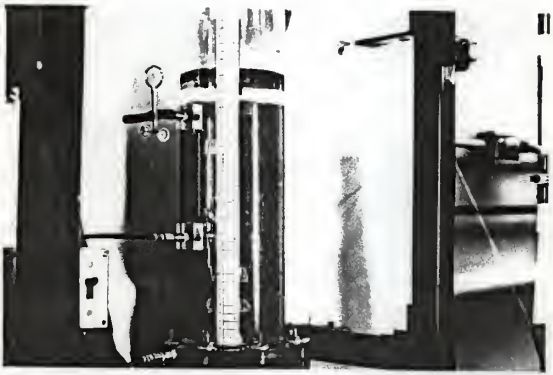

Figure VII-2. Photograph of the semifluidized-bed filter during the course of backwashing.

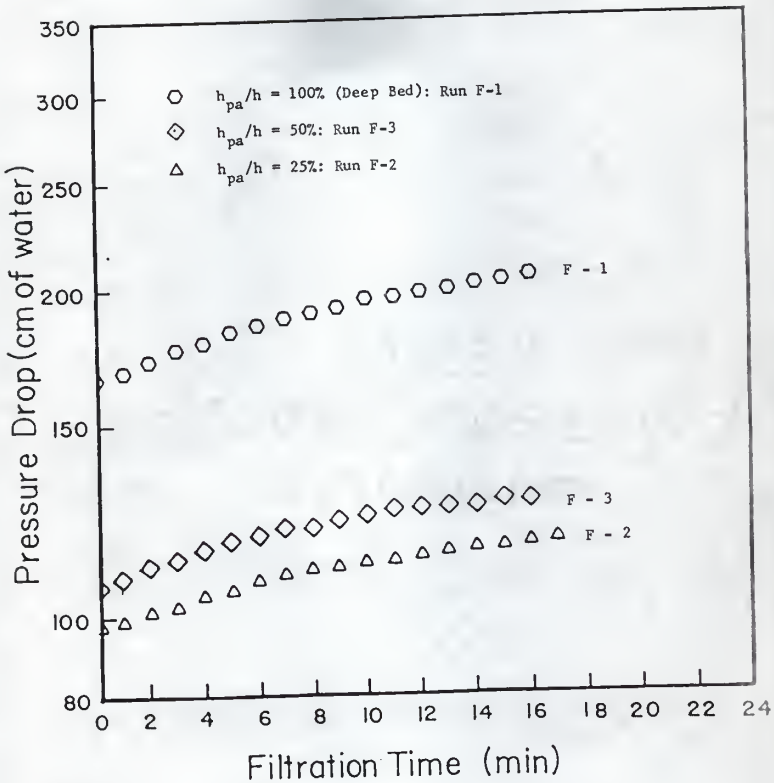

Figure VII-3. Increase in the pressure drop as a function of filtration time : suspension concentration, 0.0227 wt%;
Runs; F-1, entire bed height, 20 cm; pH, 8.0; T, 20.8 ℃;
F-2, entire bed height, 23.6 cm; pH, 8.1; T, 21.0 ℃;
F-3, entire bed height, 22.4 cm; pH, 8.0; T, 20.7 ℃.

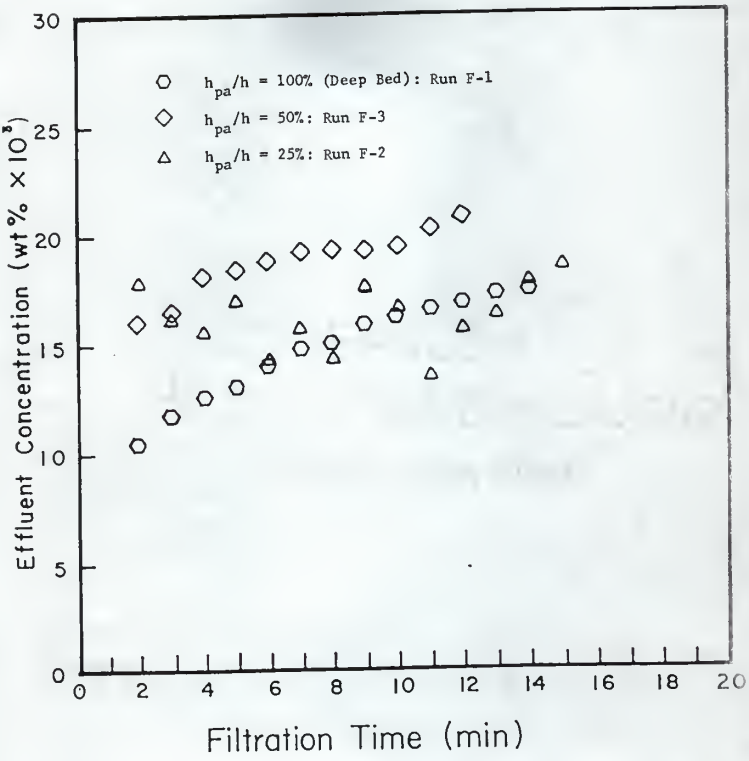

Figure VII-4. Effluent concentration of suspended particles as a function of filtration time : suspension concentration, 0.0227 wt%; Runs F-1 through F-3.

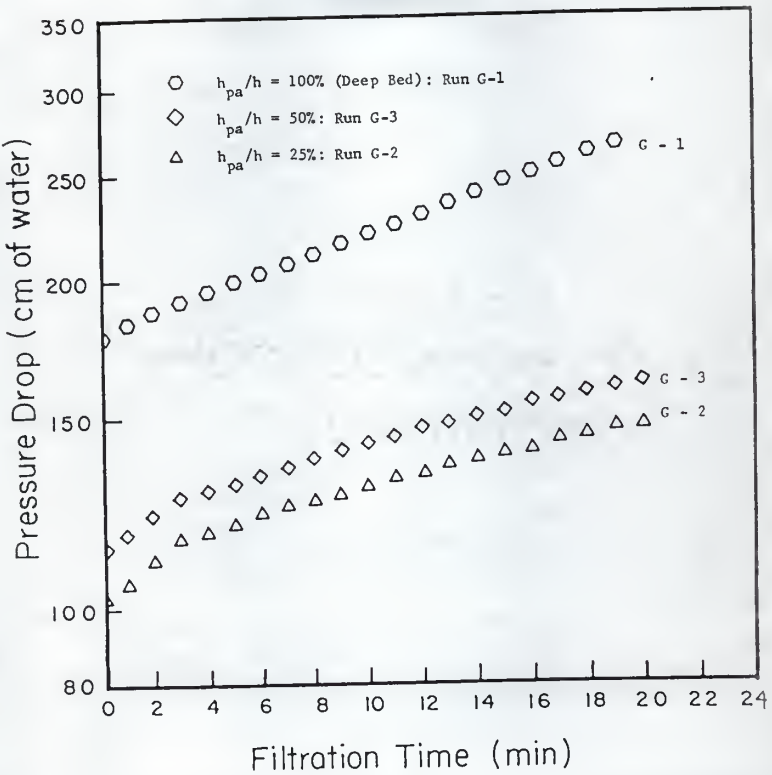

Figure VII-5. Increase in the pressure drop as a function of filtration time : suspension concentration, 0.0164 wt%;
Runs; G-1, entire bed height, 20 cm; pH, 8.5; T, 22.1 °C;
G-2, entire bed height, 23.6 cm; pH, 8.5; T, 21.9 °C;
G-3, entire bed height, 22.4 cm; pH, 8.5; T, 21.8 °C.

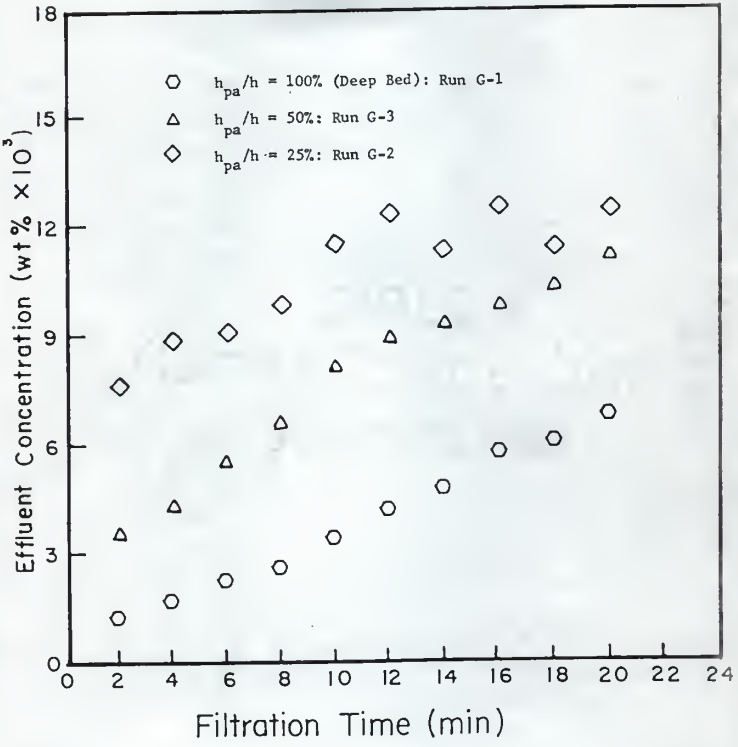

Figure VII-6. Effluent concentration of suspended particles as a function of filtration time : suspension concentration, 0.0164 wt%; Runs G-1 through G-3.

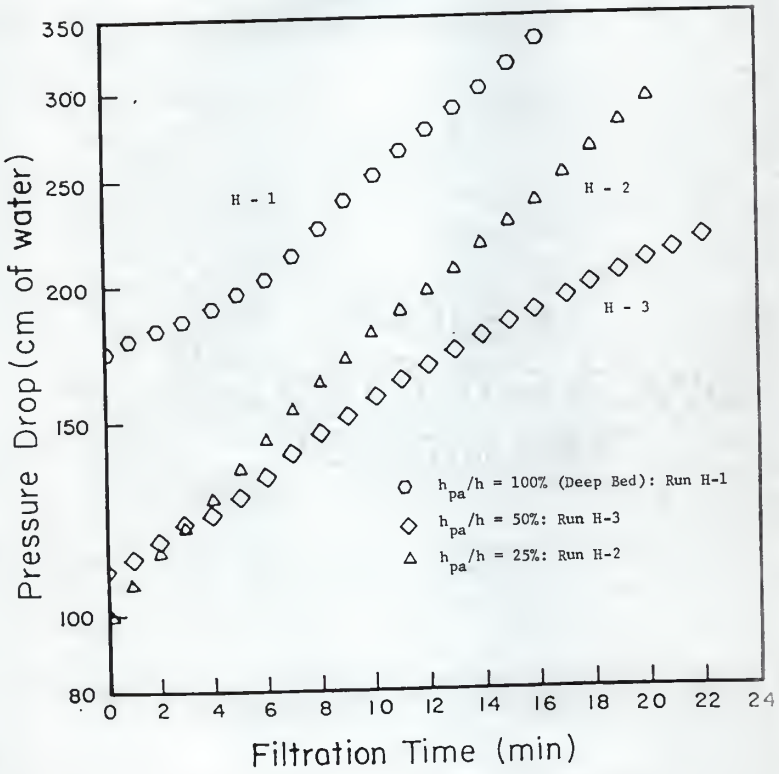

Figure VII-7. Increase in the pressure drop as a function of filtration time : suspension concentration, 0.0149 wt%;
Runs; H-1, entire bed height, 20 cm; pH, 9.4; T, 16.6 °C;
H-2, entire bed height, 23.6 cm; pH, 9.3; T, 16.5 °C;
H-3, entire bed height, 22.4 cm; pH, 9.3; T, 16.4 °C.

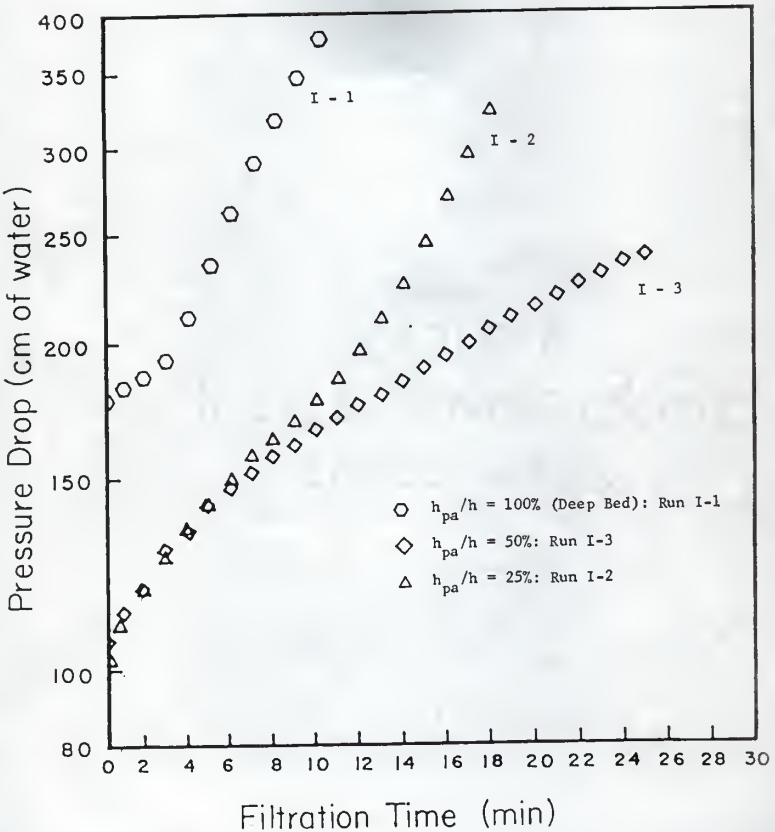

Figure VII-8. Increase in the pressure drop as a function of filtration time : suspension concentration, 0.0140 wt%;
Runs; I-1, entire bed height, 20 cm; pH, 9.1; T, 17.0 °C;
I-2, entire bed height, 23.6 cm; pH, 9.0; T, 17.1 °C;
I-3, entire bed height, 22.4 cm; pH, 9.1; T, 17.2 °C.

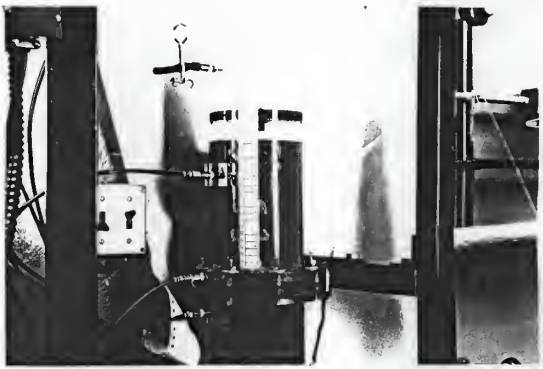

Figure VII-9. Photograph of the semifluidized-bed filter prior to the start of a filtration run: $h_{pa}/h = 25\%$.

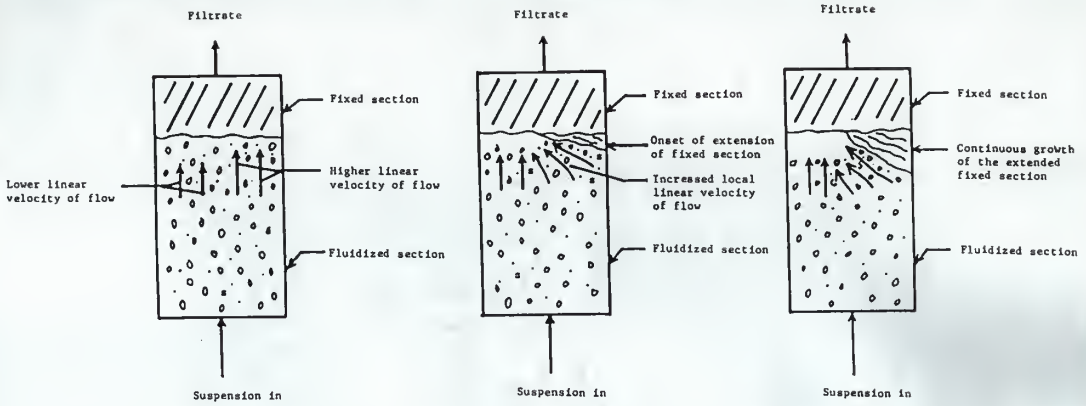

Figure VII-10. Structural evolution of the semifluidized-bed filter forming the extended fixed section : h_{pa}/h = 25%.

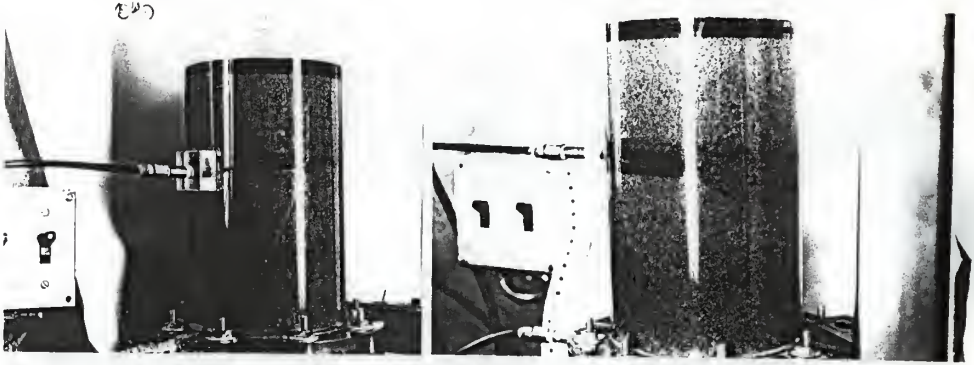

2 min 30 sec

7 min

Figure VII-11. Photographs of the semifluidized-bed filter during a filtration run: Run I-2; suspension concentration, 0.0140 wt%; entire bed height, 23.6 cm; h_{pa}/h = 25%.

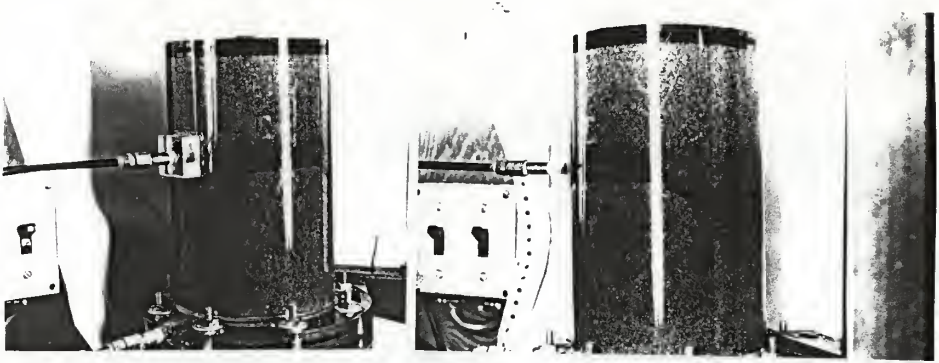

9 min 10 sec

12 min

Figure VII-11. (cont'd)

16 min

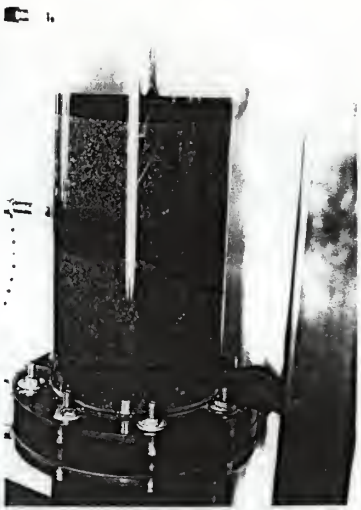

18 min

Figure VII-11. (cont'd)

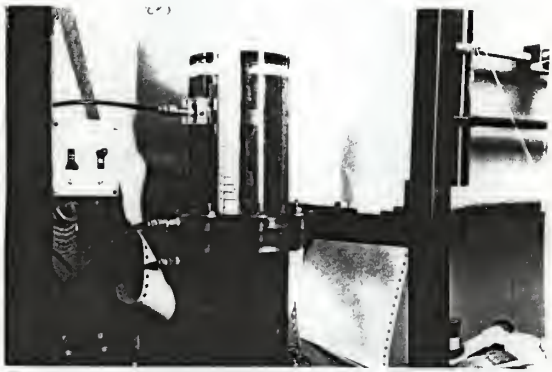

Figure VII-12. Photograph of the semifluidized-bed filter prior to the start of a filtration run: $h_{pa}/h = 50\%$.

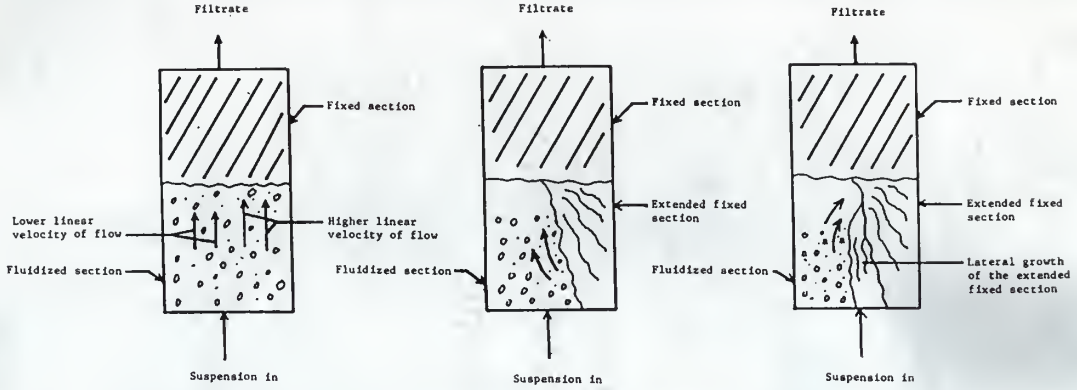

(a) Initial Stage

(b) Extension of the Fixed Section down to the Bottom Distributor Plate

(c) Lateral Growth of the Extended Fixed Section

Figure VII-13. Structural evolution of the semifluidized-bed filter forming the extended fixed section : h_{pa}/h = 50%.

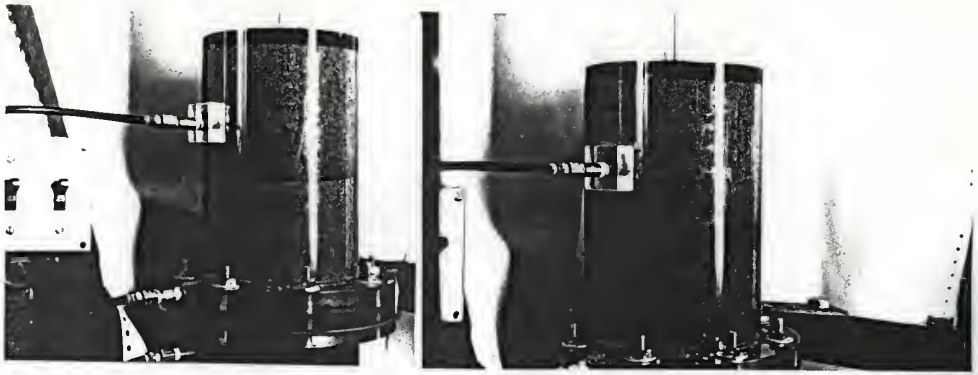

1 min 40 sec

6 min

Figure VII-14. Photographs of the semifluidized-bed filter during a filtration run: Run I-3; suspension concentration, 0.0140 wt%; entire bed height, 22.4 cm; h_{pa}/h = 50%.

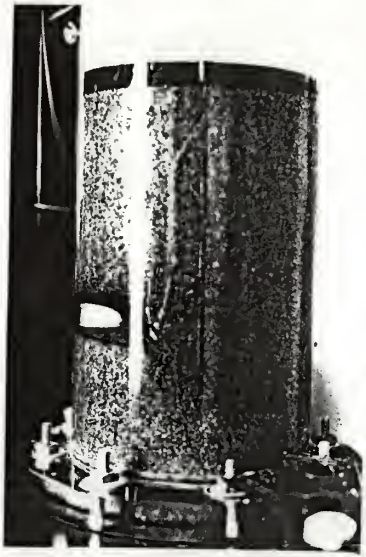

9 min

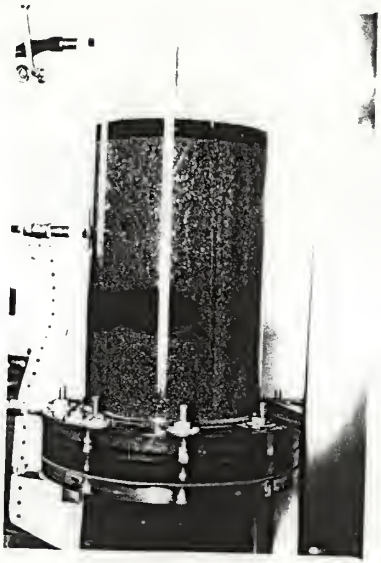

13 min 30 sec

Figure VII-14. (cont'd)

17 min 30 sec

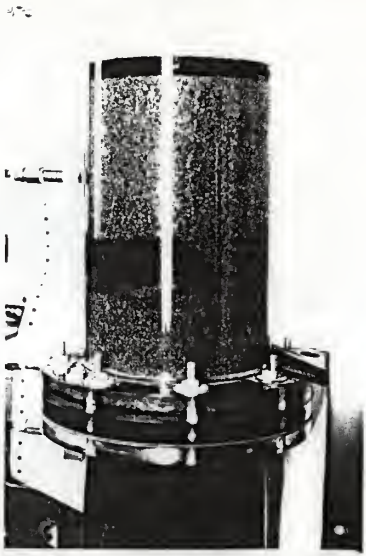

25 min

Figure VII-14. (cont'd)

CHAPTER VIII CONCLUSIONS AND RECOMMENDATIONS

In this chapter, significant conclusions of this work are summarized and possible future works are recommended.

CONCLUSIONS

The deep bed filtration is an extremely complex phenomenon involving numerous linear and nonlinear mechanisms. For such a complex system, it is impossible to construct an all-inclusive model which is capable of taking into account all known nonlinear and complex mechanisms. In fact, any model which attempts to describe every mechanism becomes excessively complex and useless. The basic tenet of the modeling is that the resultant model should be as simple as possible and yet sufficiently precise and mechanistic to represent or correlate the experimental data within their accuracy. In other words, to derive a model for such a highly complex or nonlinear system, we can not but resort to the gross or linear approximation to some degree. Needless to say, a model of any system is almost always operational in that it should be concerned with only the limited number of the significant parameters or state variables of the system, which are of interest to the modeler.

In this work, the pressure drop characteristics through the deep bed are of primary concern. To simulate the pressure drop dynamics under a constant flow condition, stochastic models, namely, the linear, birth-death process and second-order, pure birth process, in conjunction with the Carman-Kozeny equation, have been proposed. These models take into account the blockage of pores by suspended solids and/or scouring of deposited solids; the filter bed is assumed to be spatially lumped or to be composed of several compartments. In spite of this simplicity, the present models appear to represent the majority of the experimental data.

The resultant model equations, Eqs. IV-28 and V-43, are simple and easy to manipulate. Three parameters, α and β in Eq. IV-28 and k in Eq. V-43, are easily identifiable. By resorting to these parameters, the influence of various operating variables on the pressure drop characteristics can be correlated with reasonable ease. These variables include the size distributions of collector grains and suspended solids, properties of the liquid, filtration rate, bed characteristics, and suspension concentration. For design and scale-up purposes, the establishment of relationships between each of the parameters and the operating variables is the key that renders the present models useful. Based on this consideration, much effort has been spent to experimentally investigate the relationships with the size distribution of suspended solids and suspension concentration as presented in Chapter VI.

The results of the semifluidized bed filtration show that the capacity of semifluidized bed filters, expressed in terms of filtration run duration, ranged from 2 to 5 times that of the deep bed filter. Furthermore, no appreciable differences were observed in the quality of effluents obtained through the two types of filters. The results also indicate that the duration of semifluidized bed filtration runs is strongly dependent on the dynamic mechanism occurring in the fluidized portion of the filter as illustrated in Figures V-7 through V-12.

RECOMMENDATIONS

The use of the semifluidized bed filter holds great promise for increasing the filtration efficiency. To aid the design and scale-up of such filters through experimental observations and modeling, the following is recommended.

(1) To determine the performance of the semifluidized-bed filter, a companion study of the deep bed filter has been carried out to establish a basis for comparison and evaluation. Stochastic models have been developed to simulate the pressure drop change through the deep bed filter. However, the usefulness of these models as such in the design and scale-up of the deep bed filter is rather limited. For these purposes, the establishment of relationships between each of the parameters, α, β, and k, and the operating variables, including the size distributions of grains and suspended solids, size ratio of suspended solids to grains, filtration rate, bed characteristics, and suspension concentration, is the key that renders the present models useful. Thus, it is necessary to carry out an extensive experimental study of the deep bed filtration under a variety of operating conditions to determine empirically or semiempirically such relationships.

(2) The present models do not take into account the variation in the specific deposit of suspended solids. The suitability of neglecting the effect of this variation need be further justified. Furthermore, the present models are unable to simulate the phenomenon of cake formation dominent in some situations; additional modeling work should be carried out to complement this deficiency.

(3) The results of semifluidized-bed filtration show that the capacity of the semifluidized-bed filter can be increased up to several folds that of an equivalent deep bed filter. This need not be the limit; for example, this improvement will be even greater by augmenting the depth of deep bed employed in this work, which is only 20 cm. To determine the feasible and/or optimal regions of operation, an experimental study on the semifluidized-bed filter should be carried out by systematically varying the operating variables, including the entire bed height, degree of fluidization, filtration rate, size distributions of grains and suspended solids

and size ratio of suspended solids to grains.

(4) A rather high flow rate, greater than 13.1 m/h, was necessary in maintaining the fluidization of grains in the semifluidized-bed filters in this work. On the other hand, for the purification of potable water and the treatment of waste water, filtration runs are usually performed under the flow rate in the neighborhood of 5 m/h and with the suspended solids of the average diameter between 1 and 50 μm. To operate semifluidized-bed filters under such conditions, particles smaller and lighter than the 20x30 mesh sand used in this work ought to be employed as the filtering medium.

(5) The suspended solids in the potable water or waste water often vary widely in size either by the flocculation from the secondary effluent or by the addition of filter aid. Recall that the pressure drop increase was quite large for the deep bed filtration with suspended solids varying widely in size because the larger solids tended to clog the bed, preventing the penetration of smaller solids into the bed. However, it may be possible that in filtering such suspended solids with the semifluidized bed, the larger solids will tend to clog the bed and cause the extension of the fixed section; this extended fixed section will aid substantially the capture of the smaller solids, reducing the rate of pressure drop increase. Therefore, it is possible that the improvement by the semifluidized-bed filter will be even greater than that observed for the filtrations with suspended solids with a narrow size range. This possibility should be experimentally demonstrated.

(6) A mathematical model of the semifluidized-bed filtration should be developed for the design and scale-up of the filter. At the initial stage of filtration, the semifluidized bed will behave like a deep bed; the present models for the deep bed filtration are capable of simulating its performance at

this stage. As the clogging in the fixed section becomes appreciable, the fixed section will start extending. In modeling this stage of operation, two parameters are important, one being the rate of the downward extension of fixed section and the other being the rate at which the suspended solids are deposited through this extended fixed section. The estimation of these rates may result in a model for depicting the pressure drop increase during this stage. Eventually, the fixed section will extend down to the bottom of the bed, signaling the onset of the last stage of operation. At this stage, the lateral component of uneven flow in the fluidized section, as discussed in Chapter VII, will force suspended solids and fluidized sand to be captured by the extended fixed section and thicken it along the horizontal direction. Simultaneously, the flow will tend to bypass this extended fixed section because of its high resistance to the flow, indicating that this section will contribute little to the pressure drop increase. Most of the pressure drop increase can be attributed to the suspended solids, not captured by the extended fixed section, but deposited mainly in the initial fixed section through which the flow pass.

LITERATURE CITED

Babu Rao, K. and L. K. Doraiswamy, "A Generalized Equation for Solids Distribution in the Semifluidized MT Reactor," AIChE J., 13, 397 (1967).

Babu Rao, K. and L. K. Doraiswamy, "Combined Reactors: Formulation of Criteria and Operation of a Mixed Tubular Semifluidized Reactor," ibid., 16, 273 (1970).

Beranek, I. J., "Fluidizing Plant and Its Design," Brit. Chem. Eng., 3, 358 (1958).

Besik, F., "High Rate Adsorption-Bio-Oxidation of Domestic Sewage," Water & Sewage Works, 6, 68 (1973).

Camp, T. R., "Theory of Water Filtration," J. of the Sanitary Eng. Div., Proc. of ASCE, 90 (SA4), 1 (1964).

Chementator, "Japanese Report First Large-Scale Use of Continuous Ion Exchange," Chem. Eng., Nov., 1962.

Chementator, "Fluidized Bed Ion Exchange Systems Are Available," ibid., July, 1972.

Chern, S. H., K. Muroyama, and L. S. Fan, "Hydrodynamics of Constrained Inverse Fluidization and Semifluidization in a Gas-Liquid-Solid System," Chem. Eng. Sci., 38, 1167 (1983).

Chern, S. H., K. Muroyama, and L. S. Fan, " Hydrodynamics of Cocurrent Gas-Liquid-Solid Semifluidization with a Liquid as the Continuous Phase," AIChE J., 30, 288 (1984).

Chiang, C. L., Introduction to Stochastic Processes and Their Applications, Robert E. Krieger Publishing Company, Huntington, New York, 1980.

Corella, J. and R. Bilbao, "Fluid Dynamic Study of a New Type of Solid-Gas Contactor: the Fluidized/Fixed or Fluidized Bed," Ind. Eng. Chem. Process Des. Dev., 21, 545 (1982).

Craft, T. F. and G. G. Eickholz, "Mechanism of Rapid Filtration in a Uniform Filter Bed," Water Resources Res., 6, 527 (1970).

Deb, A. K., "Theory of Sand Filtration," J. of San. Eng. Div. Proc. of ASCE, 95, (SA3), 399 (1969).

Diaper, E. W. J. and K. J. Ives, "Filtration Through Size Graded Media," ibid, 91 (SA3), 89 (1965).

Dunbar, Dr., and H. T. Calvert, Principles of Sewage Treatment, Charles Griffin & Co., Ltd., Publishers, London, 1908.

Eliassen, R., "An Experimental and Theoretical Investigation of the Clogging of a Rapid Sand Filter," Doctor of Science Dissertation, MIT, Boston, Mass., 1935.

Ergun, S., "Fluid Flow Through Packed Columns," Chem. Eng. Progr., 48, 89 (1952).

Fan, L. T., Personal Communication (1958).

Fan, L. T., Y. C. Yang and C. Y. Wen, "Semifluidization: Mass Transfer in Semifluidized Beds," AIChE J., 5, 407 (1959).

Fan, L. T., Y. C. Yang and C. Y. Wen, "Mass Transfer in Semifluidized Beds for Solid-Liquid System," ibid, 6, 482 (1960).

Fan, L. T. and C. Y. Wen, "Mechanics of Semifluidization of Single Size Particles in Solid-Liquid Systems," ibid, 7, 606 (1961).

Fan, L. T. and C. Y. Wen, "System for Solid Particle - Fluid Contact Operations," U.S. Patent 3,374,052, March 1968.

Fan, L. T. and H. Hsu, "Semifluidized Bed Bioreactor," presented at the VIth International Fermentation Symposium, London, Ontario, Canada, July, 1980; also appeared in the Symposium Proceedings.

Fan, L. T. and C. Y. Wen, "Method for Wasterwater Treatment in Fluidized Bed Biological Reactors," U.S. Patent 4,253,947, March, 1981; Japanese Patent 1103262, July, 1982.

Fan, L. T. and C. Y. Wen, " Method for Wastewater Treatment in Fluidized Bed Biological Reactors," U.S. Patent 4,322,296, March, 1982.

Fan, L. T. and H. Hsu, "Method of Filtration Using Semifluidized Beds," U.S. Patent Pending, 1984.

Fan, L. T., Personal Communication (1983).

Fuller, G. W., The Purification of the Ohio River Water at Louisville, Kentucky, D. Van Nostrand Co., New York, 1898.

Govindrajan, P. N. and P. Sen Gupta, "Mass Transfer in Semifluidized Bed," Indian Chem. Engr., 18, 51 (1976).

Hall, W. A., "Analysis of Sand Filtration," J. of the San. Eng. Div., Proc. of ASCE, 83, (SA3), 1276 (1957).

Happel, J., "Viscous Flow in Multiparticle Systems: Slow Motion of Fluids Relative to Beds of Spherical Particles," AIChE J., 4 (2), 197 (1958).

Hsu, H., "Porous Medium Filtration in Semifluidized Beds," Ph.D. Dissertation, KSU, Manhattan, Kansas, 1981.

Hsu, H. and L. T. Fan, "A Novel Porous Medium Filter," Proc. World Filtration Congress III, Philadephia, PA, Sept., 1982.

Hsu, H. and L. T. Fan, "Experimental Study of Deep Bed Filtration: A Stochastic Treatment," AIChE J., 30, 267 (1984).

Huang, J. Y., "Granular Filters for Tertiary Wastewater Treatment," Ph.D. Dissertation, ISU, Ames, Iowa, 1972.

Ives, K. J., "Rational Design of Filters," Proceedings, Inst. of Civil Engrs., London, 16, 189 (1960).

Ives, K. J., "Filtration Using Radioactive Algae," J. of San. Eng. Div. Proc. of ASCE, 87 (SA3), 23 (1961).

Iwasaki, T., "Some Notes on Sand Filtration," J. of the Am. Water Works Assoc., 29, 159 (1937).

Jeris, J. S. and R. W. Owens, "Pilot-Scale, High-Rate Biological Denitrification," J. of Water Poll. Contr. Fed., 47, 2043 (1975).

Jeris, J. S., R. W. Owens and R. Hickey, "Biological Fluidized-Bed Treatment for BOD and Nitrogen Removal," ibid., 49, 816 (1977).

Jewell, W. J., H. R. Davis, W. W. Gunkel, D. V. Lathwell, J. H. Martin, Jr., T. R. McCarty, G. R. Morris, D. R. Price and D. W. Williams, " Bioconversion of Agricultural Waste for Pollution Control and Energy Conservation," NTIS Report TID-27164, Sept., 1976.

Jewell, W. J., H. R. Capener, S. Dell'orto, K. J. Fanfoni, T. D. Hayes, A. P. Leushner, T. L. Miller, D. F. Sherman, P. J. Van Soest, M. J. Wolin and W. J. Wujcik, "Anaerobic Fermentation of Agricultural Residue: Potential for Improvement and Implementation," NTIS Report EY-72-S-02-2981-7, 1978.

Kurian, J. and M. Raja Roa, " Hydrodynamics of Semi-Fluidization," Indian J. of Tech., 8, 275 (1970).

Leva, M., M. Weintraub, M. Grummer and E. L. Clark, "cooling of Gases Through Packed Tubes," Ind. Eng. Chem., 40, 747 (1948).

Leva, M., Fluidization, McGraw-Hill, New York, 1959.

Lewatit, "The Lewatit Fluidized Bed Process - A simple System for Counter-Current Ion Exchange," Company Brochure, 1972.

Lewis, W. K., E. R. Gilliland and W. C. Bauer, "Characteristics of Fluidized Particles," Ind. Eng. Chem., 41, 1104 (1949).

Litwiniszyn, J., "Colmatage Considered as a Certain Stochastic Process," Bulletin De L'Académie Polanaise Des Sciences, Serie des sciences techniques, 11 (3), 117 (1963).

Litwiniszyn, J., "Colmatage-Scouring Kinetics in the Light of Stochastic Birth-Death," ibid., 14 (9), 561 (1966).

Litwiniszyn, J., "Colmatage with Reference to the Model of a Random Walking," ibid., 15 (6), 345 (1967).

Litwiniszyn, J., "The Phenomenon of Colmatage Considered in the Light of Markov Processes," ibid., 16 (4), 183 (1968a).

Litwiniszyn, J., "On a Certain Markov Model of Colmatage-Scouring Phenomena. I," ibid., 16 (11-12), 533 (1968b).

Litwiniszyn, J., "On a Certain Markov Model of Colmatage-Scouring Phenomena. II," ibid., 17 (1), 57 (1969).

Marquardt, Donald W., " An Algorithm for Least-Squares Estimation of Non-linear Parameters," Journal for the Society of Industrial and Applied Mathematics, 11, 431 (1963).

Mathews, A. P. and L. T. Fan, " Comparison of Performance of Packed and Semifluidized Beds for Adsorption of Trace Organics," presented at the National AIChE Meeting, Denver, CO, Aug., 1983a.

Mathews, A. P. and L. T. Fan, " Wastewater Treatment and Water Reuse in the Fermentation Industries," presented at the AIChE Annual Meeting, Washington, DC., Oct.-Nov., 1983b.

Mintz, D. M., "Kinetics of Filtration," Dokl. AK. Nauk. U.S.S.E. 78, No. 2, (1951).

Mintz, D. M., "Modern Theory of Filtration," Special Subject No. 10, Proc., The Seventh International Water Supply Congress, 1966.

Mintz, D. M., Paskutskaya, L. N. and Chernova, Z. V., "The Mechanism of the Filtration Process on Rapid Water Treatment Filters," Zh. Priklad. Khim. 8, 1695 (1967).

O'Melia, C. R. and W. Stumm, "Theory of Water Filtration," J. of Am. Water Works Assoc., 59, 1393 (1967).

Payatakes, A. C., "A New Model for Granular Porous Media. Application to Filtration Through Packed Beds," Ph.D. Dissertation, Syracuse University, 1973.

Payatakes, A. C., C. Tien and R. M. Turian, "A Model for Granular Porous Media: Part 1. Model Formulation," AIChE J., 19, 58 (1973).

Payatakes, A. C., R. Rajagopalan and C. Tien, "Application of Porous Media Models to the Study of Deep Bed Filtration," Canadian J. of Chem. Eng., 52, 722 (1974).

Pense, H. C., C. Tien, R. Rajagopalan and R. M. Turian, "Dispersion Measurement in Clogged Filter Beds: A Diagnostic Study on the Morphology of Particle Deposits," AIChE J., 24, 473 (1978).

Poddar, S. K. snd D. K. Dutt, "Studies on Semifluidization Characteristics for Solid-Liquid Systems. Prediction of Minimum and Maximum Semifluidization Velocity," Indian Chem. Engr., 11, 80 (1969).

Purnachander Rao, S. and R. Kaparthi, "Heat Transfer in Semifluidized Bed," ibid., 11, April, 1969.

Rajagopalan, R. and C. Tien, "Trajectory Analysis of Deep-Bed Filtration with the Sphere-in-cell Porous Media Model," AIChE J., 22, 523 (1976).

Richardson, J. F. and W. N. Zaki, "Sedimentation and Fluidization: Part I," Trans. Inst. Chem. Engr., 32, 35 (1954).

Rimer, A. E., "Filtration Through a Trimedia," J. of San. Eng. Div. Proc. of ASCE, 94 (SA3), 521 (1968).

Roy, G. K., "Studies on Certain Aspects of Semifluidization," Ph.D. Thesis, Samhalpur University, India, 1971.

Roy, G. K. and K. J. R. Sarma, "Dynamics of Liquid Solid Semifluidization III. Relation Between Onset of Semifluidization and Minimum Fluidization Velocity," Chem. Eng. J., 4, 294 (1972).

Roy, G. K. and K. J. R. Sarma, "Dynamics of Liquid-Solid Semifluidization: Prediction of Semifluidization Velocity and Packed Bed Formation," Indian J. of Tech., 11, 273 (1973).

Roy, G. K. and P. Sen Gupta, "Prediction of the Pressure Drop Across a Gas-Solid Semi-Fluidized Bed," Chem. Eng. J., 5, 191 (1973).

Roy, G. K. and K. J. R. Sarma, "Relation Between Maximum Semi-Fluidization and Minimum Fluidization Velocity in Liquid-Solid Systems," J. of Inst. of Engr. (India), 54, 34 (1974a).

Roy, G. K. and K. J. R. Sarma, "Dynamics of Liquid-Solid Semi-Fluidization (IV)," Indian Chem. Engr., 16, 31 (1974b).

Roy, G. K. and P. Sen Gupta, "Prediction of the Packed Bed Height in Gas-Solid Semifluidization," Ind. Eng. Proc. Des. Dev., 13, 219 (1974).

Roy, G. K. and P. Sen Gupta, "Semi-Fluidization: Design Study," Processing, 10, Jan., 1975.

Roy, G. K. and J. Dash, "Liquid-Solid Semi-Fluidization of Homogeneous Mixtures - II: Prediction of Maximum Semi-Fluidization Velocity," Indian Chem. J., 24, Jan., 1976.

Roy, G. K. and H. N. Sharat Chandra, "Liquid-Solid Semi-Fluidization of Heterogeneous Mixtures II: Prediction of the Minimum Semi-Fluidization Velocity," Chem. Eng., 12, 77 (1976).

Scott, C. D. and C. W. Hancher, "Use of a Trappered Fluidized Bed as a Continuous Bioreactor," Biotech. and Bioeng., 18, 1393 (1976).

Streander, P. B., "Sewage filtration with silica sand filters I," Water Works and Sewerage, 87, 351 (1940).

Tchobanoglous, G., "Filtration Techniques in Tertiary Treatment," J. of Water Pollution Control Federation, 42, 604 (1970).

Tchobanoglous, G. and R. Eliassen, "Filtration of Treated Sewage Effluent," J. of the San. Eng. Div., ASCE, 96, 243 (1970).

Tien, C. and Payatakes, A. C., "Advances in Deep Bed Filtration," AIChE J., 25, 737 (1979).

Tien, C., R. M. Turian and H. Pense, "Simulation of the Dynamic Behavior of Deep Bed Filters, ibid., 25, 285 (1979).

Van Kampen, N. G., Stochastic Processes in Physics and Chemistry, North-Holland Publishing Company, Amsterdam, New York, Oxford, 1981.

Weber, W. J. Jr., C. B. Hopkins, and R. Bloom, Jr., "Physicochemical Treatment of Wastewater," J. Water Poll. Contr. Fed., 42, 83 (1970).

Wen, C. Y., S. C. Wang and L. T. Fan, "Semifluidization in Solid-Gas System," AIChE J., 9, 316 (1963).

Wen, C. Y. and Y. H. Yu, "Mechanics of Fluidization," Chem. Eng. Progr. Symposium Series, 62, 100 (1966).

Wen, C. Y. and L. T. Fan, "Method of Filtration Using Convertible (Semi-fluidized) Beds," U.S. Patent 4,157,959, June 1979; U K GB 2 002 250B, Jan., 1982, Japanese 1176738, Nov., 1983.

Wilhelm, R. H. and R. Kwauk, "Fluidization of Solid Particles," Chem. Eng. Progr., 44, 201 (1948).

Yao, K. M., M. T. Habibian and C. R. O'Melia, "Water and Waste Water Filtration: Concepts and Application," Environ. Sci. & Tech., 5, 1105 (1971).

Yutani, N. and L. T. Fan, Personal Communication (1984).

Zenz, F. A. and D. F. Othmer, Fluidization and Fluid-Particle System, Chapter 5, Reinhold Publishing Corp., New York, 1960.

A STUDY OF SAND-BED FILTERS: Filtration of Suspended Solids with Narrow Size Ranges

by

SHYH-HONG HWANG

B. S., NATIONAL TAIWAN UNIVERSITY, 1980

AN ABSTRACT OF A MASTER'S THESIS

submitted in partial fulfillment of the

requirements for the degree

MASTER OF SCIENCE

Department of Chemical Engineering

KANSAS STATE UNIVERSITY
Manhattan, Kansas

1984

The present study aimed to carry out a comprehensive investigation of the performance of the semifluidized-bed filter. Because the filtration in a semifluidized-bed involves the deep bed filtration, a reasonable model of semifluidized-bed filtration requires the incorporation of a deep bed filtration model. Therefore, a companion study on the deep bed filter has also been carried out.

Stochastic models, namely, the linear, birth-death process and the second-order, pure birth process, have been employed in conjunction with the Carman-Kozeny equation to simulate the performance of the deep bed filter in terms of the pressure drop dynamics under a constant flow condition. These models take into account the blockage of pores by suspended aolids and/or scouring of deposited solids; the filter bed is assumed to be spatially lumped or to be composed of several compartments. The present models appear to represent the majority of the experimental data.

A series of experimental runs of deep bed filtration was conducted with suspensions of solids of various sizes, size distributions and concentrations. For each run, the pressure drop and effluent concentration were measured as functions of filtration time. The results are treated and analyzed stochastically.

The operation of deep bed filters is often inefficient; it is typically characterized by the shallow penetration of suspended solids and rapid clogging in the bed. Fortunately, these disadvantages can be overcome by the use of semifluidized-bed filters. The results of an experimental study show that the filtration capacity of the semifluidized-bed filter is conaiderably greater than that of an equivalent deep bed filter. In addition to pressure drop and effluent quality data, a series of photographs is included to describe and explain the mechanisms of the semifluidized-bed filter, giving rise to its superior performance over the deep bed filter.

The present study aimed to carry out a comprehensive investigation of the performance of the semifluidized-bed filter. Because the filtration in a semifluidized-bed involves the deep bed filtration, a reasonable model of semifluidized-bed filtration requires the incorporation of a deep bed filtration model. Therefore, a companion study on the deep bed filter has also been carried out.

Stochastic models, namely, the linear, birth-death process and the second-order, pure birth process, have been employed in conjunction with the Carman-Kozeny equation to simulate the performance of the deep bed filter in terms of the pressure drop dynamics under a constant flow condition. These models take into account the blockage of pores by suspended aolids and/or scouring of deposited solids; the filter bed is assumed to be spatially lumped or to be composed of several compartments. The present models appear to represent the majority of the experimental data.

A series of experimental runs of deep bed filtration was conducted with suspensions of solids of various sizes, size distributions and concentrations. For each run, the pressure drop and effluent concentration were measured as functions of filtration time. The results are treated and analyzed stochastically.

The operation of deep bed filters is often inefficient; it is typically characterized by the shallow penetration of suspended solids and rapid clogging in the bed. Fortunately, these disadvantages can be overcome by the use of semifluidized-bed filters. The results of an experimental study show that the filtration capacity of the semifluidized-bed filter is conaiderably greater than that of an equivalent deep bed filter. In addition to pressure drop and effluent quality data, a series of photographs is included to describe and explain the mechanisms of the semifluidized-bed filter, giving rise to its superior performance over the deep bed filter.